Characterisation of human surfactant protein A and recombinant human vimentin in their modulation of HPV16 pseudovirus infection

---

Sinead Carse

Supervisor:

Dr Georgia Schäfer

Co-supervisor:

Professor Arieh Katz

Presented for the Degree

Master of Science in Medicine

Medical Biochemistry

Division of Medical Biochemistry and Structural Biology

Department of Integrative Biomedical Sciences

Faculty of Health Sciences

University of Cape Town

20th December 2019

Declaration

I, Sinead Carse, hereby declare that the work on which this dissertation/thesis is based is my original work (except where acknowledgements indicate otherwise) and that neither the whole work nor any part of it has been, is being, or is to be submitted for another degree in this or any other university.

I empower the university to reproduce for the purpose of research either the whole or any portion of the contents in any manner whatsoever.

Signature: Signed by candidate

Date: 20th December 2019

Acknowledgements

I would first and foremost like to thank my amazing supervisor Dr Georgia Schäfer. I have been so fortunate to have her as a supervisor since my honour's year and have learnt so much from her over the past few years. Georgia, thank you for being so patient with me over the past few years and for going above and beyond by making my experience as a postgraduate student so exciting and fulfilling. I am so grateful for the opportunities you have given me, not least of which was to present my Master's work overseas and have a paper published!

A big thank you to my co-supervisor, Professor Arieh Katz, for his mentorship and guidance with my writing. Thank you for making me feel so welcome in your lab.

I would like to thank Graham Christians, Xolani Nonzinyana and Roshan Ebrahim for everything they do in the lab and office. I really appreciate all the hard work that goes into keeping the lab up and running!

I would like to thank Sylvia Ujma for teaching me many of the techniques I used in this study and for establishing the mouse model I used for my thesis. An even bigger thank you for advising me to choose Georgia as my supervisor at the beginning of my honour's year!

I would like to thank Ms. Alisha Chetty and Dr. Schäfer for their assistance and guidance with the mouse work and myeloid panel studies. Ms. Chetty put in many hours to help us even when she was writing up her PhD. I would also like to thank Associate Professor Dirk Lang and Mrs. Susan Cooper for their assistance with confocal microscopy and image analysis. I really appreciated the friendly assistance as well as the occasional cup of coffee! Thank you to Dr Mohamed Jaffer for all his expertise and assistance with the transmission electron microscopy.

I would like to thank everyone of my friends and members of my family for being there for me throughout the years. A big thank you to my friend and lab mate, Melissa, for being so kind and thoughtful. I have the utmost admiration for you Melis! Thank you to my parents, Genene and Fred Carse for everything they have given me, most especially for all their love and support. Thank you to Gabriel Stein for loving me and for giving me the much-needed strength and support to get me to this point.

I would like to thank Dr Schäfer, Dr Lisa Graham as well as the Poliomyelitis Research Foundation for funding my studies, as well as the University of Cape Town for funding my conference attendance. Without the financial support I would not have been able to pursue my postgraduate studies and so I am eternally grateful.

Table of Contents

List of Figures

List of abbreviations

Listed are only terms that have been used more than once in the document. When mentioned for the first time in the text, all terms were written out followed by the abbreviation in brackets.

°C	Degrees Celsius
ACE2	Angiotensin converting enzyme 2
AF488	Alexa Fluor 488
AF555	Alexa Fluor 555
AF647	Alexa Fluor 647
AIDS	Acquired Immunodeficiency syndrome
A. phagocytophilum	*Anaplasma phagocytophilum*
ANOVA	Analysis of variance
APCs	Antigen presenting cells
BSA	Bovine serum albumin
CMC	Carboxymethylcellulose
CMV	Cytomegalovirus
CPMV	Cowpea mosaic virus
CRD	Carbohydrate recognition domain
CsCl	Caesium chloride
CTCs	Circulating tumour cells
C. trachomatis	*Chlamydia trachomatis*
DCs	Dendritic cells
DMEM	Dulbecco's modified medium

DNA	Deoxyribonucleic acid
DOH	Department of Health
ECM	Extra-cellular matrix
E. coli	*Escherichia coli*
EDTA	Ethylenediaminetetraacetic acid
EMT	Epithelial-mesenchymal transition
EV71	Enterovirus 71
FACS	Fluorescence Activated Cell Sorter
FMO	Fluorescence minus 1
FRT	Female reproductive tract
FSC	Forward scatter
GLuc	Gaussia luciferase
Gly	Glycine
HEPES	4-(2-hydroxyethyl)-1-piperazineethanesulfonic acid
H. influenza	*Hemophilus influenza*
HIV	Human immunodeficiency virus
HLA	Human leukocyte antigen
HPV	Human papillomavirus
HPV16-PsVs	Human papillomavirus type 16 pseudovirions
HSB	High-salt buffer
HSPGs	Heparan Sulphate proteoglycans
HSV-1/2	Herpes simplex virus type 1 and 2
IAV	Influenza A virus

IF	Intermediate filaments
IHC	Immunohistochemistry
IFN	Interferon
IRF	Interferon regulatory factor
i.vag.	Intravaginal
JEV	Japanese encephalitis virus
kb	Kilobase
KCl	Potassium chloride
kDa	Kilo Daltons
KLK8	Kallikrein-8
kV	kilo Volts
L	Litre
LCs	Langerhans cells
LMIC	Low-to-middle-income countries
-m	-meter
m-	Milli-
M	Molar
MF	Microfilaments
$MgCl_2$	Magnesium chloride
MT	Microtubules
M.tb	*Mycobacetrium tuberculosis*
N	Nano-
NaCl	Sodium chloride

N-9	Nonoxynol-9
OCT	Optimal cutting media
ori	Origin of replication
P. aeruginosa	*Pseudomonas aeruginosa*
PAMPs	Pathogen associated molecular patterns
PBS	Phosphate buffered saline
p.i.	Post infection
PVs	Papillomaviruses
Rb	Retinoblastoma
RCF	Relative Centrifugal Force
rhVim	Recombinant human Vimentin
RPM	Revolutions per minute
RSV	Respiratory syncytial virus
SARS-CoV	Severe acute respiratory syndrome *coronavirus*
S. aureus	*Staphylococcus aureus*
s.c.	Subcutaneous
SDS-PAGE	Sodium Dodecyl Sulphate Polyacrylamide Gel Electrophoresis
SPs	Surfactant proteins
SP-A	Surfactant protein A
S. pneumoniae	*Streptococcus pneumoniae*
S phase	Synthesis phase
SSC	Side scatter

TEM	Transmission electron microscopy
U	Units
ULF	Unite length filament
VLPs	Virus-like particles
Vol	Volume
v/v	Volume/volume
w/w	Weight/weight
α	Alpha
µ	Micro-

Abstract

Infection by oncogenic human papillomavirus (HPV) is the primary cause of cervical cancer, where low-and middle-income countries (LMIC) have the highest incidence. Prophylactic HPV vaccines exist but LMIC have limited access. Therefore, alternative preventative measures against HPV infection and cervical cancer progression are needed. Two human proteins have been identified in our laboratory that modulate HPV16 pseudovirus (HPV16-PsVs) infection *in vitro*, namely surfactant protein A (SP-A) and recombinant human vimentin (rhVim).

Previous work suggested SP-A mediated immune recognition of HPV since SP-A-coated HPV16-PsVs enhanced viral uptake by RAW264.7 murine macrophages. These initial observations were confirmed using a murine C57BL/6 cervicovaginal challenge model: pre-incubation of HPV16-PsVs with purified human SP-A significantly reduced the level of HPV16-PsV infection *in vivo.* Moreover, when isolated cells from female reproductive tracts of naïve C57BL/6 mice were incubated with HPV16-PsVs and stained for selected innate immune cell populations by flow cytometry, significant increases in viral uptake by eosinophils, neutrophils, monocytes and macrophages were observed over time using SP-A-pre-coated virions compared to control particles.

Compared to SP-A mediated modulation of HPV infection through activation of innate immune responses, rhVim was suggested to directly interfere with HPV entry into host cells. Indeed, supplementation with non-filamentous rhVim resulted in decreased viral uptake by NIKS cells which was confirmed *in vivo* using the murine C57BL/6 cervicovaginal HPV16-PsVs challenge model. Co-localisation analysis employing confocal imaging, revealed that rhVim-coated HPV16-PsVs co-localised, to a lesser degree, with surface-expressed heparan sulphate proteoglycans (HSPGs) than control particles. Removal of surface HSPGs on NIKS cells decreased HPV16-PsVs cell surface binding and internalisation, while pre-incubation of HPV16-PsVs with rhVim decreased viral particle binding and internalisation to a greater extent. This indicates that rhVim may modulate HPV16 infection by interfering with its attachment to HSPGs as well as viral engagement with the yet unknown entry receptor(s).

In summary, both SP-A and vimentin modulate HPV16-PsVs infection by different mechanisms. These *in vivo* studies strongly confirm previous *in vitro* observations, rendering both proteins potentially suitable for further development into possible candidates for use in topical microbicides, which may provide protection against new HPV infections.

1 Introduction

1.1 Human papillomavirus and cervical cancer

Papillomaviruses (PVs) belong to the highly diverse family of *Papillomaviridae* (1). There are over 100 characterised types of human papillomaviruses (HPVs), which have been classified as either low-risk or high-risk, depending on their ability to cause malignancy (1). HPVs are highly prevalent and are contracted through sexual activity, thus leading to significant disease burden globally. Infection with high-risk (oncogenic) HPVs are associated with 5% of all human cancers, and are the etiological agents for the development of virtually all cases of cervical cancers (2, 3). More than 20 oncogenic HPV types have been characterised, of which HPV types 16 and 18 are the most common oncogenic types globally and are the major causes of cervical cancer. These two high-risk HPV types contribute to 70% of all documented cases (2, 4).

Although HPV infection is necessary, it is not sufficient for cancer development. Many co-factors have been established for the initiation and progression of cervical cancer, some of which include: long-term use of contraceptives, tobacco smoking, chronic inflammation, and co-infection with human immunodeficiency virus (HIV) (4–6). Likely co-factors include co-infection with *Chlamydia trachomatis (C. trachomatis)* and herpes simplex virus type-2 (HSV-2), as well as genetic and immunological factors (5, 8–11).

Cervical cancer is more prevalent in low-and middle-income countries (LMIC). Globally, cervical cancer ranks fourth for both incidence and mortality in women (12). However, it is the second most common cancer in South Africa (8, 12) as well as the leading cause of female cancer-associated deaths in Sub-Saharan Africa (13). The higher incidence rate in LMIC has been attributed to the HIV/acquired immunodeficiency syndrome (AIDS) epidemic in Southern Africa (see section 1.1.3) (14).

As infection with oncogenic HPVs is almost always the cause of cervical cancer, it has the potential to be preventable. Highly efficient vaccines targeting the most common oncogenic HPV types are on the market, but access to these vaccines by the target groups in LMIC has proven challenging for a number of reasons (see section 1.1.4). Therefore, alternative means to protect against sexually transmitted HPVs are much needed.

1.1.1 HPV genome and structure

HPVs are small non-enveloped DNA viruses. They are characterised by their circular double-stranded DNA genomes, which are approximately 8 kilobases (kb) in length. The HPV genome is broken down into “early” and “late” genes (Figure 1.1A). E1 and E2 have been implicated in replication and transcription (15). E1 has ATPase, DNA helicase as well as origin of replication (ori)-specific DNA binding and unwinding activities (16). Contrarily, E2 acts as a transcriptional activator protein (16). It has been shown that E1 complexes with E2 for enhanced binding of the ori (15, 16). E4 has roles in successful genome amplification and virus synthesis, as well as a role in viral particle release (17).

The function of E5 is not well described, and controversy exists about its role in the HPV life cycle. A study has elucidated a role for E5 in immune evasion, showing that E5 selectively downregulates surface human leukocyte antigen (HLA) class I molecules (18).

E6 and E7 are proteins with oncogenic properties, where both have been implicated in neoplastic transformation of cells (19). E6 specifically binds to p53, a tumour suppressor protein involved in controlling the cell cycle, DNA repair and apoptosis (19). Suppression of p53 by E6 results in dysregulation of the cell cycle, promotes cell proliferation and increases the frequency of spontaneous mutations, all of which are hallmarks of malignancy (19, 20). E7 binds to the retinoblastoma protein (Rb), another major tumour suppressor (19, 21). E7 binding to Rb releases the E2F transcription factor from Rb complexes, which results in the activation of genes that control cell proliferation (19, 20, 22). Furthermore, both E6 and E7 also play a role in immune evasion (detailed in section 1.1.3).

The late proteins L1 and L2 encode for the major and minor capsid proteins, respectively. L1 spontaneously assembles into pentameric capsomeres and comprise the majority of the icosahedral viral capsid (23, 24). L2 remains hidden and embedded in the pentamers and stabilises the shape and stability of the capsid (Figure 1.1B) (23).

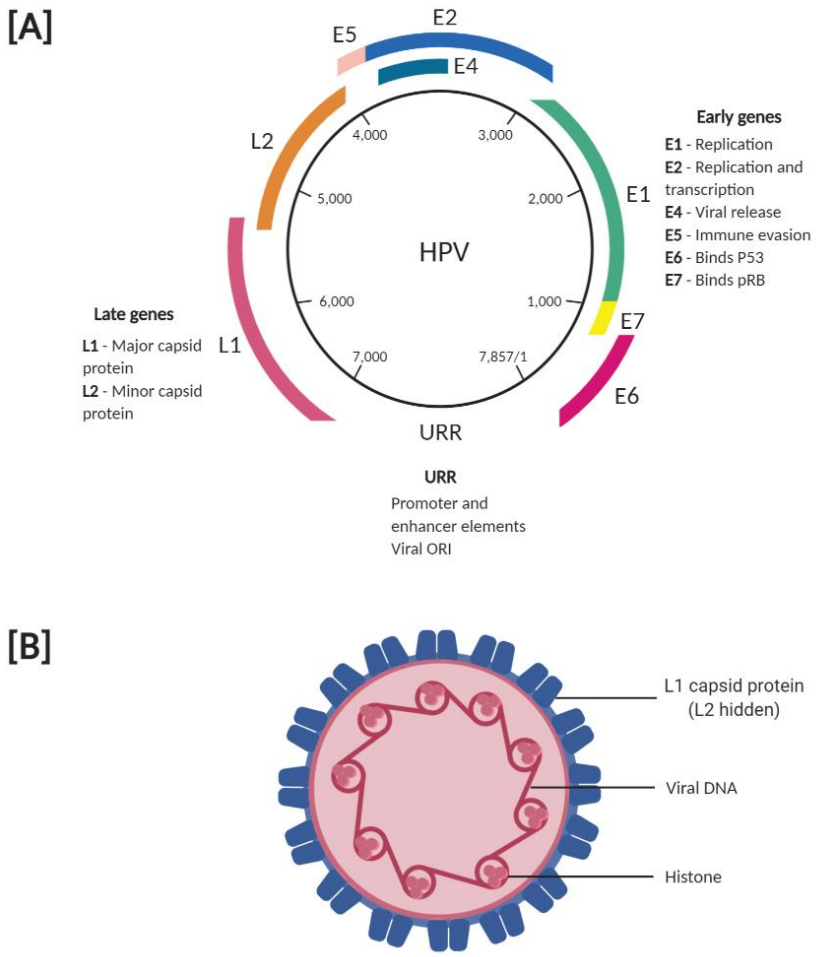

Figure 1.1: Schematic representation of the HPV genome and viral particle structure. [A] Depicted is the arrangement of the early E (non-structural) genes, the capsid genes (L1 and L2) and the upstream regulatory region (URR). Genome size as well as the position of the genes are marked in base pairs (bp). **[B]** Depicted is the structure of the HPV particle. Figure adapted from (25).

1.1.2 HPV infectious cycle and malignant transformation

HPV displays a rather specific target cell tropism and primarily infects basal keratinocytes of squamous epithelium, such as is found in the mucosal epithelial lining of the cervix (23, 26). It is well established that epithelial wounding (or damage) is a pre-requisite for efficient HPV infection in an *in vivo* setting (27–29). It is likely that abrasions in the outermost protective layers help the virions gain access to the mitotically-competent basal epithelial cells in the inner layers of the epithelium, as these are the cells that are able to establish episomal viral genome replication (26, 27). Both the major L1 capsid protein, and the mainly hidden minor L2 capsid protein have been

shown to be involved in the initial binding and entry steps into the target cells of the basal epithelium. However, the exact mechanisms and surface receptors used by HPV for successful entry and subsequent establishment of infection remain unknown.

What is known is that the initial cell surface molecules that HPV interact with are heparan sulphate proteoglycans (HSPGs) (27, 30, 31). It has also been proposed that HPV binds in a transient manner to laminin 332 (a protein secreted into the extracellular matrix by migrating keratinocytes), which results in uptake by proliferating keratinocytes expressing α6 integrin (32).

Many infectious pathogens and viruses interact with HSPGs on the cell surface, or on the basement membrane, for attachment and subsequent cellular entry (33). Specifically, the L1 capsid protein of HPV binds to the glycosaminoglycan (GAG) chains of HSPGs (27). This binding induces conformational changes in the capsid and facilitates proteolytic cleavage of L1 by the secreted serine-protease kallikrein-8 (KLK8) (27, 34). This cleavage allows for interactions between the capsid and cyclophilin B, which results in further conformational changes that exposes the L2 N-terminus containing a conserved consensus cleavage site for the host extracellular proprotein convertase furin (35, 36). This interaction has been shown to be essential for successful infection of HPV, as furin cleavage results in the exposure of a binding site on L1, postulated to be recognised by an unknown receptor, or receptor complex (27, 33, 34, 37). The described changes in virion conformation further facilitate the reduction in the binding affinity to HSPGs, thereby facilitating the engagement with the unknown receptor(s), or receptor complex (38).

The mechanisms and pathways used by HPV for intracellular trafficking remains elusive, however, most studies indicate a clathrin-mediated endocytosis pathway for most HPV types, including HPV16 (39). This involves the localisation of HPV into early endosomes within 4 hours of cellular internalisation, followed by uncoating of the viral particle within the late endosome (12 hours after internalisation). Most studies suggest the release of a L2/viral DNA complex from the late endosome, followed by nuclear trafficking of this complex and subsequent viral DNA replication and gene expression (39). Furin cleavage has also been in implicated in successful endosomal escape prior to transport of the L2/viral DNA complex to the nucleus, emphasising the necessity of furin cleavage for successful infection of HPV (36, 37, 40).

The HPV life cycle is closely linked to the differentiation program of the host keratinocyte (20). Low levels of viral DNA are made in infected mitotically active keratinocytes within the basal epithelial layer (approximately 100 genomes per cell), where expression of the E1 and E2 proteins help maintain this low level of replication, as well as the subsequent separation of the viral DNA into the dividing cells (5, 20). The infected daughter cells leave the mitotic phase and migrate to the upper epithelial layers (spinous layer), where they enter the differentiation phase (25). This results in upregulation of viral E6 and E7 protein expression, which disrupts the normal cell cycle control and drives these differentiating cells into the S phase. This disruption allows for viral DNA replication, amplifying the copy number to thousands per cell, as well as the expression of the late viral L1 and L2 capsid proteins (25, 41). The capsid proteins spontaneously assemble to encapsidate the viral genome, where the newly formed virions are released from the outermost layer of the epithelium (the cornified layer, Figure 1.2) (25). The time from infection to viral release is relatively slow and takes approximately three weeks (26) .

For malignancy to occur, the viral genome must integrate into the host keratinocyte genome (5, 19). Integration from the perspective of HPV is “accidental” as it results in a dead-end for virus production (42). However, viral genome integration into the host genome results in a constant level of E6 and E7 expression (5). Integration disrupts the expression of E4, E5, and E2, the latter of which controls expression of the E6 and E7 proteins (19). Overexpression of E6 and E7 genes results in overproduction of the E6 and E7 oncoproteins (19), consequently leading to the repression of the tumour suppressor proteins, p53 and Rb (see section 1.1.1). This results in uncontrolled cell proliferation and increased incidence of DNA damage (19, 20, 41).

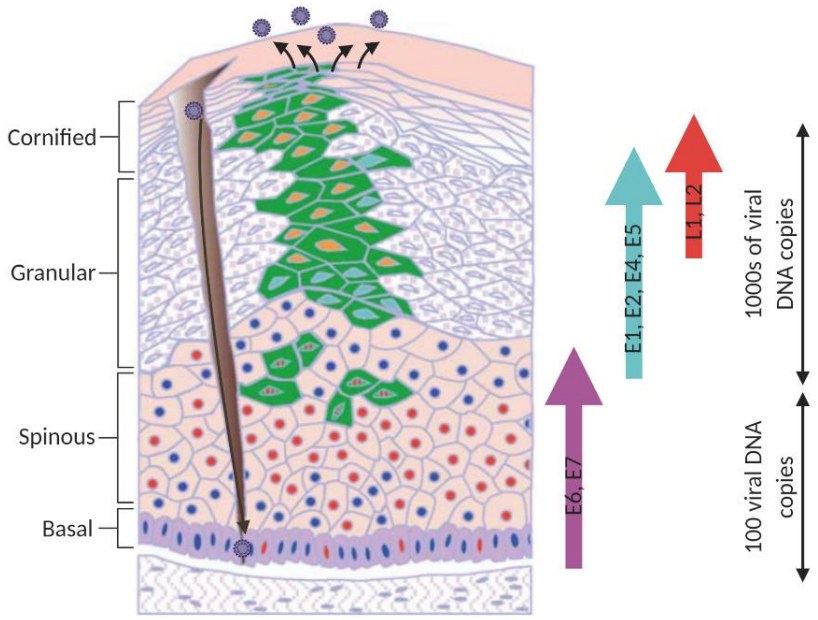

Figure 1.2: Life cycle organisation of HPV upon infection of basal keratinocytes. Diagrammatic representation of the skin (layers indicated on the left) to reveal the pattern of HPV gene expression and viral DNA copy number (indicated on the right), upon HPV infection resulting from an abrasion that exposes the basal epithelial layer. Figure adapted from (43).

1.1.3 Immune evasion strategies of HPV

HPV employs several mechanisms to effectively evade the innate immune responses. As stated previously, the infectious life cycle of HPV is closely linked to the differentiation of the host keratinocyte (20, 25). There is no cytolysis as a result of low viral replication throughout most of the viral life cycle, where viral release only occurs after the basal keratinocyte has migrated to the outer epithelial layers and has fully differentiated. Viral particles are therefore only released where immune surveillance is minimal, thus making antigen presenting cells (APCs) ineffective (25).

Under normal conditions, keratinocytes can either constitutively or be induced to secrete a range of pro-inflammatory cytokines, including interleukin (IL)-1, -6, -10, and -8. IL-1 in particularly plays a vital role in activation of APCs such as Langerhans cells (LCs) and macrophages, which in turn present antigens to T-helper cells (25, 44). As low levels of viral protein are produced at the early stages of the viral life cycle, as well as the fact that there is no cytolysis as a consequence of viral

replication, little to no pro-inflammatory cytokines are released by infected keratinocytes. As a result, no immune response is elicited as the APCs - dendritic cells (DCs) and macrophages - are ineffective in non-inflammatory environments (25). Throughout its life cycle, HPV remains within the epithelium and does not have a viraemic or blood-borne phase, resulting in minimal exposure to host immune defences (25). Evidence has shown that HPV, from the start of the infectious cycle, dampens keratinocyte cytokine responses (25).

Like many other DNA viruses, HPV has evolved mechanisms for inhibiting the synthesis and release of the cytokine molecules named interferons (IFNs). Type I IFN-α has antiviral and immunostimulatory properties, and infection with high-risk HPVs downregulates its expression (25). As mentioned previously, HPV E6 and E7 have been implicated in immune evasion. Both oncoproteins suppress the type I IFN response by directly interacting with the components of the IFN signalling cascades (25, 45, 46). For example, E7 binds to and inactivates the interferon regulatory factor (IRF)-1, an IFN-β promoter binding transcription factor and an established tumour suppressor protein (45). E6 has been shown to bind to IRF-3 and this interaction is proposed to inhibit IRF-3 transcriptional activity, thus providing the virus with a way to evade the immune response of infected cells (47). HPV E5 causes retention of major histocompatibility (MHC) class I complexes (HLAs) in the Golgi apparatus and prevents their transport to the cell surface (18). Furthermore, E5 downregulates the surface expression of HLA-A and HLA-B molecules which present viral peptides to cytotoxic T lymphocytes (18).

Despite these innate and early adaptive immune evasion strategies, HPV infection is cleared in most cases after several months by cell-mediated immunity, driven by a Th1-based immune response (18, 48). LCs take up viral antigens (made up of viral particles or proteins) from infected and dead keratinocytes (48). Subsequent activation of these LCs results in presentation of the antigen to naïve T-cells that become activated effector T-cells, capable of migrating to infected keratinocytes and destroying them (48).

However, in 10 % of all cases, HPV infection is persistent, which greatly enhances the risk of progression to malignancy. As discussed previously, several co-factors contribute to this process. The major co-factor affecting South Africa is co-infection with the highly prevalent HIV. Both these viruses share the same route of transmission, and HIV infection has been shown to promote

HPV infection in women at both the molecular and cellular levels, such as HPV entry into keratinocytes, establishment of persistent HPV infection, and immune evasion (49). HIV-1 infection and low CD4 count have been shown to be significantly associated with increased risk of HPV infection and HPV-related disease progression. Immune response to HPV infection is modulated by $CD4^+$ T cell-dominated Th1 response, therefore in HIV positive individuals who have low CD4 cell counts, HPV immune responses are dampened even further (14). As a result of increased risk of persistent HPV infection in HIV positive women, the risk of cancer development in HIV positive women increases. Indeed, HIV-infected women present with cervical cancer 15 years earlier than HIV negative women (14). Usually, the administration of anti-retroviral therapy decreases the risk of AIDS-defining cancers (such as Kaposi's sarcoma and non-Hodgkin's lymphoma), but this is not the case for HPV-associated cancers (14).

1.1.4 HPV prophylaxis and challenges

To date, there is no treatment or cure for HPV infection. However, three highly efficacious prophylactic vaccines exist against the most common and high-risk HPV types. Gardasil® (Merck) was released in 2006, which provides protection against the high-risk HPV types 16 and 18, as well as HPV types 6 and 11, the latter being low-risk types which have been implicated in 90% of genital warts cases (50). Cervarix™ (GlaxoSmithKline) became available in 2007 to the public and prevents against the two major high-risk HPV types 16 and 18 (51). Merck later released an updated version of their vaccine in 2014, named Gardasil 9, which immunises against HPV types 6, 11, 16, 18, 31, 33, 45, 52, and 58 (52).

All of the above-mentioned vaccines are composed of virus-like particles (VLPs) derived from the spontaneous assembly of individual type-specific L1 capsid proteins (50–53). For this reason, the vaccines have little to no cross protection against other HPV types not included in the vaccine as the immune response is highly type-specific. Furthermore, these vaccines do not provide treatment for individuals who are already infected with HPV. The South African Department of Health (DOH) began a vaccination program and rolled out Cervarix™ to school girls (Grade 4, approximately 9 years of age) in 2014 (8). However, the vaccine programme, along with cervical

cytology screenings provided for women by the state, have not been sufficient to overcome the high HPV infection/cervical cancer rate in South Africa, due to financial and cultural strains (54). Many young girls are thought to have missed the opportunity to be immunised through the DOH vaccination programme as a result of absenteeism and limited access to school health teams (55). The need for a cold chain (controlled storage at low temperatures) has been difficult to maintain in South Africa and other LMIC countries with substandard infrastructure and low funding, which would more than likely make administration of vaccines to school girls in rural areas even more challenging (54).

As the DOH program in South Africa is limited to young girls in the fourth grade of state schools, a large portion of young girls will not have had the opportunity to receive the vaccine through this programme. The likelihood of adolescent women being immunised outside of the school-based programme is low as an adolescent health platform does not exist (54, 55). This means that little emphasis is put on increasing the knowledge and awareness around the need for vaccination to prevent HPV and cervical cancer in adolescent women. Many of those who are aware of the vaccine are challenged with the high cost of the vaccines (55).

Another challenge faced by current HPV prevention by means of vaccination is the stigma and lack of knowledge surrounding cervical cancer, HPV and HPV vaccination, as well as reproductive health in general. A recent study was done on the understanding of cervical cancer, HPV and prevention among female students at a university in South Africa. It revealed that a large proportion of young women had limited knowledge of cervical cancer, HPV and vaccine availability (56). Some of the public have even raised concerns about the access to the HPV vaccines being an accelerator for girls' sexual debuts, as well as a reason for young women to engage in increased sexual activity with a greater number of sexual partners. However, a study done in a cohort of college women in the US showed that there was no correlation between women receiving the vaccine and increased sexual activity at earlier ages (57). In many societies, especially in LMIC communities such as South Africa, pre-marital sexual activity is heavily frowned upon, which greatly decreases the likelihood of women seeking reproductive health care in medical facilities within their communities (58). All the above challenges greatly emphasise the need to increase awareness in young women.

Along with public education on HPV infection and prevention, alternative means of protection against HPV are needed which are broad-spectrum, more cost-effective and are easily accepted by the public. A clear example of this is the naturally derived sulphated polysaccharide carrageenan, which has been shown to inhibit early HPV infection by blocking viral attachment to cells (29, 59). Carrageenan has been formulated into the product Carraguard, a genital lubricant, where clinical trials have shown its use to be negatively associated with HPV infection, as well as with HSV-2 (60, 61). It did not, however, show any indications of prevention against vaginal transmission of HIV (62).

There are several alternative approaches that could be investigated for the prevention of HPV and other sexually transmitted infections. One of which could be activation of the innate immune response to make HPV more "visible" to the innate immune system, thereby preventing epithelial cell infection, perhaps by designing drugs based on the molecular structure of innate opsonins (see section 1.2). Another approach would be to use molecules that bind to HPV, or the host cell-surface molecules the virus uses for attachment and subsequent infection, in order to inhibit the virus/host interaction at the early steps of infection (see section 1.3).

1.2 Enhancing immune recognition of HPV with surfactant proteins

Surfactant proteins have been historically identified and described in the lung where they are part of the pulmonary surfactant, which is composed of a complex of phospholipids and proteins (63). Pulmonary surfactant is primarily responsible for reducing the surface tension at the air-liquid interface of the lung (64). The four surfactant proteins (SPs) A, B, C, and D, make up 7% of the lung surfactant, with surfactant protein A (SP-A) making up the largest portion of this percentage (5.3%) (65). While SP-B and SP-C have vital roles in phospholipid packaging and reducing lung surface tension, SP-A and SP-D have been implicated in the innate immune response and have been shown to be opsonins of a variety of respiratory pathogens (66–68). As previous work from our laboratory indicated a novel role of SP-A for immune recognition of HPV, the focus of this study was limited to this protein (see section 1.2.4) (66).

1.2.1 Structure of SP-A

SP-A (and SP-D) are large hydrophilic proteins belonging to the collectins family. This family of proteins are soluble, collagenous C-type lectin pattern recognition receptors that tend to be calcium dependent (63). Their primary structure consists of an N-terminal non-collagenous domain capable of forming inter-subunit disulphide bonds, a collagenous region of Gly-X-Y repeats, a helical neck domain, and a globular C-terminal carbohydrate recognition domain (CRD) (63). Monomeric units spontaneously self-assemble into trimers and then form higher order SP-A octadecamers (Figure 1.3) (69). SP-A preferentially binds to mannose, fucose and lipid ligands on the surface of incoming pathogens (70). SP-A has a very weak affinity to galactose and sialic acid which is important for distinguishing self from non-self, as these sugars usually form the terminals of carbohydrates on eukaryotic cells (70). SP-A (and SP-D) recognition and binding of their specific ligands usually takes place via their CRDs and elicits a variety of immune responses, including opsonisation and enhanced phagocytosis, regulating macrophage function and inflammation, and killing (70).

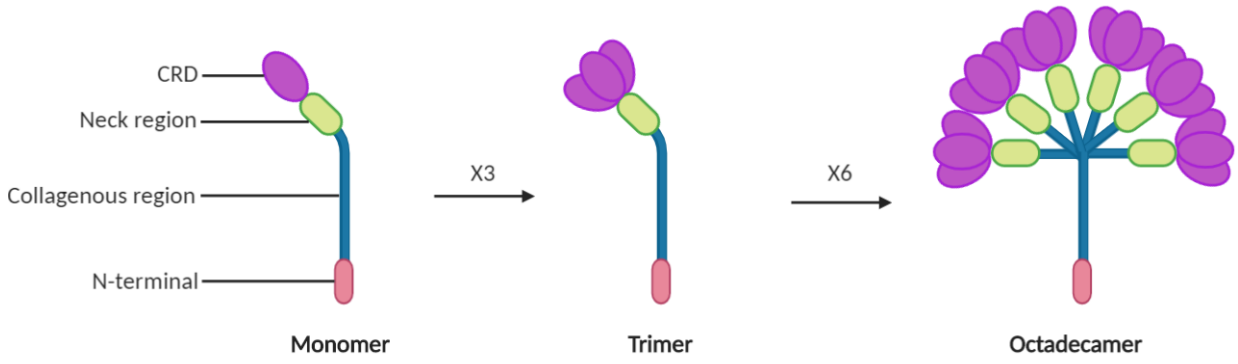

Figure 1.3: Structure and assembly of SP-A. Monomers of SP-A are composed of a carbohydrate recognition domain (CRD), neck region, collagenous region and N-terminal region. These form trimers which then multimerise to form octadecamers. Figure adapted from (66).

1.2.2 Interactions of SP-A with pathogens in the lung

SP-A has been shown to have both pathogen recognition functions as well as a role in maintaining lung homeostasis. SP-A is able to recognise and bind pathogen associated molecular patterns (PAMPs) on the surface of bacteria. These usually comprise of clustered oligosaccharides (as described in section 1.2.1). In most instances, the recognition of bacterial PAMPs results in clearance of the infection. Studies have shown that SP-A mediates macrophage phagocytosis and neutrophil uptake of a number of bacteria, including of *Escherichia coli (E. coli)*, *Streptococcus pneumoniae (S. pneumoniae)*, *Staphylococcus aureus (S. aureus),* and *Hemophilus influenza (H. influenza)* (71). SP-A has also been shown to mediate *Mycobacterium tuberculosis* (*M. tb*) phagocytosis by alveolar macrophages, by binding to macrophage mannose receptors (67). Macrophages, however, serve as the major host cell niche for the growth and survival of *M. tb*, and so these results suggest SP-A assists *M. tb* growth and survival (72). SP-A has also been shown to play an important role in the pathogenesis of mucoid *Pseudomonas aeruginosa* (*P. aeruginosa*) infection in the lung *in vivo*, also by enhancing macrophage phagocytosis (73).

SP-A has also been implicated in early innate immune responses to a variety of viral infections. Influenza A virus (IAV), a common respiratory tract infection, has been demonstrated to be controlled by SP-A. IAV clearance by SP-A is initiated by recognition of IAV glycoproteins haemaglutinin and neuramidase by the CRD of SP-A. This interaction leads to aggregation of the IAV particles, followed by enhanced neutrophil binding to the virus, resulting in clearance of IAV from the lung (74). SP-A has also been shown to have neutralising capabilities against respiratory syncytial virus (RSV) by binding to the F glycoprotein of RSV and blocking viral entry (68). It also recognises HSV-1 which generally infects the mucosal layer of the mouth, but can also cause infections in the respiratory tract (75). SP-A recognition of HSV-1 enhances viral uptake by alveolar macrophages.

In addition to the recognition of viral and bacterial infection, SPs also play a role in the regulation of fungal infection and allergens, such as pollen grains from a variety of plants (69).

1.2.3 Presence of SP-A in the female reproductive tract

While SP-A has been historically identified in the lung where it plays an important role as an innate immune molecule protecting against pulmonary infections of a variety of pathogens (as outlined above), SP-A has recently been shown to express at various non-pulmonary sites (63). In the human female reproductive tract (FRT,) SP-A (and SP-D) has been detected in the myometrium, vaginal epithelium and vaginal lavage fluid (76, 77). It has been suggested that SPs play protective roles during pregnancy as well as contribute to innate defences against sexually transmitted pathogens (78, 79). It has recently been reported that supplementation with SP-A resulted in decreased uropathogenic *E. coli* growth in the urinary tracts of mice (80).

SP-A (and SP-D) has been shown to interact with HIV via oligosaccharides on the HIV envelope protein gp120 *in vitro* (78, 81). SP-A binding to HIV inhibits its infectivity of CD4 T-cells, perhaps by blocking the CD4 binding site of gp120 (78). However, SP-A plays a dual role in HIV infection as SP-A was shown to enhance HIV uptake by DCs *in vitro*, where DCs transfer the virus to CD4 cells, although no *in vivo* studies have validated this (81).

1.2.4 SP-A enhances innate immune recognition of HPV16-PsVs

In an attempt to identify novel molecules that enhance immune recognition of oncogenic HPV, our laboratory has demonstrated for the first time that SP-A binds directly to HPV16-PsVs (Figure 1.4A), and that this binding was calcium dependent and independent of the lectin-binding domain (Ujma MSc thesis, 66). It was also shown that SP-D had little to no binding to HPV16-PsVs (Ujma MSc thesis, 66). To test whether this physical interaction between SP-A and HPV16-PsVs had any functional consequences on immune cell recognition, virus internalisation assays using the murine macrophage cell line RAW264.7 were performed. Pre-incubation of HPV16-PsVs with purified SP-A at a 1:10 (w/w) ratio prior to infection of RAW264.7 macrophages resulted in increased viral particle uptake (Figure 1.4B) (Ujma MSc thesis, 66). Infection assays revealed increased viral pseudogenome expression by RAW264.7 macrophages when HPV16-PsVs was pre-coated with SP-A (Figure 1.4C, (66)). Although overall infectivity of RAW264.7 macrophages compared to the human cervical cancer cell line HeLa cells was extremely low (Figure 1.4C), pre-

incubation of HPV16-PsVs with SP-A had no effect on HeLa cell infection (Ujma MSc thesis, 66). To date, macrophages have not been shown to be infected by HPV, which explains the low levels of infection in RAW264.7 cells. It was therefore hypothesised that macrophages may prevent infection by effectively killing most of the internalised virus, and this was facilitated by exogenous addition of SP-A (Ujma MSc thesis, 66).

Although the *in vitro* findings above elucidated a role of SP-A in enhancing immune recognition of incoming HPV16-PsVs, the HPV infection environment in the FRT is more intricate since a number of different cell types could be involved upon infection with HPV. For this reason a murine cervicovaginal challenge study model was used to elucidate the impact of SP-A on HPV16-PsVs infection in a biologically relevant setting (29). Interestingly, SP-A was not detected in the murine FRT, neither in naïve C57BL/6 mice (Figure 1.4D) nor in HPV challenged mice (data not shown, Ujma MSc thesis (66). This was surprising as SP-A is known to be expressed in the FRT in humans (63). Furthermore, a preliminary mouse infection study indicated a reduction in HPV16-PsVs infection for SP-A pre-incubated pseudovirions (Ujma MSc thesis 66). The data described above suggest a protective role of SP-A for HPV infection, and thus formed the basis for further studies on the effect of SP-A supplementation on HPV16-PsVs infection. These preliminary results, along with the results in this thesis, have recently been published in the journal Pathogens (82).

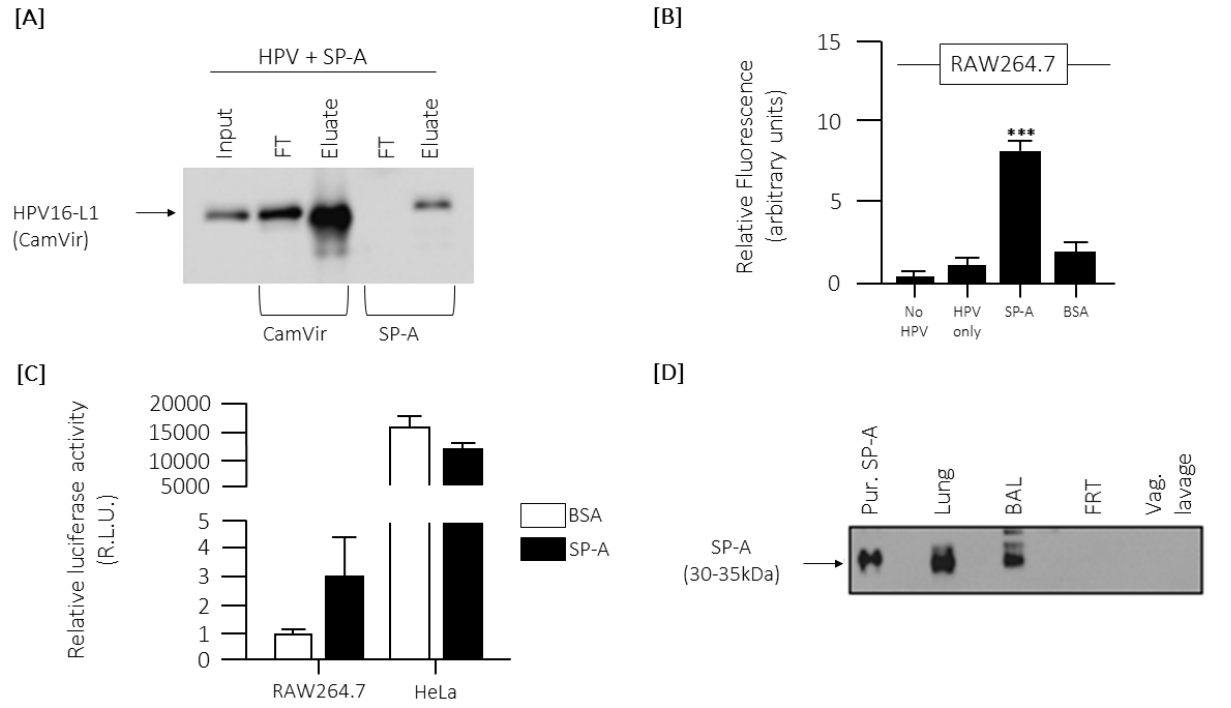

Figure 1.4: Binding of HPV16-PsVs to SP-A results in increased viral uptake by RAW264.7 macrophages but not by HeLa cervical epithelial cells. [A] Co-immunoprecipitation experiments displaying the input, flow through (FT) and eluate samples of HPV16-PsVs incubated with SP-A. Complexes were incubated for 1 hour at 4°C, followed by precipitations with anti-HPV16-L1 (CamVir) or anti-SP-A antibodies. Western Blots were performed using the CamVir antibody to detect the presence of HPV16-L1**. [B]** RAW264.7 cells were infected with fluorescently labelled HPV16-PsVs (pre-absorbed with SP-A or BSA control where indicated) for 1 hour at 37°C. Cells were washed extensively and lifted with trypsin/EDTA to remove surface-bound virions and subjected to flow cytometry to quantify viral internalisation. Experiments were performed in triplicate, quantified by quadrant analysis of the dot blots of three independent experiments and presented as x-fold increase relative to the mean fluorescence intensity of cells infected with untreated HPV16-PsVs which was set as 1. Significances were calculated by means of one-way ANOVA and Tukey post-hoc tests. *** indicates statistical significance between uptake of HPV16-PsVs in the presence of SP-A as compared to the other tested conditions (*** = $p<0.001$). **[C]** RAW264.7 and HeLa were infected with HPV16-PsVs encapsidating the firefly luciferase reporter plasmid pGL3-control for 48 hours. Where indicated, the viral particles were pre-absorbed with purified SP-A protein (or BSA control) before infection. Firefly luciferase activity in the cell lysates as a measure for successful infection is presented as Relative Light Units relative to RAW264.7 cells infected with untreated HPV16-PsVs which was set as 1. Bars in [B] and [C] depict mean values, with error bars showing SEM. **[D]** Western Blot assessing SP-A expression in lung, bronchoalveolar lavage fluid (BAL), female reproductive tract (FRT) tissue, and vaginal lavage (vag. lavage) fluid of naïve wildtype C57BL/6 mice. 20µg of each sample was loaded per lane, while 0.5µg of purified human SP-A protein was loaded as control. Figure adapted from (66).

1.3 Modulation of the interaction between HPV and host cell surface molecules by vimentin

1.3.1 The intermediate filament vimentin

The cytoskeleton of mammalian cells provides structural integrity and support to their largely aqueous and susceptible internal constituents. Three major cytoskeletal networks run through vertebrate cells, namely actin/micro- filaments (MF), microtubules (MT) and intermediate filaments (IF). Intermediate filaments have been termed due to their diameter (10nm) being between that of actin microfilaments (7-10nm) and microtubules (24nm) in metazoan cells (83, 84).

IFs, the least structurally characterised of the three filament systems, are expressed by a large family of at least 65 genes that produce minor variations of a homologously conserved polymer structure, suggesting its vital role in cellular physiology (85–87). They are divided into 5 types (I to V), based on the properties of their amino acid sequences. Of those, vimentin is the major constituent of all the type III IFs which additionally include desmin, glial fibrillary acidic protein, and peripherin (84). Vimentin is present in cultured fibroblasts, endothelial cells, lymphocytes, and epithelial cells, which are cells with a mesenchymal heritage (88–90). Importantly, vimentin is the sole IF that exists in almost all sarcomas, meningiomas, schwannomas, and melanomas, giving evidence to its crucial role in cancer cell biology and making it a promising cancer diagnostic marker (90).

1.3.2 Cellular functions of vimentin

It has taken some time for researchers to understand the importance of this intermediate filament protein, mainly because vimentin knockout mice expressed a very mild phenotype and initially appeared healthy (91). Further studies revealed vimentin's role in a variety of cellular functions ranging from integrating into the entire cytoskeleton, responding to mechanical stress, cellular adhesion, to signalling (92, 93). It appears that vimentin is able to help the cell respond to stress in a variety of forms, including heat, infection, and toxins (94, 95). The highly complex and regulated phosphorylation of vimentin appears to control some of these diverse functions (96).

As a characteristic protein of cells of mesenchymal origin, the expression of vimentin correspondingly increases in cells transitioning from an epithelial to mesenchymal state (EMT). EMT is associated with increased motility and is important during development, wound healing and during cancer invasion and metastasis (97). Vimentin has also been shown to play a crucial role in transcellular migration of lymphocytes across endothelial cells (98). Mice lacking vimentin displayed lymphocytes with retarded homing and ability to adhere and cross the endothelium (98). In addition, vimentin has been shown to be a central player in the programmed cell death process of apoptosis, as cleavage of intracellular vimentin leads the way into cellular breakdown (99).

1.3.3 Structure of vimentin

The structural organisation of a vimentin monomer is composed of a central α-helical rod domain, flanked by an intrinsically disordered N-terminal ("head") and a C-terminal ("tail") domain (74, 75). The monomers are fairly stable in denaturing conditions, and spontaneously assemble into coiled-coil dimers, followed by assembly of two of these dimers into antiparallel tetramers (Figure 1.5) (101). It has been shown *in vitro* that the assembly of the vimentin tetramers into full-length filaments is instigated by the addition of monovalent salts, such as potassium chloride (KCl) and sodium chloride (NaCl) (101, 102). Typically, eight of these tetramers further associate laterally to form what is called a unit length filament (ULF). ULFs can associate end to end to form longer filaments, however, it is not precisely known what the exact mechanism of this elongation reaction is (101).

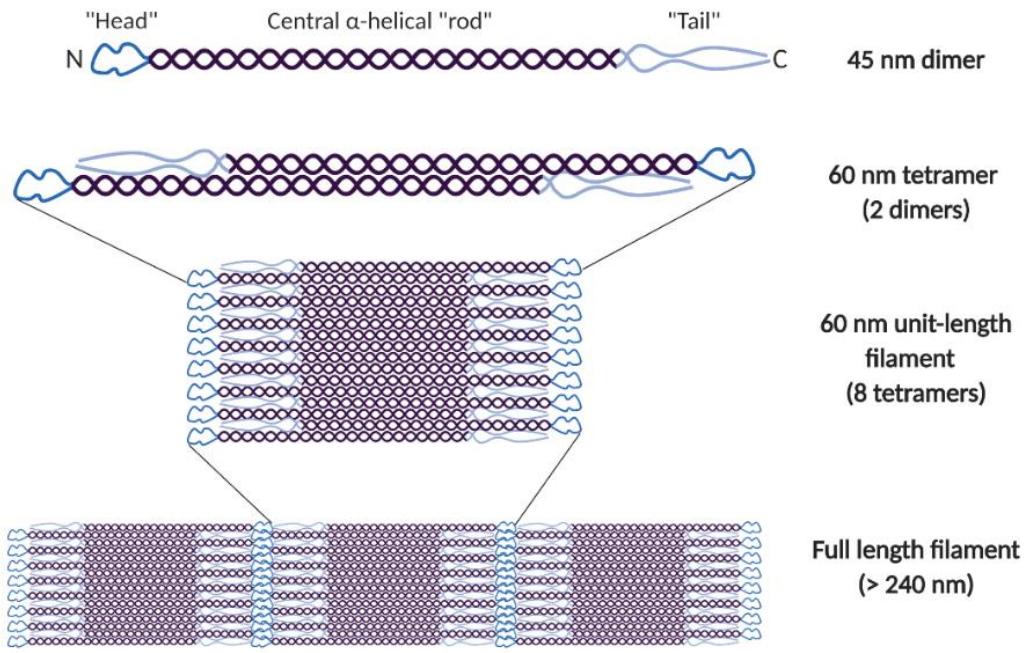

Figure 1.5: Structure of vimentin filaments. The vimentin monomer, consisting of an elongated rod domain flanked by a "head" N-terminal domain and "tail" C-terminal domain, spontaneously form dimers. Two dimers associate laterally to form an offset tetramer. Eight tetramers associate to form a unit length filament (ULF). Figure adapted from (103).

1.3.4 Interactions of surface-expressed and secreted vimentin with pathogens

Although best described as a cytosolic protein involved in cellular processes such as cell adhesion and cell migration, vimentin has been identified on the surface as well as in the extracellular spaces of cells of various origins (104–107). However, the biological role of cell surface and secreted vimentin is only beginning to be elucidated. Levels of surface expression have been shown to be altered during the cell cycle, and differ among cell lines (108). In addition, cell surface vimentin functions as an endogenous, activating ligand for Dectin-1, a non-toll like pattern recognition receptor, present on inflammatory cells (109). Here, it has been linked to the inflammation of the arterial wall and oxygen production, suggesting that by activating Dectin-1 it contributes to the oxidation of lipids and cholesterol accumulation in atherosclerosis (109). Promisingly, cell surface vimentin has the potential to be exploited as a marker for detecting mesenchymal circulating tumour cells (CTCs) derived from patients with sarcomas (110).

In addition to vimentin's diverse roles described above, vimentin has also been observed to be affected by, or play a role in infection of, a variety of pathogens. It has been shown that vimentin is secreted by macrophages in response to pro-inflammatory cytokines produced as a response to *E. coli* infection, where the secreted vimentin interacts with *E. coli* and favours bacterial killing (106). In contrast, several bacterial pathogens have been shown to utilise vimentin for successful infection. *Anaplasma phagocytophilum* (*A. phagocytophilum*) infection induces re-organisation of the vimentin filament network and this is necessary for infection (111). *C. trachomatis* replicates within a membrane-bound vacuole termed an ''inclusion'' (112). Vimentin and other intermediate filaments are also reorganised upon *C. trachomatis* infection, where this has been shown to be necessary for maintaining the structural integrity of the inclusion, and was hypothesised to also hinder the exposure of *C. trachomatis* to the innate immune system (112).

Many viruses have been described to utilise the vimentin protein network for cell surface attachment and entry, which is often accompanied by drastic changes in intermediate filament arrangement. Cowpea mosaic virus (CPMV) is one such virus that utilises cell surface vimentin to attach to its host cells. CPMV is a plant *Comovirus* and a member of the Picornavirus superfamily (113). Vimentin was shown to bind to CPMV, and knocking down vimentin resulted in reduced infection by CPMV (113).

Japanese encephalitis virus (JEV), a mosquito born *Flavivirus*, was found to interact with vimentin (114). The role of vimentin as a receptor for viral entry was then validated when an antibody against vimentin resulted in inhibition of cellular entry of JEV into porcine kidney cells, possibly by disrupting the binding of the JEV envelope protein to vimentin (115). This interaction was not observed in other cell lines tested (114). Furthermore, it was found that JEV infection was attenuated upon vimentin knockdown (115). These studies infer a crucial role for vimentin in entry of JEV into certain mammalian cells.

The entry of the ubiquitous Human Cytomegalovirus (CMV) into fibroblasts is also affected by a lack of vimentin (116). CMV is a herpesvirus that can cause grave complications when present in immunocompromised individuals. Studies in human fibroblasts showed that disarrangement of the vimentin network via either acrylamide, or in vimentin$^{-/-}$ mice resulted in severely reduced

cellular entry with two disparate strains of CMV, one with a restricted and another with a wide cell tropism (116).

Enterovirus 71 (EV71) is a highly transmissible single-stranded RNA virus that belongs to the human enterovirus species A of the genus *Enterovirus* within the Picornaviridae family (117). Infection with EV71 results in extreme central nervous system malfunction in infected infants and small children (117). It was shown that the N-terminus portion of vimentin filaments is involved in binding to EV71 on the host cell surface, and blocking vimentin using either soluble vimentin, or antibodies resulted in reduced binding of EV71 to the cell surface (117).

A novel C*oronavirus* was implicated as the etiological agent of severe acute respiratory syndrome (SARS), a life threatening respiratory illness, and therefore named SARS-CoV (118). SARS-CoV has been detected in the lung, bronchi, trachea, and surprisingly in non-respiratory tissues as well (119). SARS-CoV binds to the angiotensin-converting enzyme 2 (ACE2), the type I integral transmembrane protein, for cellular entry (120). ACE2, however, is not adequate enough for maintaining viral infection. Vimentin was shown to be a cellular factor that is copiously present in the SARS-CoV spike protein-ACE2 complexes (121). Vimentin was shown to directly bind to the SARS-CoV spike protein in kidney epithelial cells and has been shown to play an essential role in the cellular entry of SARS-CoV (121).

1.3.5 Interactions of HPV and vimentin

A study done by Schäfer *et al* aimed to discover novel host surface molecules that interact with high-risk HPV16 with the aim to modulate infection (36). Biochemical pull-down experiments showed that surface-expressed vimentin interacted with HPV16-PsVs, regardless of whether the pseudovirions underwent furin cleavage, a step shown to be necessary for successful infection (Figure 1.6A) (36, 37, 40). Unlike most viruses that use vimentin to aid in internalisation, this study demonstrated that both surface-expressed and recombinant human vimentin (rhVim) functioned as an inhibitory molecule for HPV16-PsVs entry. When HeLa, HaCaT and NIKS cells[1] were

[1] All cell lines representing physiologically relevant cell culture models, where NIKS in particular have been found to support the complete HPV life cycle (36).

challenged with HPV16-PsVs that were pre-incubated with rhVim prior to infection, infectious internalisation was significantly lower when compared to the BSA control across all cell lines (Figure 1.6B) (36). Knockdown of surface vimentin of NIKS cells led to an increase in HPV16-PsVs infection, which was more pronounced when HPV16-PsVs underwent furin treatment (36). Conversely, transient overexpression of surface vimentin significantly decreased HPV16-PsVs binding, uptake, and infection of NIKS cells, which was independent of furin treatment (36).

Schäfer *et al* hypothesised that both cell surface or soluble vimentin bind to viral particles and modulates the early steps of HPV infection (i.e. cell surface binding and cellular entry) either by masking portions of the virus necessary for interactions with cell surface molecules/receptors, or by causing steric hindrance which would destabilise, or prevent host-virus interactions necessary for infectious internalisation (36). Further characterisation of the mechanisms by which artificial supplementation with rhVim modulates HPV16-PsVs infection may enable the development of novel inhibitors to HPV infection.

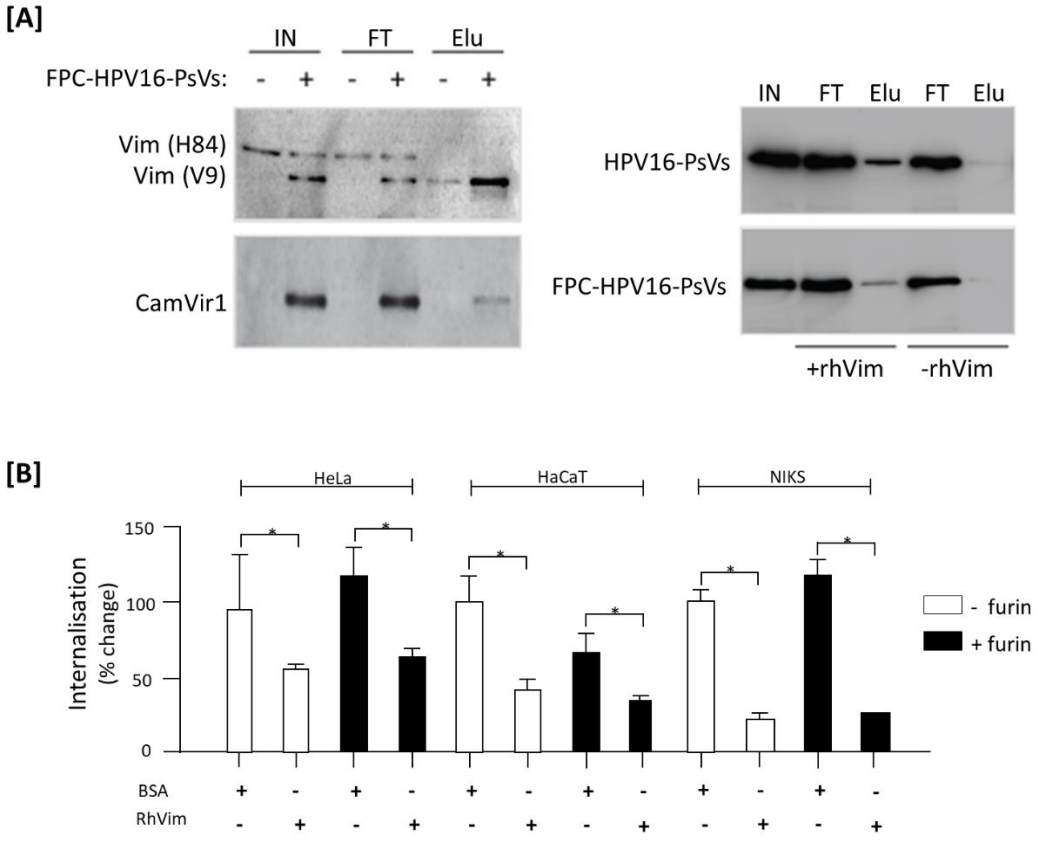

Figure 1.6: Identification of cell surface and recombinant human vimentin (rhVim) as binding proteins for HPV16-PsVs, modulating HPV16-PsVs infection *in vitro* (36)**. [A]** Western Blot (left gel) of a pull-down experiment (pgsD677[2] surface proteins bound to furin pre-cleaved (FPC)-HPV16-PsVs pulled-down by the HPV16-L1 specific antibody CamVir1), probed simultaneously with the anti-vimentin antibodies H84 and V9 (upper panel) and re-probed with the antibody CamVir1 (lower panel). Note that in the presence of HPV16-PsVs the size of the vimentin protein is slightly reduced. IN, input; FT, flow-through; Elu, eluate. Pull-down of HPV16-PsVs (with or without furin pre-treatment) using immobilised rhVim (right gel). Proteins were detected by Western Blot using the antibody CamVir1. **[B]** AF488-conjugated HPV16-PsVs (with or without prior furin cleavage) were pre-treated with soluble rhVim or BSA before infection of HeLa, HaCaT and NIKS cells. Internalisation of viral particles was assessed by flow cytometry and presented as change in mean fluorescence intensities of AF488-positive cells compared to untreated particles which was set as 100%. Quadrant statistics of three independent experiments performed in triplicate were used to calculate the means ± S.D. with the Student's t test used for determination of statistical significance compared to controls (* = $p<0.05$). Figure adapted from (36).

[2] In order to biochemically pull-down surface molecules that interact with HPV16-PsVs, the HSPG-deficient pgsD677 cell line was used. This, along with furin pre-cleavage of the HPV16-PsVS, allowed for the bypassing of the initial extracellular HSPG-mediated attachment steps that result in viral uptake (36).

1.4 Hypotheses

Hypothesis 1: Purified human SP-A protein reduces HPV16-PsVs infection by enhancing immune recognition of the virions by recruitment of innate immune cells to the site of infection, resulting in immune cell uptake of viral particles.

Hypothesis 2: RhVim modulates HPV16-PsVs infection by interfering with the early (and crucial) steps of HPV infection, namely cell-surface binding and internalisation, by preventing receptor-virus binding necessary for successful infection.

1.5 Aims and Objectives

Aim 1: To further characterise the mechanisms elicited by purified SP-A in reducing HPV16-PsVs infection through enhancing immune recognition of HPV16-PsVs using an established *in vivo* mouse cervicovaginal challenge model.

This aim will be addressed by the following two objectives:

- To determine whether SP-A enhances recruitment of macrophages in HPV16-PsVs infected mouse FRT tissue.
- To set up an adaptation of the HPV16-PsVs cervicovaginal challenge model (29) in order to observe the effects of SP-A on the FRT innate immune cell populations[3] by flow cytometry of both HPV16-PsVs infected and uninfected tissue, as well as to establish any changes in viral uptake of these immune cells in the presence of SP-A.

[3] Macrophages, monocytes, eosinophils, and neutrophils.

Aim 2: To further characterise rhVim in its ability to modulate the early events of HPV cellular entry and infection, using both *in vitro* and *in vivo* approaches.

This aim will be addressed by the following two objectives:

- To determine whether the structure of rhVim (filamentous or globular) affects its ability to reduce HPV16-PsVs infection *in vitro* and *in vivo* using an established mouse cervicovaginal challenge model (29)
- To determine if rhVim has an effect on HPV16-PsVs surface binding and internalisation in the absence and presence of heparan sulphate proteoglycans (HSPGs) *in vitro.*

2 Materials and methods

2.1 General materials

Chemicals of analytical/reagent grade were used and generally purchased by Merck, or Sigma Aldrich, unless indicated otherwise. Solutions made up in the laboratory are detailed in the Appendix.

2.2 Cell culture

The human keratinocyte cell line NIKS (ATCC CRL-12191) was cultured in complete F-Medium (Appendix) and the virus packaging cell line HEK293TT (122, 123) as well as the human epithelial cervical adenocarcinoma cell line HeLa (ATCC® CCL-2™) were cultured in complete Dulbecco's Modified Eagle Medium (DMEM) (Appendix). Cell culture procedures were performed under sterile conditions to prevent the risk of contamination.

All cells were cultured in 75cm^2 cell culture flasks (SPL Life Sciences) and incubated in a humidified atmosphere containing 5% CO_2 at 37°C. Cells were passaged as follows:

The old media was removed from the cells followed by adding 5mL 0.025% trypsin/0.01% Ethylenediaminetetraacetic acid (EDTA) in phosphate buffered saline (PBS) for 5 to 15 minutes[4] at 37°C, to lift the cells from the flask. 5mL F-medium, or complete DMEM was then added to the respective cells in order to stop the trypsin/EDTA reaction. The cell suspensions were transferred to 15mL Falcon tubes (SPL Life Sciences), where the cells were pelleted by centrifugation (2800rpm for 2 minutes). The cell pellets were re-suspended in 10mL of their respective growth medium, where 2 to 3mL of the resuspended cells was transferred to a 75cm^2 cell culture flask, along with 10mL of sterile medium. Cells were passaged twice a week, to allow the cells to reach approximately 80% confluency.

Where precise numbers of viable cells were required before seeding, manual cell counting by means of a counting chamber and trypan blue staining were used. 10µL cell suspension was

[4] The HEK293TT and HeLa cell lines required approximately 5 minutes of trypsinisation before all the cells lifted from the flask, whereas NIKS cells required an extended period of 15 minutes before the cells completely lifted.

added to 90µL trypan blue (Appendix), which allows for the distinguishing of viable and dead cells as the blue dye enters the porous membrane of the dead cells. 10µL of this solution was placed on a Neubauer hemocytometer (Marienfeld) and covered with a glass coverslip. Bright unstained live cells were counted using a microscope (Nikon TMS) and cell concentration was determined using the following calculation:

$$\frac{cells}{ml} = \frac{x}{4^*} \times 10^{\text{֍}} \times 10^{3\oplus}$$

Where:
x: *number of cells counted*
*: *4 chambers of hemocytometer*
֍: *dilution factor*
⊕: *volume of cells below coverslip = 0.01ml*

The cell densities for each experimental procedure are described below.

2.3 Studying HPV infection using HPV16-PsVs

To study HPV16 infection *in vitro* and *in vivo*, non-oncogenic infectious HPV16 pseudovirions (HPV16-PsVs) were generated according to a procedure by Christopher Buck (122). These pseudovirions encapsidate a reporter plasmid representing the pseudogenome, which allows for the quantification of infection once the pseudovirions have successfully infected cells and reached the host cell nucleus. HPV16-PsVs particles containing the Gaussia luciferase (GLuc) reporter plasmid pCMV-GLuc 2 (New England Biolabs) were used to measure infection. Gaussia luciferase is an oxidative enzyme originally produced by the marine copepod *Gaussia princeps*, and contains an internal signal peptide for extracellular secretion (124). Because this protein is secreted from the cell cytoplasm, using HPV pseudoparticles encapsidating Gaussia luciferase can be beneficial for certain experiments, such as time course experiments, as luciferase activity can be measured directly from cell supernatants or from body fluids (such as vaginal lavages) without needing to lyse cells or sacrifice the animal (see section 2.7) (66).

Fluorescently labelled HPV16-PsVs particles (AF488-HPV16-PsVs) were also used to determine viral internalisation and cell surface binding by flow cytometry and microscopy. In these

experiments, Alexa Fluor 488 (AF488) was used to fluorescently label HPV16-PsVs (see section 2.3.2).

2.3.1 Production of HPV16-PsVs

To produce HPV16-PsVs, HEK293TT cells were plated on a total of 16 10cm dishes, and co-transfected with the pXULL plasmid (122) (which encodes codon-optimised HPV16 L1 and L2 capsid proteins) and the pCMV-GLuc 2 plasmid (the Gaussia luciferase reporter plasmid), using the calcium phosphate method described in previous studies (122, 125). 48 hours later, the cells were harvested by trypsinisation and pelleted by centrifugation (2000rpm for 2 minutes) in a 50mL Falcon tube. The cell pellet was resuspended in 1mL 1X PBS and transferred to a 1.5mL siliconised Eppendorf tube[5].

The cells were centrifuged again (3000rpm for 5 minutes), before being resuspended in a 1:1 (v:v) of PBS and 9.5mM $MgCl_2$. 1/20 Vol fresh 5% Brij58 was added in order to lyse the cells, and 1µL Benzonase and 1µL Exonuclease V (New England Biolabs) was added to digest any un-encapsidated DNA (66, 122).

The solution was incubated at 37°C for 24 hours, where the solution was occasionally mixed to allow for particle maturation. The lysate was then chilled on ice and 0.17 Vol PBS + 5M NaCl was added, followed by three freeze/thawing cycles at -80°C/25°C (66). The lysate was then centrifuged at 8000g for 10 minutes at 4°C to pellet any cell debris, followed by AF488 labelling (for confocal and flow cytometry analysis, section 2.3.2) and HPV16-PsVs purification (section 2.3.3).

2.3.2 HPV16-PsVs labelling with Alexa Fluor 488

HPV16-PsVs particles were fluorescently labelled with AF488 succinimidyl ester (Invitrogen) before CsCl (caesium chloride) gradient purification, as described in Bergant *et al.* (126). Before fluorescently labelling the viral particles (produced as described in 2.3.1.), the pH of the lysate

[5] The use of siliconised tubes is essential as the HPV16-PsVs absorb non-specifically to polypropylene (145).

was adjusted by adding 1/10 Vol 1M $NaHCO_3$, to a final pH of 8.8. 1/10 Vol AF488 (10mg/mL in DMSO) was then added to the cell lysate before incubating for 1 hour at room temperature with continuous rotation. Thereafter, the lysate was adjusted to pH 6.5 using 1/25 Vol 1M $NaPO_4$ (126).

2.3.3 HPV16-PsVs purification

CsCl ultracentrifugation was used to isolate the HPV16-PsVs from cell lysates (66). This was achieved by loading the lysate onto a discontinuous CsCl gradient. 4mL light CsCl (1.25g/mL in 1X HSB, see Appendix) was loaded to a 13.2mL Ultra-Clear™ centrifuge tube (Beckman Coulter), followed by carefully adding 4mL heavy CsCl (1.4g/mL in 1 X HSB) underneath the light CsCl layer (Appendix). The cell lysate was then made up to 3.5mL with 1 X HSB buffer and gently placed on top of the CsCl gradient. Tubes were centrifuged between 16 and 18 hours at 20 000rpm in a Beckman SW40Ti swinging bucket rotor. Viral particles were harvested from the gradient by inserting an 18-gauge needle attached to a 5mL syringe into the tube just below the interface. The sample, now containing the pseudovirions, was then transferred to an Amicon Ultra-4 Centrifugal filter unit (Millipore) and centrifuged at 3000rpm for 10 minutes, to concentrate the pseudovirions. The pseudovirions were then rinsed with 3mL HSB buffer and centrifuged at 3000rpm for 10 minutes, or until the sample was concentrated to approximately 100mL. The protein concentration of HPV16-PsVs preparations was then quantified using the Pierce™ BCA Protein Assay Kit (Thermo Scientific), according the manufacturer's instructions. HPV16-PsVs and AF488-HPV16-PsVs preparations were stored at -80°C in siliconised 1.5mL Eppendorf tubes.

2.3.4 Quality checks of HPV16-PsVs preparations

2.3.4.1 SDS-PAGE and silver staining

SDS-PAGE gels were used to determine the purity of HPV16-PsVs preparations. 3µL of each HPV16-PsVs preparation was loaded and electrophoresed according to conventional protocols (4,5). AF488-HPV16-PsVs preparations were visualised using a Biospectrum™ 500 Imaging System (Ultra Violet Products, UVP) to detect fluorescent bands at 55kDa and 75kDa, corresponding to

AF488 labelled L1 and L2 capsid proteins, respectively, with the L1 protein being at a 10-fold excess compared to L2 (122). Gels were then stained to visualise the L1 and L2 proteins (as well as any possible impurities) of the HPV16-PsVs using the Pierce™ Silver Stain Kit (Thermo Scientific), according to the manufacturer's instructions.

2.3.4.2 Luciferase infection assay

Luciferase assays were performed to determine the infectivity of HPV16-PsVs preparations, and for measuring infection *in vivo* under various experimental conditions (section 2.7.1). For quality control purposes, HeLa cells were seeded as described in Schäfer *et al* 2017 (36), where the following luciferase infection assays were performed:

• HPV16-PsVs only

• Positive control: HPV16-PsVs pre-incubated for 1 hour at 4°C with the HPV16 neutralising antibody H16.V5[6] . This was expected to abolish infection.

• HPV16-PsVs treated for 1 hour at 37°C with DNase I endonuclease (Thermo Scientific). This would cleave any plasmid that was not packaged in the viral capsid, so any measured luciferase was due to infection only.

To measure infection, 5µL cell supernatant (or vaginal lavage, see section 2.7.1) was added to a white 96-well plate (Nunc) and measured using a GloMax® Explorer Multimode Microplate Reader (Promega) following the Gaussia Luciferase Assay Kit (New England Biolabs) protocol. Per sample, freshly prepared GLuc Assay Solution consisting of 0.5µL BioLux GLuc Substrate added to 50µL BioLux Assay Buffer (New England Biolabs) was added per well and luminescence measured with 2 seconds lag time over 10 seconds integration time.

[6] Provided by Neil D. Christensen, Pennsylvania State University College of Medicine, USA

2.4 Negative staining transmission electron microscopy

Negative staining transmission electron microscopy (TEM) was employed to visualise viral particles as well as to determine the structure of recombinant human vimentin (rhVim) under various conditions. Samples of 0.08µg/µL rhVim and NaCl with concentrations ranging from 0mM to 100mM were pre-incubated for 1 hour before negative staining and viewed as described below. Samples of HPV16-PsVs were made to a final concentration of 0.08µg/µL as subsequent rhVim experiments used a 1:1 molecular ratio to the L1 protein of the HPV16-PsVs (see section 2.5 for details).

With the assistance of Dr Mohamed Jaffer from the UCT Electron Microscope Unit, samples were analysed as described in Varsani *et al* 2007 (128). 3µL of sample was absorbed onto a carbon-coated copper grid (Agar Scientific) and left for 30 seconds before blotting with filter paper. The carbon-coated copper grid had been glow-discharged using the Glow Discharge Unit (Agar Scientific) to render the carbon surface hydrophilic, allowing for the sample to adhere to the grid. The sample was then washed twice with a drop of deionised water, blotting with filter paper after each application, and subsequently stained with 2 drops of 2% aqueous uranyl acetate (SPI supplies), followed by blotting with filter paper. The grid was air-dried before being viewed with a Philips Tecnai F20 equipped with a field emission gun operating at 200kV. Images were taken with a Gatan US 4000 4kX4k CCD camera using the Digital Micrograph software suite.

2.5 Viral binding and internalisation assays

Various flow cytometry experiments were conducted to quantify viral internalisation and binding of NIKS cells. These involved using AF488-HPV16-PsVs, as AF488 emits fluorescence when excited by a 488 nm laser, allowing for detection of any bound or internalised virus. All conditions tested were performed in triplicate on NIKS cells, with three independent biological repeats for each experiment.

For virus binding and internalisation assays, NIKS cells were seeded in 12-well plates (Greiner Bio-One) at a density of $5x10^3$ cells per well and incubated overnight at 37°C. Before addition to cells, per well 0.35µg AF488-HPV16-PsVs were incubated with 0.35µg purified rhVim or BSA (i.e. 1:1

(w/w)[7], unless stated otherwise) for 1 hour at room temperature. Where indicated, pseudovirus/protein incubations occurred in the presence of varying concentrations of NaCl (0-100mM) and/or in the presence 3% carboxymethyl cellulose (CMC).

Moreover, to determine the effect of HSPGs on virion internalisation, NIKS cells were treated with heparinase I (Sigma, derived from *Flavobacterium heparinum*) before binding and internalisation assays were performed. Briefly, NIKS cells were treated, rinsed and covered with KCl isotonic buffer (Appendix) before adding 5U of heparinase I per well for 1 hour at 37°C (32). Cells were washed three times with 1X PBS before adding fresh F-media and the pre-incubated virions. Successful removal of HSPGs was determined by confocal microscopy (see section 2.6).

Cells were infected with pre-incubated AF488-HPV16-PsVs for 30 minutes at 37°C in order to achieve internalisation of the pseudovirions, or for 1 hour at 4°C to achieve pseudovirus cell-surface binding. Following infection, medium was aspirated from each well and cells were washed 3 times with 1X PBS. With regards to internalisation assays, cells were harvested by incubating cells with 300µL trypsin/EDTA for 15 minutes at 37°C, which removed any cell-surface bound virus and therefore allowed for quantification of internalisation only (36). For binding assays, cells were harvested by incubating with 300µL lidocaine/EDTA for 15 minutes at 37°C, which does not remove any cell-surface bound AF488-HPV16-PsVs, allowing for quantification of cell-surface binding (36).

Once all the cells had been lifted, 400µL F-medium was then added to each well to neutralise the trypsin or lidocaine reactions. Cell suspensions were transferred to 1.5mL Eppendorf tubes and centrifuged at 700g for 2 minutes at 4°C. The supernatant was removed, and each cell pellet resuspended in 500µL FACS wash (Appendix). Cells were centrifuged at 700g for 2 minutes at 4°C and the supernatant removed. Cells were fixed by resuspending the cell pellets in 100-300µL FACS fix (Appendix) and samples were subjected to a short spin in a microcentrifuge before being

[7] A 1:1 (w/w) for rhVim and HPV16-PsVs is equivalent to a 1:1 (mol/mol) for rhVim and the L1 capsid protein:
1 ng rhVim (54.3 kDa) = $1.1x10^{10}$ rhVim molecules.
1 ng L1-only HPV particles (20 000 kDa) = $30x10^{6}$ HPV virions. Assuming each particle contains 72x5 L1 molecules (145), the number of molecules in 1 ng of HPV L1-only particles is $1.08x10^{10}$.
Therefore, when using vimentin and HPV particles at a 1:1 (w/w) ratio the molar ration between 1 molecule vimentin and 1 molecule L1 is approximately also 1:1.
BSA (66.5 kDa) = $9.1x10^{9}$ (comparable to vimentin, therefore BSA was also used at 1:1 (w:w) BSA:HPV16-PsVs.

transferred to 5mL polystyrene round-bottom tubes (Falcon) and kept in the dark at 4°C until analysis to prevent fading of the AF488 fluorescence.

Data were acquired using a BD FACSCalibur™ together with the BD CellQuest™ Pro software (Version 5.2.1, BD Biosciences), and at a later stage with a BD LSRFortessa™ together with BD FACSDiva™ software. Acquisition parameters were determined using uninfected cells (negative control). The cell population was gated using the dot plot showing forward scatter (FSC) versus side scatter (SSC) of the negative control using the BD FlowJo™ software. Gating was performed to exclude any contaminants and cell debris. Dot plots of fluorescence in the FL1 channel (AF488 positive cells) versus SSC were generated in BD FlowJo™ and quadrant statistics determined (see Supplementary Figure 1).

Statistical analysis was performed on the percentage of AF488 positive cells (cells observed in the lower right quadrant) for the gated cell population. Data was assessed for normality using the Shapiro-Wilk test in STATA. One-way analysis of variance (ANOVA) and Tukey post-hoc tests were performed using Graph Pad Prism 5 or 8 (Graph Pad Software), to determine the differences in viral internalisation and binding between different conditions tested.

2.6 Staining of surface HSPGs on HPV16-PsVs infected NIKS cells

In order to visualise surface HSPGs on NIKS cells by immunohistochemistry (IHC), NIKS cells were seeded in 12-well plates (Greiner Bio-One) containing sterile round coverslips (Marienfeld) at a density of $5x10^3$ cells per well and incubated overnight at 37°C. The cells were either infected as described in section 2.5, or left untreated, before being rinsed in cold F-medium and incubated with a mouse anti-heparan sulphate monoclonal antibody (Seigaku, 10E4 epitope) at a dilution of 1:100 for 1 hour at 4°C. Cells were rinsed with cold 1X PBS and fixed with 4% (v/v) paraformaldehyde in 1X PBS for 10 minutes at room temperature, before being washed 3 times for 5 minutes with 1X PBS and blocked with blocking solution (Appendix) for 1 hour at room temperature.

Cells were then stained with an AF647-conjugated donkey anti-goat antibody (Jackson ImmunoResearch Laboratories, Inc) with a dilution of 1:1000 in blocking solution for 1.5 hours at

room temperature. The cells were rinsed with 1X PBS prior to being counterstained with Hoechst (Sigma) at a dilution of 1:6000 in 1X PBS. Cells were washed with 1X PBS and mounted on glass slides with Mowiol (Sigma) containing n-propylgallate for its anti-fade properties. Slides were stored at 4°C protected from light until viewing.

Slides were viewed using a Zeiss LSM880 Airyscan confocal microscope together with Zen 2.3 SP1 software (Zeiss). Co-localisation analysis was performed for each optical section in z-stacks of individual cells. Quantification of co-localisation was performed on approximately 50 cells for each experimental condition tested, using the Zen software. Co-localisation coefficients for the fluorescence channels representing AF647-labeled heparan sulphates and AF488-labeled HPV16-PsVs, respectively, as well as overlap coefficients were determined according to the method of Manders *et al*. (129).

Z-stack dimensions were then normalised to 10 optical sections per image stack, and maximum intensity projections were done for display purposes. The lower and upper thresholds were set at 14 and 230 greyscale levels, respectively, for each maximum intensity projection. This was done to remove background signal so that the measured signal for AF647 corresponded to the area representing 10E4 Heparan Sulphate staining.

2.7 *In vivo* infection of female C57BL/6 mice with HPV16-PsVs

In order to study the effects of rhVim and SP-A on HPV16 infection *in vivo*, a murine cervicovaginal challenge model was applied as described by Roberts *et al* (29). All *in vivo* experiments were performed on female, 6 to 10 week-old C57BL/6 mice. The mice were housed and monitored in the UCT Research Animal Facility (RAF) Biosafety Level 2 laboratory, as described in (66). All experiments were approved by the Faculty of Health Sciences Research Animal Committee at UCT (ethics number: 016/008).

4 days prior to infection, mice were injected subcutaneously (s.c.) with 100µL 2mg/20g Depo-Provera (Pfizer) in sterile 1X PBS to equilibrate hormone levels as well as to help facilitate infection by thinning the vaginal epithelium (Figure 2.1) (29). 6 hours before infection, mice were lightly anaesthetised by intra-peritoneal (IP) injection with 125µL 1.5mg/20g ketamine +

0.2mg/20g xylazine. Following this, vaginal lavages were performed with 2X 50µL sterile 1X PBS. 25µL 4% nonoxynol-9 (N-9, US Pharmacopeia) in 3% carboxymethylcellulose (CMC) was then added to the genital tract, as N-9 is known to chemically disrupt the vaginal and cervical epithelium, facilitating HPV infection (130). After 6 hours, mice were anaesthetised as described above and infected intravaginally (i.vag.) with 1µg HPV16-PsVs encapsidating the pGluc reporter gene (pre-incubated with rhVim or SP-A as indicated) in 3% CMC. For time course experiments, vaginal lavages were performed daily with 2X 50µL sterile 1X PBS and stored at -80°C until analysis.

Mice were euthanised using halothane 3 days post infection (p.i.), followed by cervical dislocation as a confirmation of death. For early infection experiments (see sections 2.7.2 and 2.7.3), mice were euthanised 2 hours p.i. (h.p.i.) and the genital tract dissected. Briefly, using dissection tools, the peritoneal cavity was opened, and the cecum and colon was moved to expose the genital tract. The bladder was then excised from the vagina, and the genital tract removed from the body cavity. Fat and connective tissue were then carefully removed from the genital tract tissue. The fallopian tubes and ovaries were removed, and the remaining genital tract, which included the uterus, cervix and vagina, was processed as described in sections 2.7.2 and 2.7.3.

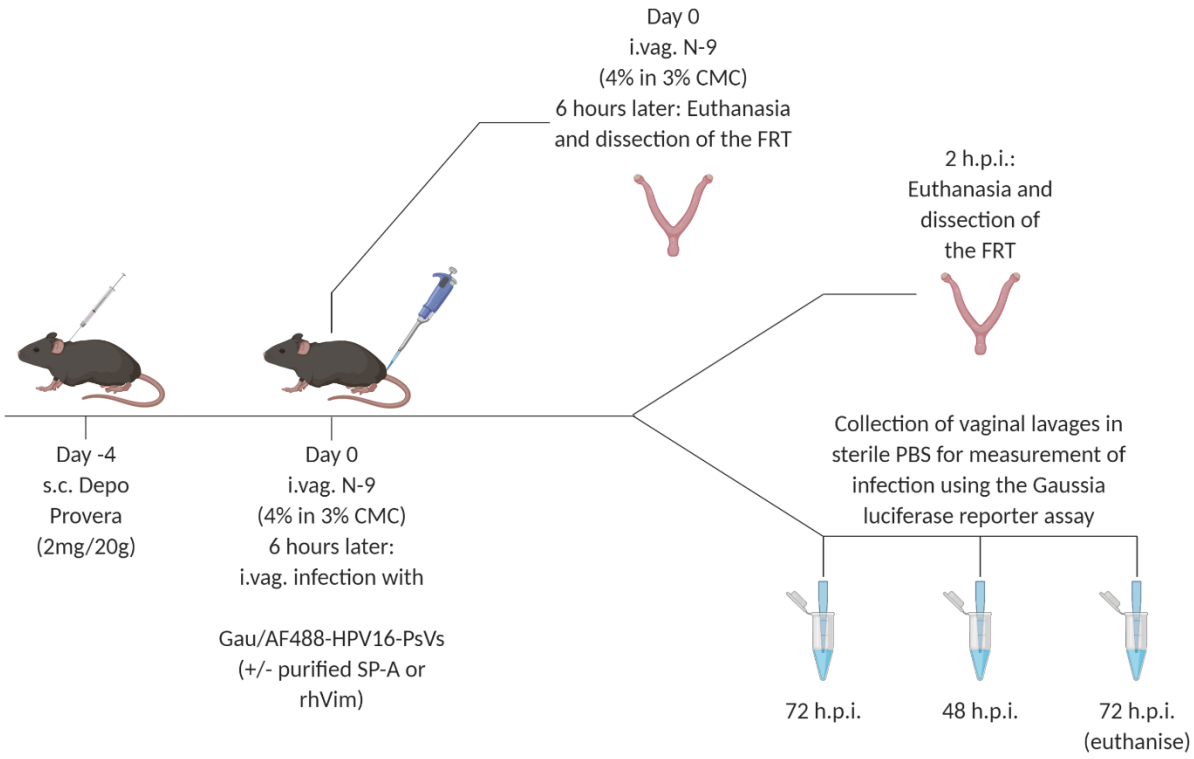

Figure 2.1: Mouse model for HPV16-PsVs infection using C57BL/6 mice, adapted from Roberts *et al.* (29)**.**

2.7.1 Processing of samples from HPV16-PsVs infected female C57BL/6 mice

To measure luciferase activity in the vaginal lavages of mice infected with GLuc HPV16-PsVs, the vaginal lavages collected in Eppendorf tubes were centrifuged for 1 minute at 700g to remove any vaginal mucus from the sample. Thereafter, 5µL lavage was added directly to a white 96-well plate and measured using a Fluoroskan™ Ascent Microplate Fluorometer and Luminometer (Thermo Scientific) or a GloMax® Explorer Multimode Microplate Reader (Promega) following the Gaussia Luciferase Assay Kit (New England Biolabs) protocol (see section 2.3.4).

2.7.2 Flow cytometry analysis of HPV16-PsVs infected mouse FRT single cell suspensions

In order to recapitulate the early events of human sexual HPV transmission and elucidate the early immune responses subsequent to infection with SP-A pre-incubated viral particles, different approaches were followed involving single cell suspensions prepared from female reproductive tracts of mice treated as outlined below. Cells were analysed by flow cytometry using an innate immune cell (myeloid) panel. In all cases, the cervicovaginal challenge model of Depo-Provera and N-9-treated mice was applied.

In order to create FRT single cell suspensions, the FRT was dissected (see section 2.7), finely cut, and digested in complete DMEM containing 1% HEPES and 20µg/ml Liberase™ TL (Roche), for 1 hour at 37°C with gentle shaking. Digested tissue was passed through a 70µm cell strainer and resuspended in fresh complete DMEM. Single cell suspensions were counted by trypan blue exclusion, using a haemocytometer slide and resuspended at a concentration of 1 x 10^6 cells/mL, where 100µL of the suspension was plated in clear 96-well plates (Greiner Bio-One).

Innate immune cell populations were analysed by multi-colour flow cytometry. The following fluorochrome-conjugated antibodies were used: CD45 Alexa Fluor 700 (Biolegend, Clone: 30-F11), CD11b Brilliant Violet (BV) 421™ (Biolegend, Clone: M1/70), SigLecF PE (Biolegend, Clone: S17007L), Gr-1 (Ly-6G+Ly-6C) APC Cy7 (eBioscience, Clone: RB6-8C5), F4/80 BV605 (Biolegend, Clone: BM8). Cells were stained in staining buffer (0.5% BSA, 2mM EDTA in 1 X PBS) for 20 minutes at 4°C (dark), washed and resuspended in staining buffer for acquisition using the BD LSR Fortessa. Data was analysed using FlowJo software (V10). Innate immune cell populations were identified as $CD45^+CD11b^+/SigLecF^+/SSC^{high}$ (eosinophils), $CD45^+CD11b^+/Gr\text{-}1^{high}$ (neutrophils), $CD45^+CD11b^+/Gr\text{-}1^{intermediate}$ (monocytes) and $CD45^+CD11b^+/F4/80^+$ (macrophages) (Figure 2.2). Uptake of internalized AF488-labelled virions by immune cells were defined as $AF488^+$ cells, based on fluorescence minus one (FMO) controls.

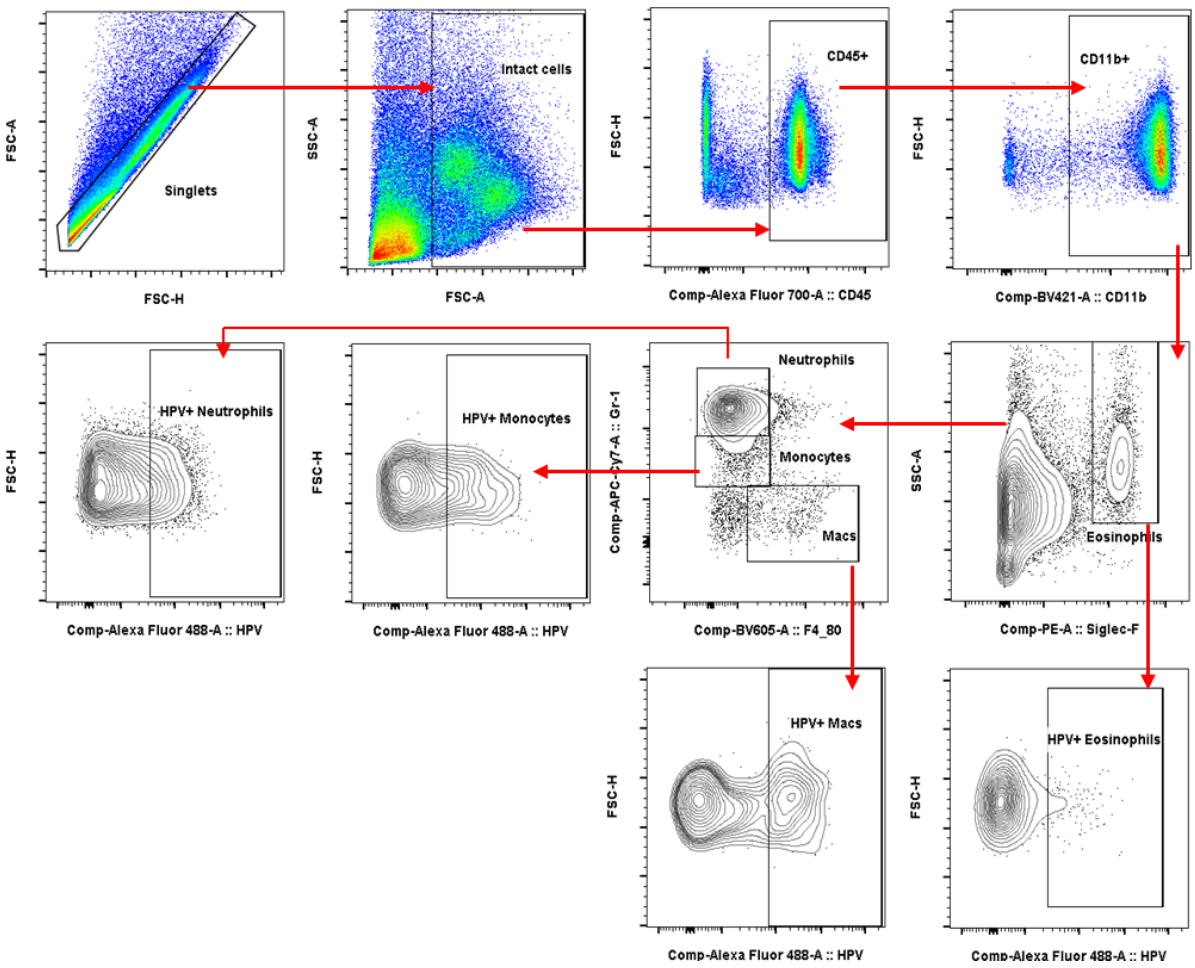

Figure 2.2: HPV/SP-A *ex vivo* infection. Innate immune cell gating strategy. 6 to 10 week-old female wildtype C57BL/6 mice were treated with Depo-Provera (s.c.) for 4 days, and then pre-treated with N-9 for 6 hours. Thereafter, mice were killed and the FRTs were dissected for the preparation of single cell suspensions. Cells were infected with AF488-labelled HPV16-PsVs that had been pre-incubated with BSA (control) or SP-A in a ratio of 1:10 (w/w) for 1 hour at room temperature. At various time points, cells were stained to visualise and gate the following innate immune cell populations by flow cytometry: eosinophils ($CD11b^+/SiglecF^+/SSC^{high}$), neutrophils ($CD11b^+/Gr\text{-}1^{high}$), inflammatory monocytes ($CD11b^+/Gr\text{-}1^{intermediate}$), and macrophages ($CD11b^+/F4/80^+$). AF488-labelled HPV16-PsVs uptake/co-localisation by innate genital cells were gated as $AF488^+$ innate cells, based on FMO (uninfected) controls.

Three different approaches were taken with regards to analysing the single cell suspensions. These were performed to fine-tune the most accurate procedure and subsequent analysis that would reflect biologically relevant changes in innate immune cell populations in the early stages of HPV16 infection.

2.7.2.1 First approach: *in vivo* infection

6 to 10 week-old female wildtype C57BL/6 mice were treated with Depo-Provera (s.c.) for 4 days, and then pre-treated with N-9 for 6 hours, as described above. The mice were infected intravaginally for 2 hours with 1µg AF488-labelled HPV16-PsVs that had been pre-incubated with BSA (control) or SP-A in a ratio of 1:10 (w/w) for 1 hour at room temperature. The mice were euthanised and the FRTs dissected and single cell suspensions were produced and analysed by flow cytometry as described in section 2.7.2 (Figure 2.3).

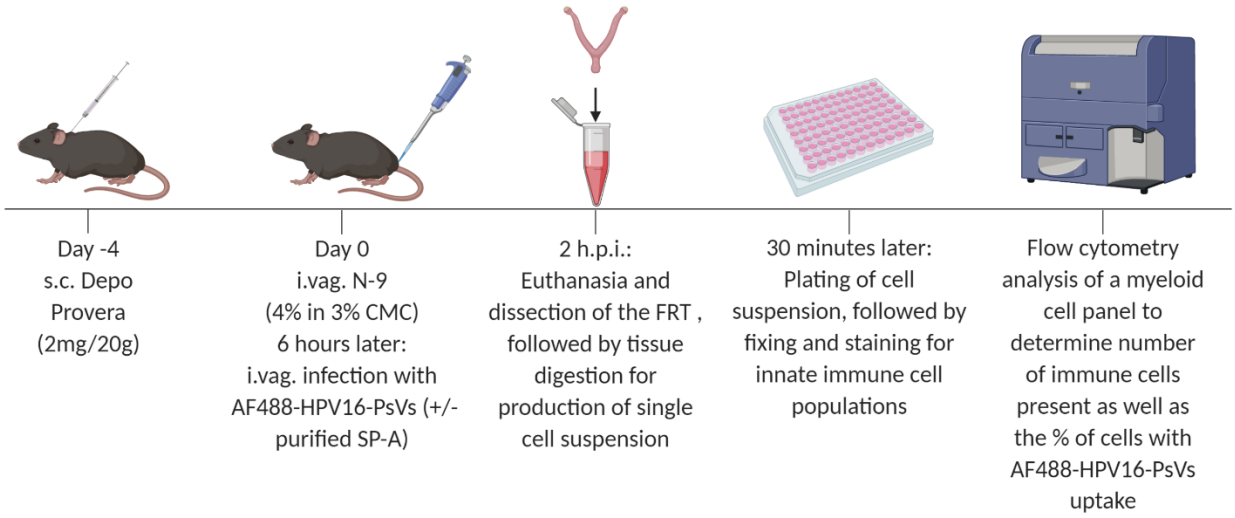

Figure 2.3: Flow cytometry analysis of mouse FRT single cell suspensions upon *in vivo* infection with SP-A pre-incubated HPV16-PsVs (*in vivo* approach). N-9-treatment of naïve C57BL/6 female mice followed by infection with SP-A/BSA pre-incubated AF488-HPV16-PsVs 6 hours later. This was followed by dissection of the FRT 2 hours p.i. to create a single cell suspension with fixing, staining and flow cytometric analysis performed all at once. Protocol adapted from (29).

2.7.2.2 Second approach: *ex vivo* infection with a reverse order time-staggered infection of FRT single cell suspensions

6 to 10 week-old female wildtype C57BL/6 mice were treated with Depo-Provera (s.c.) for 4 days, and then pre-treated with N-9 for 6 hours, as described above. The mice were then euthanised followed by dissection of the FRTs and production of the single cell suspensions. The single cell suspensions were plated as described in section 2.7.2. Infection of the cells was performed for 0 to 8 hours, and this was done in a time staggered, reverse-ordered fashion (Figure 2.4), where the cells that were infected for a total of 8 hours at 37°C were infected first, and the cells infected

for 30 minutes were infected last. In each well, 1µg AF488-labelled HPV16-PsVs that had been pre-incubated with BSA (control), or SP-A in a ratio of 1:10 (w/w) for 1 hour at room temperature was added.

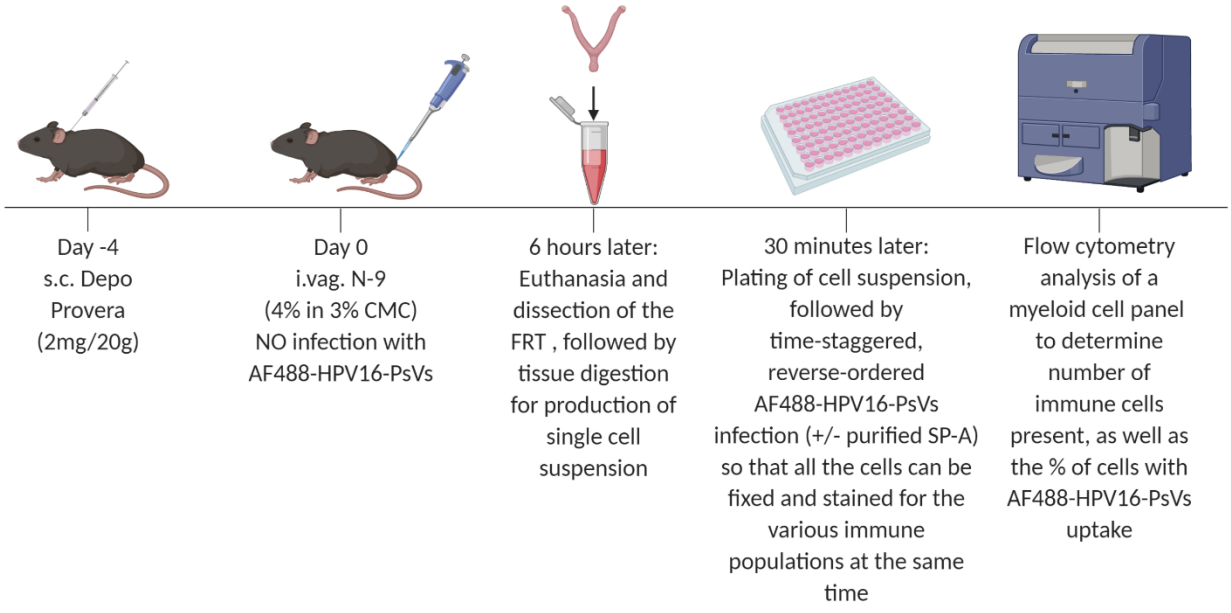

Figure 2.4: Flow cytometry analysis of mouse FRT single cell suspensions upon *ex vivo* time-staggered infection with SP-A pre-incubated HPV16-PsVs (*ex vivo* approach I). N-9-treatment of naïve C57BL/6 female mice followed by dissection of the FRT to create a single cell suspension for subsequent time-staggered infection of SP-A/BSA pre-incubated AF488-HPV16-PsVs, with fixing, staining and flow cytometric analysis performed all at once. Protocol adapted from (29).

2.7.2.3 Third approach: *ex vivo* infection with fixing, staining and flow cytometry acquisition after each infection

In order to prepare single cell suspensions for this approach, the FRTs of uninfected mice were removed 6 hours post N-9-treatment (Figure 2.5). 1 x 10^6 cells were plated as described and infected at 37°C for 30 minutes to 6 hours with 1µg AF488-conjugated HPV16-PsVs which had been pre-incubated with purified human SP-A protein or BSA at a w/w ratio of 1:10 for 1 hour at room temperature. All cells were infected at the same time, followed by fixing and staining of the cells for each indicated time point, and analysis by flow cytometry (as described in section 2.7.2).

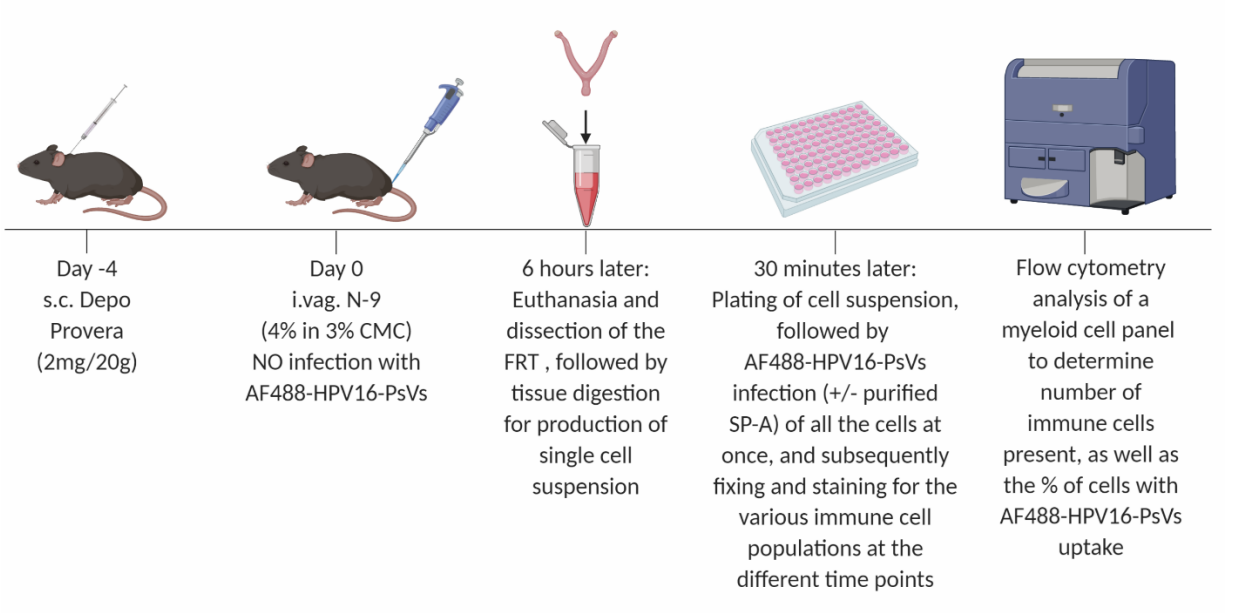

Figure 2.5: Flow cytometry analysis of mouse FRT single cell suspensions upon *ex vivo* "all at once" infection with SP-A pre-incubated HPV16-PsVs (*ex vivo* approach II). N-9-treatment of naïve C57BL/6 female mice followed by dissection of the FRT to create a single cell suspension for subsequent "all at once" infection of SP-A/BSA pre-incubated AF488-HPV16-PsVs, with fixing, staining and flow cytometric analysis at different time points: t=0 hours, t=2 hours, t=4 hours, t=6 hours. Protocol adapted from (29)**.**

2.7.3 Staining for macrophages in the mouse female reproductive tract

To visualise macrophages and viral particles by IHC, the FRT was dissected from Depo/N-9 treated naïve and AF488-HPV16-PsVs (pre-incubated with BSA or SP-A) infected mice (Figure 2.1). The tissue was prepared for cryosectioning 2 hours p.i. (or 6 hours after N9 treatment for naïve mice) following standard procedures. Briefly, the genital tract tissue was first placed in 4% paraformaldehyde for 1 hour to fix the tissue which was then washed 3 X 10 minutes in sterile 1X PBS. Following washing steps, the tissue was suspended in a 30% sucrose solution overnight at 4°C in order to displace any water from cellular spaces and therefore "cryoprotect" the tissue. Remaining sucrose was then removed from the tissue by gently blotting with paper towel, and tissue was embedded in Optimal Cutting Temperature (OCT, Sakura Finetec USA) compound in a plastic mould (Sakura Finetec USA) and frozen over dry ice. Tissue blocks were stored at -80°C until cryosectioning. Tissue sections of 20µm were cut using a Leica CM1850 cryostat. These sections were placed on microscope slides coated with 3-Aminopropyltriethoxysilane (APES),

which allowed the tissue to adhere to the slides. Samples were then air-dried overnight, protected from light. Slides were stored at 4°C for up to a week or at -80°C long-term, protected from light.

Before any IHC staining, samples were removed from storage and left at room temperature for 30 minutes. Sections were then immersed in cold methanol and incubated for 10 minutes at -20°C to fix and permeabilise sections. Sections were then washed 3 times in 1X PBS, 10 minutes each. Following washing, sections were incubated in IHC blocking solution (Appendix) for 1 hour at room temperature to reduce non-specific staining. To stain for macrophages, sections were incubated with a specific antibody against murine macrophage surface protein F4/80 (rat-anti-mouse F4/80, Thermo Scientific) at a dilution of 1:1000 in IHC blocking solution overnight at 4°C in a sealed humidified chamber. Non-specific background signal was controlled for by using a rat IgG2B isotype control (Invitrogen) at a dilution of 1:1000 in blocking solution overnight at 4°C in a sealed humidified chamber. Sections were then washed 3 times in 1X PBS, 10 minutes each. Goat-anti-rat AF555 secondary antibody (Invitrogen) was added to the sections at a 1:500 dilution in blocking solution for 90 minutes at room temperature. This was followed by washing as described above. Sections were then incubated in Hoechst Nuclear Stain (0.5µg/mL in 1X PBS) for 10 minutes at room temperature, protected from light. After incubation, slides were washed in 1X PBS for 10 minutes. Sections were then mounted with 20mm x 20mm coverslips using Mowiol, which contained n-propylgallate for its anti-fade properties. Slides were stored at 4°C protected from light until viewing.

Tissue sections were viewed using a Zeiss LSM880 Airyscan confocal microscope together with Zen 2.3 SP1 software (Zeiss). Ten areas in the epithelium were randomly selected for each condition, using the Hoechst channel only to eliminate bias. Z-stacks were then taken with the Hoechst, AF488 and AF555 channels selected. Z-stack dimensions were then normalised to 18 optical sections per image stack, and maximum intensity projections were done. The area occupied by macrophages (positive for F4/80) in the epithelium was determined by outlining the epithelium in each maximum intensity projection and determining the area of the AF555 stain in these selected regions (Supplementary Figure 2). This was normalised to the area occupied by the AF488-conjugated HPV16-PsVs, as the number of pseudovirions surrounding the basal

epithelium was predicted to impact the level of immune response, i.e. the number of macrophages that are recruited to the basal epithelium. Normalising was done for each individual maximum intensity projection by setting the lower and upper thresholds at 18 and 256 greyscale levels, respectively. This was done to remove background signal so that the measured signal for AF555 corresponded to the area representing F4/80 macrophage staining.

3 Results

Two proteins, rhVim and SP-A have been previously shown by our laboratory to modulate HPV16-PsVs infection *in vitro*, and in the case of SP-A, *in vivo* as well (36, 66). SP-A has been hypothesised to modulate HPV16-PsVs infection indirectly by enhancing innate immune cell recognition and clearing of HPV16-PsVs in the female reproductive tract (66). RhVim, on the other hand, has been hypothesised to modulate HPV16 pseudovirus infection by binding to the HPV16-PsVs and preventing binding to cell surface, internalisation, and subsequent infection of epithelial cells (36).

This study aimed to further elucidate the mechanisms with which these two proteins modulate HPV16-PsVs infection by means of various *in vitro* and *in vivo* experiments.

3.1 Production and evaluation of HPV16-PsVs

Before any *in vitro* and *in vivo* experiments using HPV16-PsVs were performed, the purity and infectivity of every new preparation was tested. Firstly, SDS-PAGE followed by silver staining was used to assess the purity of the HPV16-PsVs preparations (Figure 3.1A, left panel). A predominant L1 band at 55 kDa as well as a less predominant L2 band at 75 kDa were expected in pure preparations. For HPV16-PsVs that had been labelled with AF488 the SDS gels were illuminated with a 488 nm light source, which resulted in visualisation of the successfully labelled fluorescent bands before silver staining (Figure 3.1A, right panel).

Secondly, the infectivity of HPV16-PsVs preparations was assessed by infecting HeLa cells with viral particles that had undergone the treatments detailed in section 2.3.4.2. As expected, pre-incubation of HPV16-PsVs with the neutralising antibody H16.V5, which is HPV16 type specific, completely abolished infection (Figure 3.1B). Treatment with DNase I endonuclease was also performed to determine whether the measured luciferase activity was as a result of any un-encapsidated plasmid. In pure preparations, such as the one depicted in Figure 3.1B, DNAse treatment showed a similar HPV16-PsVs infectivity compared to untreated control.

Thirdly, selected pure and highly infectious HPV16-PsVs preparations were visualised by negative staining electron microscopy (Figure 3.1C). The pseudoparticles were found to exhibit similar morphology to that of native HPV, where distinct capsomeres to form complete capsids can be seen (131).

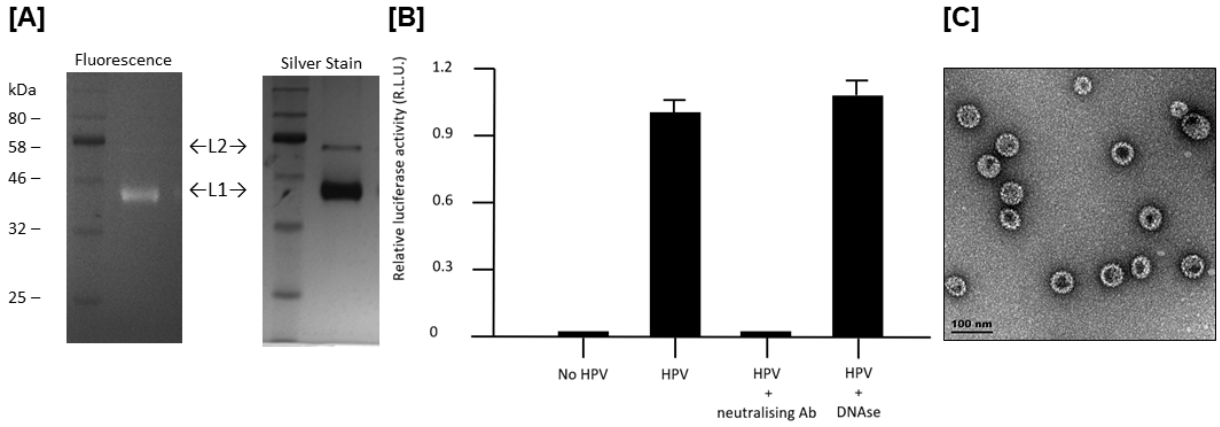

Figure 3.1: Quality control tests to assess purity and infectivity of HPV16-PsVs preparations. [A] SDS-PAGE gel showing the same representative AFF488-labelled HPV16-PsVs preparation, visualised by fluorescence (left gel) followed by silver staining (right gel). A thick band corresponding to the L1 protein (55 kDa) as well as a thin L2 band (75 kDa) were seen in pure preparations. **[B]** HeLa cells were infected with HPV16-PsVs under various conditions (see sections 2.3.4.2) where luminescence was measured 24 hours p.i. Relative luciferase activity (R.L.U) represents luminescence (arbitrary units), and values are presented as x-fold change relative to HPV16-PsVs only, which was set as 1. **[C]** Structural analysis of a representative pure and highly infectious HPV16-PsVs preparation was performed by negative staining transmission electron microscopy.

3.2 Surfactant Protein A impairs HPV16-PsVs infection via innate immune cell activation

3.2.1 The presence of SP-A increases macrophage recruitment to the basal epithelium in the genital tract of C57BL/6 mice

As outlined in section 1.2.4 and Figure 1.4, previous work has shown that pre-incubation of HPV16-PsVs with purified SP-A protein led to a substantial increase of viral uptake into RAW264.7 murine macrophages (66). Therefore, *in vivo* experiments were performed to validate that SP-A enhances HPV16-PsVs recognition by immune cells, thereby affecting overall HPV16-PsVs infection. To confirm previous observations (Ujma MSc thesis, 66), a validation study was

performed using HPV16-PsVs encapsidating the Gaussia luciferase reporter plasmid. As shown in Figure 3.2A, pre-incubation of HPV16-PsVs with purified SP-A at a 1:10 (w/w) ratio decreased the level of infection over time compared to particles pre-incubated with BSA control, with significant reduction seen 72 hours post infection.

Thereafter, macrophage recruitment experiments by means of IHC and confocal imaging were performed to determine whether the observed reduction in infection was due to SP-A mediated changes in the overall number of macrophages in the epithelium of the mouse FRT. As innate immune cells, macrophages are expected to be involved in the very early responses to infection. Therefore, genital tract tissues were dissected 2 hours post infection with AF488-labelled HPV16-PsVs (pre-incubated with SP-A or BSA control as indicated). Figure 3.2B shows a representative image taken of the epithelium, which had been stained for macrophages (F4/80) and cell nuclei (Hoechst). The basal epithelial layer (outlined in yellow) was visually distinguishable from the rest of the genital tract epithelium and was manually outlined to quantify recruitment of macrophages for each condition (Supplementary Figure 2).

Quantification of the area occupied by macrophages (F4/80 staining) in the basal epithelial layer (outlined in yellow) of the FRT of 10 randomly selected images per condition showed a significant increase in macrophage recruitment to the basal epithelium in the presence of SP-A, when compared to the BSA control treated epithelium (Figure 3.2C). The high standard errors as a result of the highly variable and biased nature of this type of analysis should be noted. Therefore, subsequent unbiased quantitative flow cytometry analyses of FRT cell suspensions were done in order to validate the IHC results and to further analyse whether other innate immune cell populations recognise HPV16-PsVs in a SP-A dependent manner, thereby contributing to the observed overall reduction in infection (Figure 3.2A).

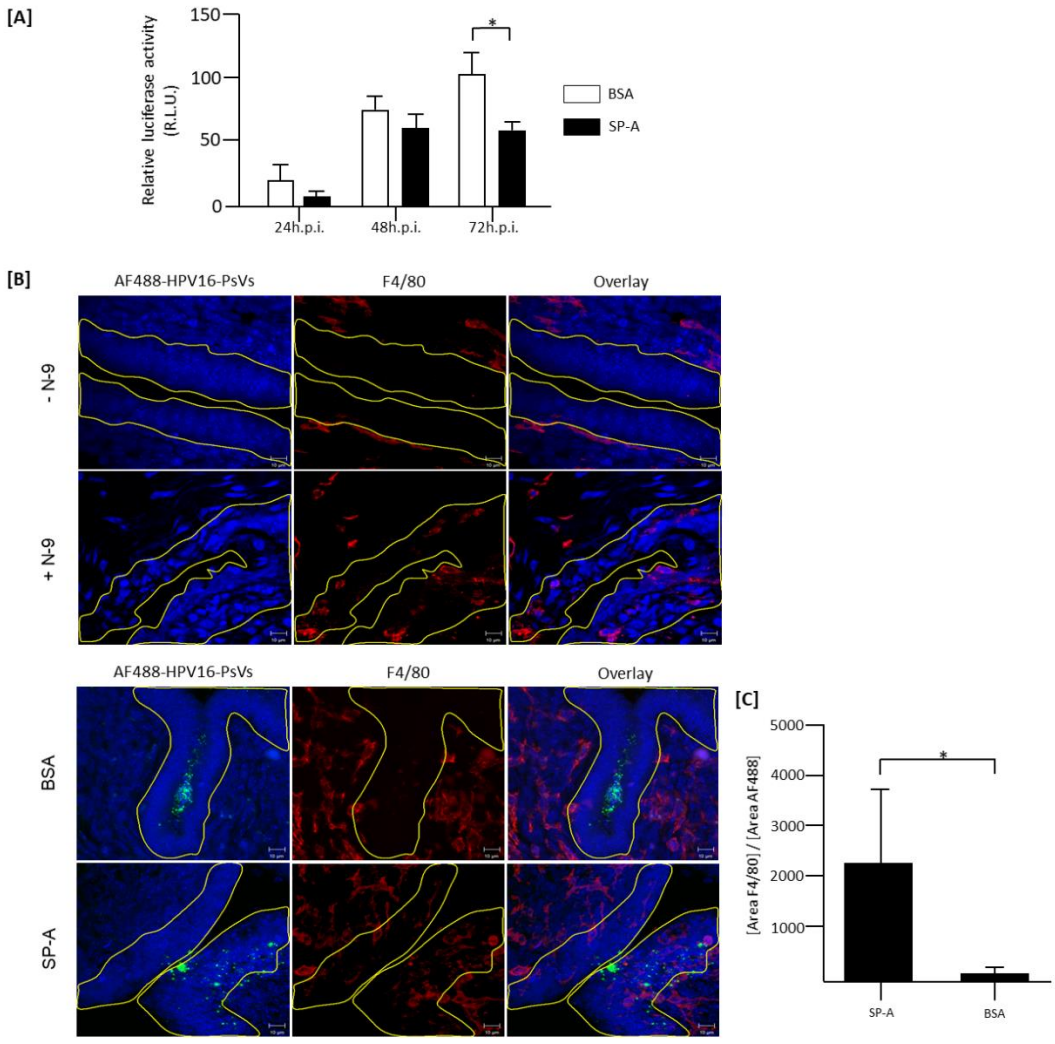

Figure 3.2: SP-A reduces HPV16-PsVs infection in C57BL/6 mice by increasing macrophage recruitment into the basal eptihelium. 6 to 10 week-old female wildtype C57BL/6 mice were pre-treated as described in in section 2.7. **[A]** HPV16-PsVs encapsidating the Gaussia luciferase reporter plasmid pGLuc were pre-incubated with a 10-fold (w/w) excess of purified SP-A protein (or BSA control) for 1 hour at room temperature, before intravaginal inoculation. Genital tracts were washed with 2 x 50µL PBS at 24 hours, 48 hours, and 72 hours post infection, and activity of the secreted Gaussia luciferase in the vaginal lavage fluid as a measure for infection was determined. Data of three independent experiments are presented relative to infectivity of the BSA control group at 72 hours which was set as 100%. Statistical significance was determined using one-way ANOVA and Bonferroni's multiple comparison tests for the individual time points. *= $p<0.05$. Bars depict mean values, with error bars showing SEM. **[B]** Mice were treated with N-9 for 6 hours as required for HPV challenge (+N-9) or left untreated (-N-9). AF488 labelled HPV16-PsVs were pre-incubated with 10-fold (w/w) excess of purified SP-A protein (or BSA control) for 1 hour at room temperature, before intravaginal inoculation (lower panel) or left uninfected (upper panel) followed by dissection 2 hours p.i. and subsequent tissue processing (see section 2.7.3 for further details). Representative confocal images of epithelial tissue (blue) exposed to fluorescent virions (green) is shown with staining for macrophages in red. The basal epithelium is outlined in yellow. **[C]** Macrophage recruitment to the epithelium in response to SP-A coated HPV16-PsVs was quantified and compared to the BSA control group. Statistical significance was determined using a Mann-Whitney test. *= $p<0.05$. Bars depict mean values, with error bars showing SEM.

3.2.2 Analysis of murine FRT single cell suspensions for SP-A mediated HPV16-PsVs uptake by innate immune cells

Since bias during the quantification of macrophage recruitment by confocal analysis (Figure 3.2C) could not be excluded, flow cytometry analysis of a myeloid cell panel was used as a more unbiased approach to determine whether SP-A had any effect on HPV16-PsVs recognition by innate immune cell populations in the FRTs of C57BL/6 mice. This analysis was carried out by creating single cell suspensions produced from the dissected genital tracts of female C57BL/6 mice, before or after infection with HPV16-PsVs. The four cell populations analysed were eosinophils, neutrophils, monocytes, as well as macrophages. Adaptations of the cervicovaginal challenge model described by Roberts *et al* (29) were performed to create these single cell suspensions, where three different infection approaches were performed while using the same flow cytometric analysis for all these approaches (see Figure 2.2). The three different approaches, their outcomes and technical limitations are described in detail below.

3.2.2.1 *In vivo* approach: Preparation and FACS analysis of FRT single cell suspension 2 hours after HPV16-PsVs infection of female C57BL/6 mice

Initially, female C57BL/6 mice were infected with AF488-HPV16-PsVs that had been pre-incubated with either SP-A or BSA, as described in section 2.7. As a negative control, two groups received either the SP-A or BSA protein only. Single cell suspensions were generated from the infected mice 2 hours p.i., where four innate immune cell types were stained and analysed by means of flow cytometry. Analysis parameters focused on the percentage of the total cell population for each innate immune cell population as well as the percentage of a particular cell population that co-localised with AF488-HPV16-PsVs.

As shown in Figure 3.3A, no significant SP-A mediated change in any of the innate immune cell populations was observed. With regards to a change in viral uptake (co-localisation with AF488-HPV16-PsVs) in the different cell populations, a decrease in viral uptake in neutrophils was observed when AF488-HPV16-PsVs had been pre-incubated wit SP-A (Figure 3.3B).

There were technical limitations to this *in vivo* approach that affected the acquisition and analysis of the cell populations. There was a long period of time between dissection of the FRTs and fixing and staining of the single cell suspensions, which means that the cells were kept alive well after the 2-hour infection period. Too many variables could have affected the cells while kept in suspension and thus this approach was determined to not be representative of the innate immune response at 2 hours p.i. in the FRT. The next approach aimed to provide more control on the length of time the cell suspensions were infected with HPV16-PsVs before being fixed, stained and analysed by flow cytometry.

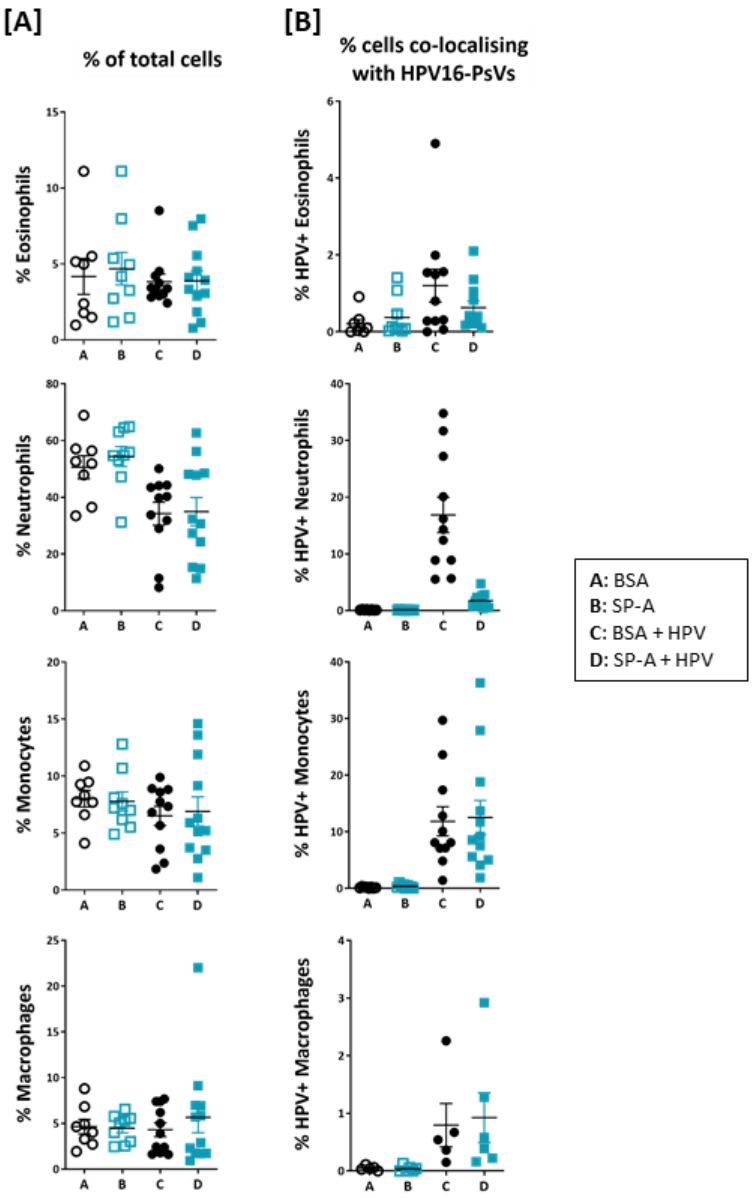

Figure 3.3: *In vivo* approach: SP-A decreases HPV16-PsVs co-localisation with neutrophils, but does not affect immune cell numbers, when FRT single cell suspensions were analysed 2 hours p.i. 6 to 10 week-old female wildtype C57BL/6 mice were treated with Depo-Provera (s.c.) for 4 days, and then pre-treated with N-9 for 6 hours. Mice were then infected with AF488-labelled HPV16-PsVs that had been pre-incubated with BSA (control) or SP-A in a ratio of 1:10 (w/w) for 1 hour at room temperature, where control mice received either SP-A or BSA only. The mice were killed 2 hours p.i. and the FRTs were dissected for the preparation of single cell suspensions. The cells were stained to visualise and gate the following immune cell populations by flow cytometry: eosinophils, neutrophils, inflammatory monocytes, and macrophages (staining details in section 2.7.2). **[A]** Shown is the percentage of the indicated immune cell populations upon infection with HPV16-PsVs pre-incubated with BSA (control) or SP-A, and the uninfected control mice. **[B]** Shown is the percentage of AF488-HPV16-PsVs uptake of each immune cell population upon pre-incubation of the viral particles with BSA (control) or SP-A, as well as the uninfected mice. Two independent experiments were performed, where pooled data from these experiments are presented.

3.2.2.2 *Ex vivo* approach I: Time-staggered HPV16-PsVs infection of FRT single cell suspensions isolated from naïve C57BL/6 mice

The next approach was to perform an *ex vivo* infection, where the female C57BL/6 mice were N-9-treated for 6 hours, followed by dissection of the FRTs. Thereafter, single cell suspensions were produced and infected with AF488-HPV16-PsVs (pre-incubated with SP-A or BSA) using a staggered (reverse) time course to allow for the fixing, staining and flow cytometric acquisition to be done for all conditions at the same time.

While there was a considerable difference in the number of most of the immune cell populations over the course of infection (with eosinophils and neutrophils decreasing, macrophage numbers increasing, and monocyte numbers remaining unchanged over time), there was no significant difference in the number of the immune cells present after each time point between the SP-A pre-incubated treatment and the BSA control (Figure 3.4A). A significant increase could be seen in viral uptake by macrophages with the SP-A pre-incubated treatment at 4 hours p.i., when comparing to the BSA control (Figure 3.4B). Other than this, no significant differences were seen when compared to the BSA control for any of the other innate immune cell populations at the other time points.

This *ex vivo* approach made it possible to analyse the immune cell populations at different time points post infection, however, this approach also had technical limitations. The single cell suspensions that were infected for the shortest period were left to incubate in a humidified atmosphere containing 5% CO_2 at 37°C for as long as 6 hours before being infected and thereafter processed for flow cytometry analysis. These cells therefore did not represent fresh immune cells and there was the potential for these immune cell populations and their viral uptake to differ from those that were left to incubate for a shorter period of time.

The next approach aimed to address this issue by infecting the cells all at once and processing the immune cells at each time point, followed by immediate flow cytometry acquisition.

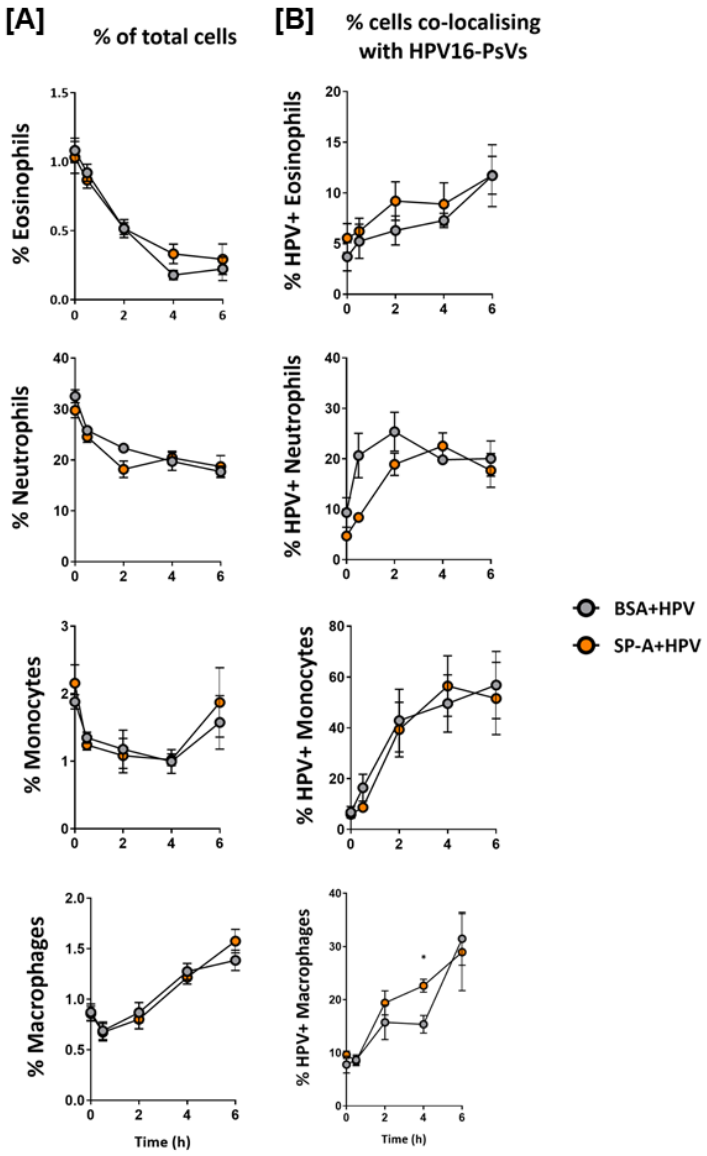

Figure 3.4: Figure 3.4: *Ex vivo* approach I: Time-staggered infection of FRT single cell suspensions with SP-A pre-incubated HPV16-PsVs reveals no changes in viral uptake by innate immune cells. 6 to 10 week-old female wildtype C57BL/6 mice were treated with Depo-Provera (s.c.) for 4 days, pre-treated with N-9 for 6 hours and killed. Thereafter, FRTs were dissected and single cell suspensions prepared which were then infected with AF488-labelled HPV16-PsVs that had been pre-incubated with BSA (control) or SP-A in a ratio of 1:10 (w/w) for 1 hour at room temperature. The infection was done in a reverse order, time-staggered manner. The cells were stained all at once to visualise and gate the following immune cell populations by flow cytometry: eosinophils, neutrophils, inflammatory monocytes, and macrophages. **[A]** Shown is the percentage of the indicated immune cell populations over time upon infection with HPV16-PsVs pre-incubated with BSA (control) or SP-A. **[B]** Shown is the percentage of AF488-HPV16-PsVs uptake for each immune cell population over time, upon pre-incubation of the viral particles with BSA (control) or SP-A. Two independent experiments were performed, where pooled data from these experiments are presented. Significances were calculated by means of two-way ANOVA and Bonferroni's multiple comparison tests for the individual time points. * = $p<0.033$; ** = $p<0.002$; *** = $p<0.001$. Depicted are mean values, with error bars showing SEM.

3.2.2.3 *Ex vivo* approach II: All-at-once HPV16-PsVs infection of FRT single cell suspension isolated from naïve C57BL/6 mice

The third and final approach was to perform an *ex vivo* infection of naïve mouse FRT single cell suspensions with AF488-HPV16-PsVs that had been pre-incubated with either SP-A or the BSA control. This approach, however, involved the infection of all the cells at once, followed by fixing, staining, and acquisition after each time point. As evident in Figure 3.5B, the percentage of eosinophils and neutrophils decreases as infection progresses, while macrophages increase over the course of HPV16-PsVs infection. However, the percentage of the indicated innate immune cell populations for any of the infection times showed no significant difference when comparing the SP-A pre-incubated with the control BSA pre-incubated cells, which is similar to the observations of the *ex vivo* approach II (Figure 3.4A). Importantly, uptake of AF488-conjugated HPV16-PsVs significantly increased in the presence of SP-A for all studied innate immune cell populations (Figure 3.5C). This is exemplified for the 2-hour time point in Figure 3.5A. This approach was the most optimal as it allowed for more control over the length of time of HPV16-PsVs infection (by performing an *ex vivo* infection) and prevented any variability between the single cell suspensions caused by varying lengths of time that the cell suspensions were incubated for before HPV16-PsVs infection (this was controlled by infecting all the cells at once and acquiring after each time point).

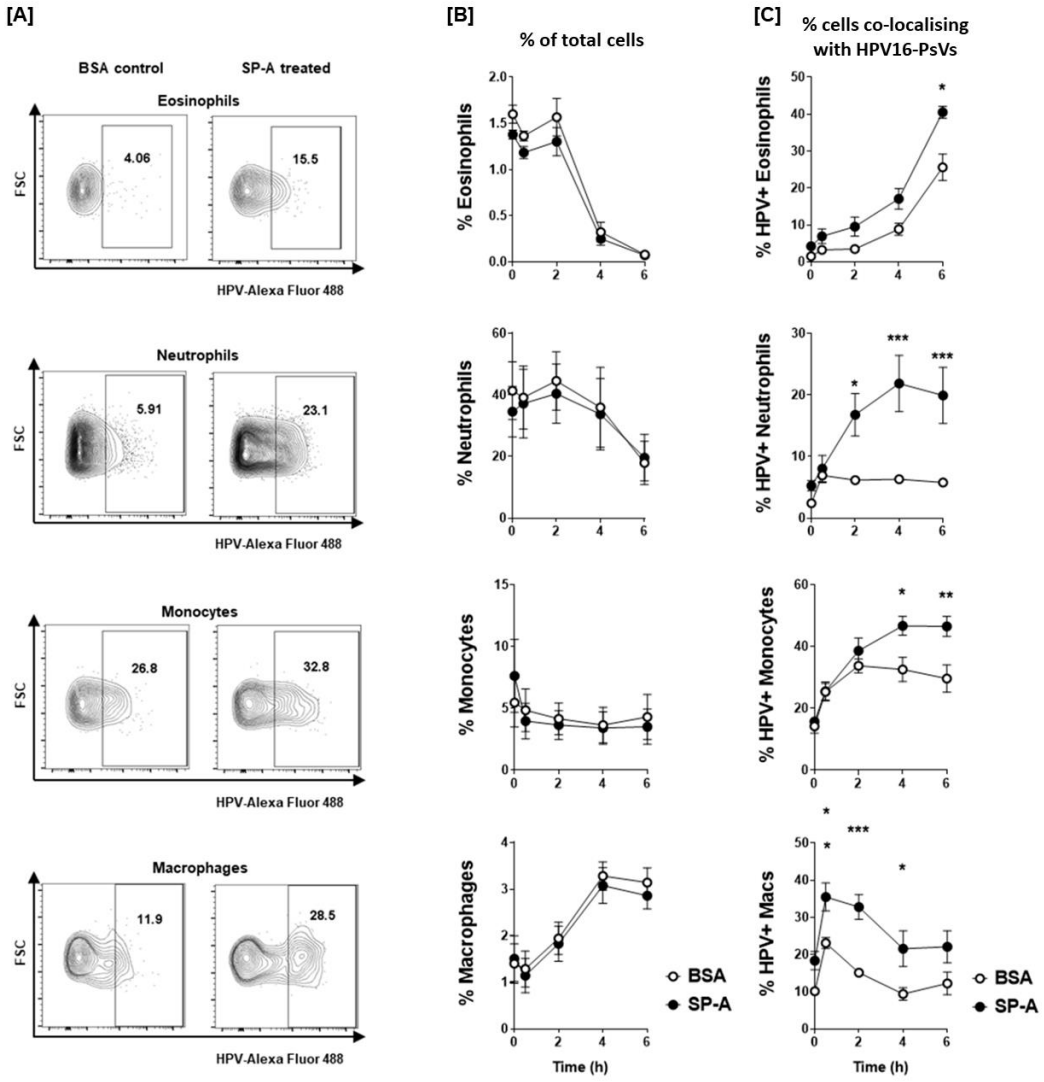

Figure 3.5: *Ex vivo* approach II: All-at-once infection of FRT single cell suspensions with SP-A pre-treated HPV16-PsVs leads to increased viral uptake by selected immune cell populations. 6 to 10 week-old female wildtype C57BL/6 mice were treated with Depo-Provera (s.c.) for 4 days, and then pre-treated with N-9 for 6 hours. Mice were killed and FRT dissected for the preparation of single cell suspensions. Cells for all time points were infected with AF488-labelled HPV16-PsVs that had been pre-incubated with BSA (control) or SP-A in a ratio of 1:10 (w/w) for 1 hour at room temperature. At the indicated time points, cells were stained to visualise and gate the following immune cell populations by flow cytometry: eosinophils, neutrophils, inflammatory monocytes, and macrophages. **[A]** Representative flow gates of AF488-labelled HPV16-PsVs uptake/co-localisation by innate genital cells at the 2-hour time point are shown. [**B]** Shown is the percentage of the indicated immune cell populations over time upon infection with HPV16-PsVs pre-incubated with BSA (control) or SP-A. **[C]** Shown is the uptake of HPV16-PsVs with the indicated immune cell populations over time dependent on pre-incubation of the viral particles with BSA (control) or SP-A. Pooled data of two independent experiments are presented. Significances were calculated by means of two-way ANOVA and Bonferroni's multiple comparison tests for the individual time points. * = $p<0.033$; ** = $p<0.002$; *** = $p<0.001$. Depicted are mean values, with error bars showing SEM.

3.3 Recombinant human vimentin modulates HPV16-PsVs infection by direct competition with the viral internalisation complex on epithelial cells

As shown in Schäfer *et al* (36) (see section 1.3.5), pre-incubation of HPV16-PsVs with rhVim led to a significant decrease in viral uptake and infection of the human keratinocyte cell line NIKS (36), suggesting an inhibitory role in the early events of the viral entry process. However, the exact mechanisms of rhVim modulation of HPV16-PsVs infection remains unknown. Therefore, *in vitro* experiments were performed to elucidate how rhVim affects the early stages of HPV16-PsVs infection, that being cell surface binding of the pseudovirions and subsequent internalisation. Furthermore, *in vivo* experiments were performed to validate whether the *in vitro* results can be applied to a biological model.

3.3.1 The formation of vimentin filaments abolishes the modulatory effect of rhVim on HPV16-PsVs infection

As vimentin has been shown to form filaments in the presence of NaCl (132), *in vitro* experiments were performed to determine whether globular and filamentous rhVim differ in their ability to modulate HPV16-PsVs uptake in NIKS cells. Initially, negatively stained electron microscopic images of rhVim under varying concentrations of NaCl were taken to determine the structure of the vimentin filaments as well as the concentration range at which these filaments start to form. Figure 3.6A shows representative images taken of the rhVim protein, where definitive filaments are formed at an NaCl concentration of 50mM, and thicker filaments form at a higher concentration of 100mM.

HPV16-PsVs uptake in the presence of rhVim at these varying NaCl concentrations were then assessed by means of FACS assays. The decrease in HPV16-PsVs uptake previously seen for a 1:1 rhVim:HPV16-PsVs (w:w) pre-incubation with 0mM NaCl (36) was abolished when the pre-incubation step occurred in the presence of NaCl concentrations 50mM and higher (Figure 3.6B). These results show that rhVim decreases HPV16-PsVs infection most effectively in the absence of NaCl when it is in a non-filamentous form.

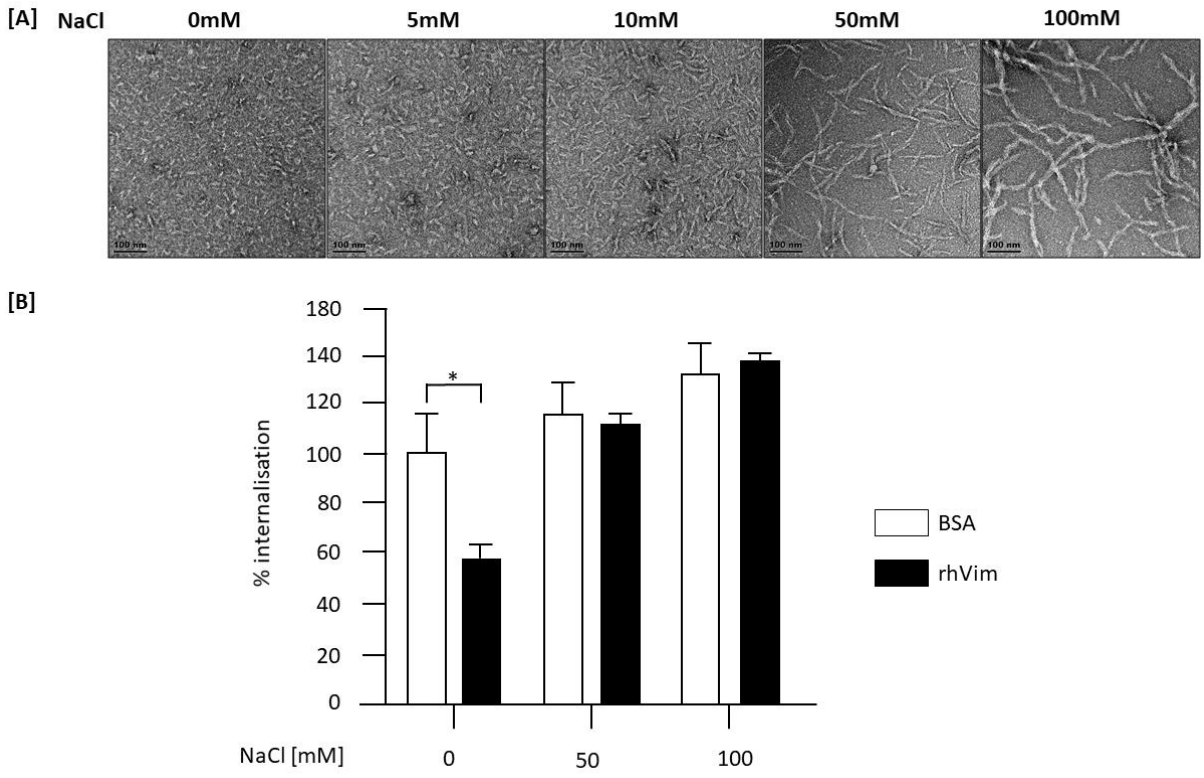

Figure 3.6: The formation of filamentous rhVim at NaCl concentrations of 50mM and higher abolishes its modulatory effect on HPV16-PsVs internalisation by NIKS cells. **[A]** Structural analysis of rhVim was performed by negative staining transmission electron microscopy. rhVim was pre-incubated with varying NaCl concentrations at room temperature for 1 hour prior to staining and imaging. **[B]** Quantification of viral internalisation was performed by flow cytometry of NIKS cells infected with AF488-conjugated HPV16-PsVs pre-incubated with rhVim or the BSA control at a 1:1 (w/w) ratio at room temperature in the presence of varying concentrations of NaCl (see section 2.5). Experiments were quantified by quadrant analysis of the dot plots and presented as % change relative to the mean fluorescence intensity of HPV16-PsVs-infected, BSA pre-incubated cells in the absence of NaCl, which was set as 100%. Combinatorial analysis of three independent experiments are presented. Significances were calculated by means of one-way ANOVA and Tukey post-hoc tests. * indicates statistical significance between uptake of HPV16-PsVs in the presence of SP-A as compared to the other tested conditions. * = $p<0.05$.

3.3.2 Pre-incubation of HPV16-PsVs with rhVim reduces pseudovirus co-localisation with surface HSPGs

The current model of HPV entry suggests that the virus initially attaches to HSPGs at the cell surface, followed by conformational changes and transfer of the virus to an unidentified receptor (30).

To further characterise the step(s) which are modulated by rhVim during the early internalisation process, more specifically at HPV/HSPG binding, HPV16-PsVs were pre-incubated with non-filamentous rhVim and subjected to NIKS cells for co-localisation studies by confocal microscopy. In order to perform these co-localisation studies, it was necessary to determine successful staining conditions of surface HSPGs of NIKS cells. Figure 3.7A shows clear staining of HSPGs, with no background signal detected with the secondary only staining control. Using a 1:1000 dilution of the AF647 secondary antibody displayed the optimal staining conditions, and so this dilution was used in subsequent experiments.

Figure 3.7B shows representative confocal images of NIKS cells that had either been uninfected, infected with AF488-HPV16-PsVs only, or infected with AF488-HPV16-PsVs that were pre-incubated with either rhVim or the BSA control. The cells were thereafter stained for HSPGs and cell nuclei. As expected, no HPV16-PsVs green signal could be detected for uninfected cells. Many HPV16 pseudoparticles (green dots) could be seen in the HPV only and BSA pre-incubated HPV treated cells. However, there were fewer HPV16 pseudoparticles detected in the cells treated with rhVim pre-incubated AF488-HPV16-PsVs when compared to the HPV only and BSA control cells.

The differences in HPV16-PsVs binding observed in Figure 3.7B, were further quantified and statistically assessed by co-localisation analysis. The co-localisation coefficients depicted in Figure 3.7C is understood as the degree of overlap between the HSPG fluorophore and the HPV16-PsVs fluorophore and vice versa, where 0 being no overlap and 1 being complete overlap. The top bar graph in Figure 3.7C represents the co-localisation coefficient of the AF647 channel (i.e. the amount of HSPGs co-localising with HPV) and the bar graph below represents the co-localisation coefficient of the AF488 channel (i.e. the amount of HPV co-localising with HSPGs). As expected,

there was a high degree of co-localisation between the HSPGs and just HPV as well as the HPV pre-incubated with BSA control. RhVim-coated viral particles showed a significantly lower co-localisation coefficient with surface-expressed HSPGs compared to control particles. Similarly, HSPGs showed less co-localisation with the rhVim coated particles, strengthening the observation that rhVim decreases binding of HPV16-PsVs to the surface HSPGs of NIKS cells.

In order to determine any statistical significance for these observations, the averaged co-localisation coefficients of fifty cells for each treatment were compared. Although this approach did indeed yield significant comparisons between the rhVim pre-incubation and the HPV only (and BSA pre-incubation controls), it is important to note the large variation and high standard error for each treatment, owing to the biased and highly variable nature of the analysis used in confocal microscopy. Similar limitations have been noted under section 3.2.1, where the same approach was used to determine macrophage recruitment in the presence of SP-A.

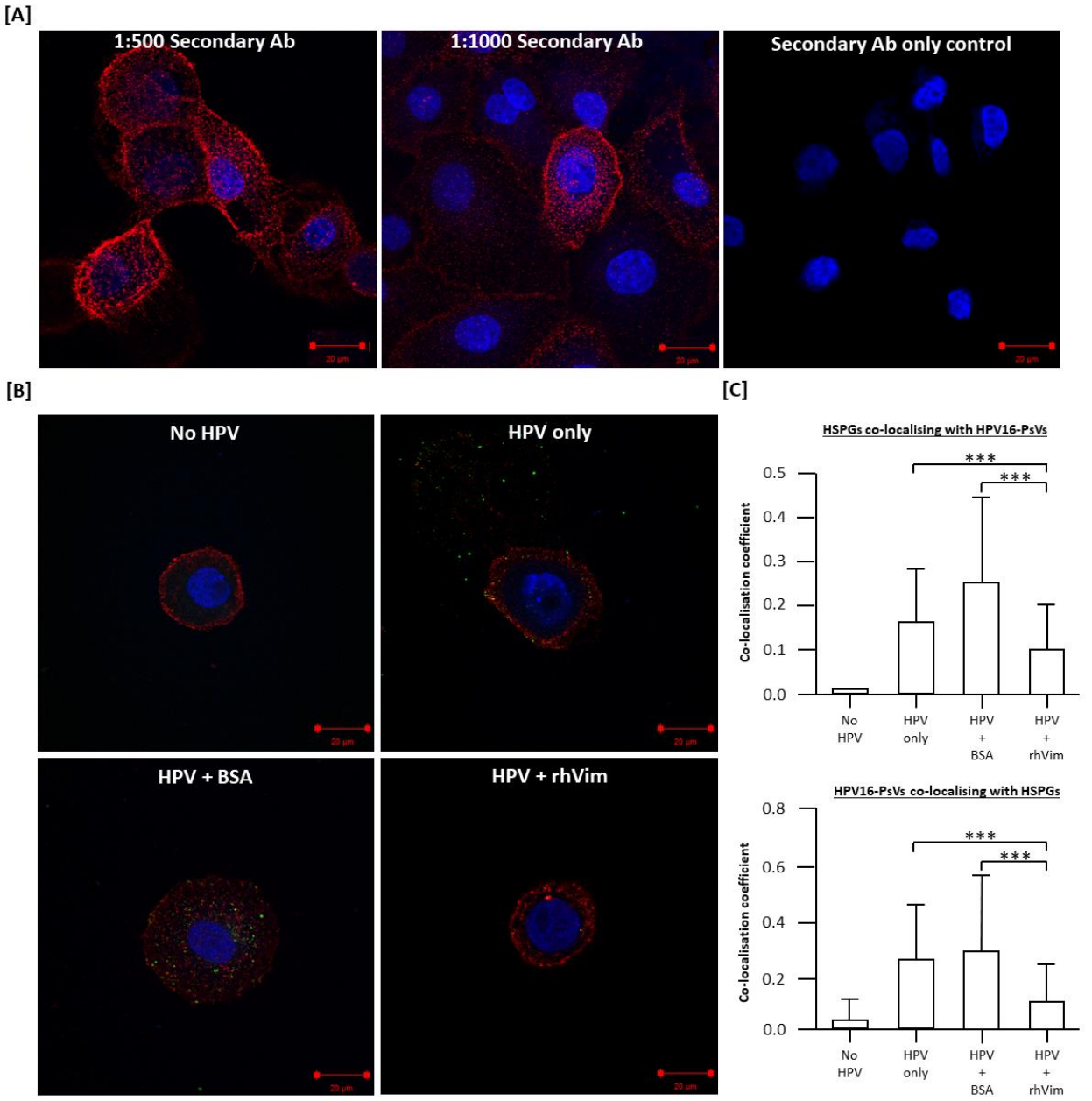

Figure 3.7: Pre-incubation of HPV16-PsVs with rhVim reduces HPV16-PsVs co-localisation with surface HSPGs of NIKS cells. [A] Successful staining for surface HSPGs of NIKS cells, with a 1:500 and a 1:1000 AF647-AffiniPure Donkey anti-Mouse IgM secondary antibody dilution, as well as staining with Hoechst nuclear stain. Cells stained with only the secondary antibody to assess any background signal and nonspecific binding is also shown. **[B] and [C]** Quantification of HPV16-PsVs binding to HSPGs in NIKS cells infected with Alexa Fluor® 488 (AF488)-conjugated HPV16-PsVs was performed by co-localisation analysis via confocal microscopy (procedures described in section 2.5 and 2.6). Images were taken and analysed using a Zeiss LSM 880 AiryScan Confocal Microscope. **[B]** Representative images of the various treatments are shown, with blue nuclei staining and red HSPG staining. **[C]** A summary of the co-localisation (Manders co-localisation coefficient) analysis as shown in **[B]** using n=50 randomly chosen images. Statistical significance was determined using a Mann-Whitney test. ***= $p<0.0001$. Bars depict mean values, with error bars showing SEM.

3.3.3 Removal of surface HSPGs decreases HPV16-PsVs binding and internalisation, and to a greater extent with rhVim pre-incubation

As demonstrated in section 3.3.2, co-localisation of HPV16-PsVs with surface HSPGs is significantly reduced upon HPV16-PsVs pre-incubation with rhVim. Co-localisation is, however, not completely abolished and therefore it cannot be concluded that the effect of rhVim on HPV16-PsVs binding to HSPGs is the sole explanation for a reduction in viral uptake and subsequent infection. The next experiment therefore focused on the effect of pseudoparticle binding and internalisation in NIKS cells upon removal of surface HSPGs by heparinase I treatment prior to infection. Figure 3.8A shows confocal images of NIKS cells that had been incubated with heparinase I for various lengths of time, as described in section 2.5. It is evident that a 1-hour heparinase I treatment completely removed surface HSPGs, and so moving forward this was used in the functional studies.

As expected, a decrease in both HPV16-PsVs cell surface binding and internalisation was observed in cells that had been treated with heparinase I (Figure 3.8B), since the surface HSPGs are known to be the initial attachment point of HPV to target cells (133). Interestingly, pre-incubation of the viral particles with rhVim significantly further decreased both viral binding and internalisation in the absence of HSPGs (Figure 3.8C).

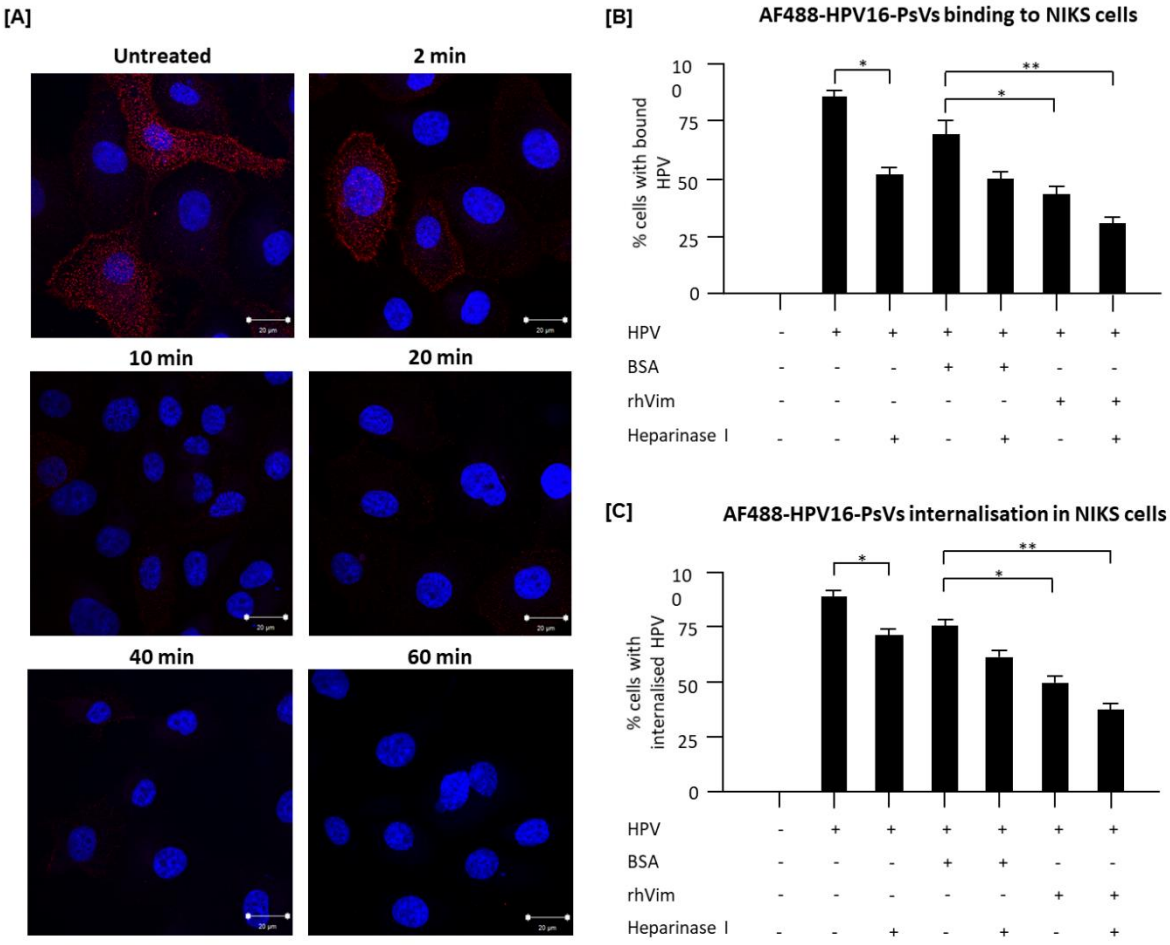

Figure 3.8: Removal of surface HSPGs from NIKS cells decreases HPV16-PsVs binding and internalisation, while rhVim pre-incubation with HPV16-PsVs decreases HPV16-PsVs binding and internalisation to a greater extent. [A] Confocal images proving successful removal of HSPGs in NIKS cells (see sections 2.5 and 2.6 for heparinase I and staining procedures). Images were taken and analysed using a Zeiss LSM 880 AiryScan Confocal Microscope. **[B]** Quantification of viral cell surface binding and **[C]** quantification of viral internalisation was performed by flow cytometry of NIKS cells infected with Alexa Fluor® 488 (AF488)-conjugated HPV16-PsVs. Combinatorial analysis of three independent experiments are presented. Experiments were quantified by quadrant analysis of the dot plots and presented as % change relative to the mean fluorescence intensity of uninfected cells which was set as 0%. Significances were calculated by means of one-way ANOVA and Tukey post-hoc tests. * indicates statistical significance between uptake of HPV16-PsVs in the presence of SP-A as compared to the other tested conditions (* = $p<0.05$, **=$p<0.005$).

3.3.4 Pre-incubation of HPV16-PsVs with non-filamentous rhVim decreases HPV16-PsVs infection in C57BL/6 mice

To confirm the *in vitro* observations on non-filamentous rhVim's capability to modulate HPV16-PsVs infection *in vivo*, the murine cervicovaginal challenge model (as already described for SP-A related experiments, see Figure 2.1) was applied.

As described in section 2.7, carboxymethyl cellulose (CMC) was used as the delivery vehicle for the intravaginal administration of all treatments in female C57BL/6 mice. CMC is a bio-adhesive polymer designed to mimic the viscosity of a typical vaginal lubricant gel (29)**.** To eliminate the possibility that CMC has any effect on the interaction between rhVim and HPV16-PsVs, *in vitro* internalisation assays in NIKS cells were performed as described in section 2.6.1. Figure 3.9 shows no significant difference between CMC pre-incubated HPV16-PsVs internalisation in NIKS cells to the respective CMC untreated cells. The inhibitory effect of non-filamentous vimentin is seen in the presence and absence of CMC. Therefore, it can be concluded that there are no significant effects of CMC on HPV16-PsVs internalisation and all subsequent *in vivo* experiments could be safely carried out in the presence of CMC.

As outlined in section 2.7.1 and shown in Figure 2.1, 6 to 10 week-old female C57BL/6 mice were inoculated intravaginally with HPV16-PsVs encapsidating pGluc that had been pre-incubated with rhVim (under filament-forming conditions or not) or BSA for 1 hour at room temperature. This was followed by welfare monitoring and collection of vaginal lavage samples at 24 and 72 hours p.i., where infection was measured using the Gaussia luciferase reporter gene assay (section 2.7.1).

HPV16-PsVs infection, regardless of whether the HPV16-PsVs had been pre-incubated with BSA or rhVim, resulted in rather low readings at 24 hours p.i. (Figure 3.10), as already observed in the SP-A *in vivo* infection experiments (see section 3.2.1, Figure 3.2A). However, although not statistically significant, a decrease in overall infection in the presence of non-filamentous vimentin (i.e. 0mM NaCl) was observed which was not seen in the presence of filamentous vimentin (100mM NaCl). These effects were much more pronounced 72 hours p.i., reaching

statistical significance, thereby supporting *in vitro* observations of the modulatory effect of non-filamentous rhVim on HPV infection (36).

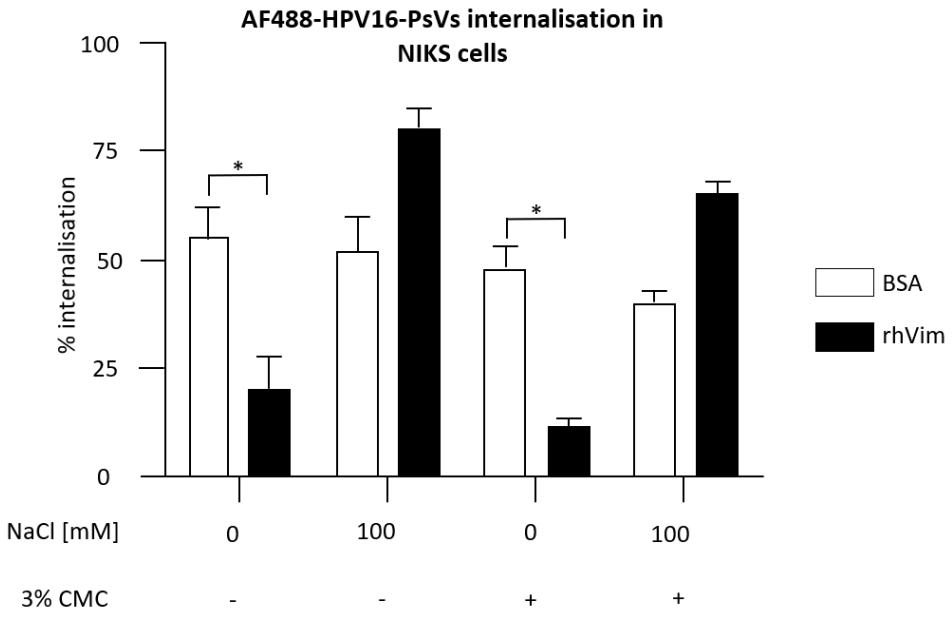

Figure 3.9: Pre-incubation of HPV16-PsVs with CMC does not affect HPV16-PsVs internalisation in NIKS cells. Quantification of viral internalisation was performed by flow cytometry of NIKS cells infected with AF488-conjugated HPV16-PsVs pre-incubated with rhVim or BSA (pseudovirus:protein = 1:1) for 1 hour at room temperature in the presence or absence of 3% CMC. Cells were washed extensively and lifted with trypsin to remove surface-bound virions, thereby allowing detection of internalised viral particles. Experiments were quantified by quadrant analysis of the dot plots and presented as % change relative to the mean fluorescence intensity of uninfected cells which was set as 0%. Combinatorial analysis of three independent experiments are presented. Significances were calculated by means of one-way ANOVA and Tukey post-hoc tests. * indicates statistical significance between uptake of HPV16-PsVs in the presence of rhVim as compared to BSA controls. * = $p<0.05$.

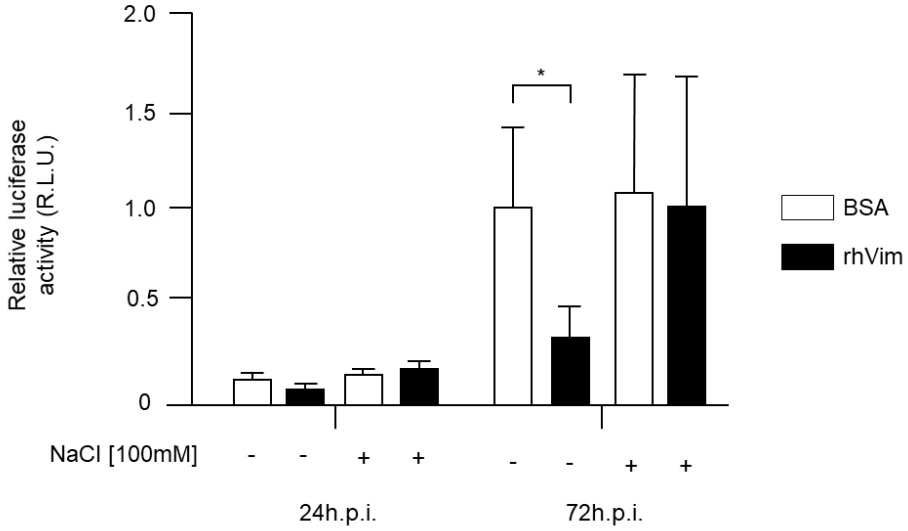

Figure 3.10: Pre-incubation of HPV16-PsVs with non-filamentous rhVim decreases HPV16-PsVs infection in C57BL/6 mice. HPV16-PsVs encapsidating the Gaussia luciferase reporter plasmid pGLuc were pre-incubated with rhVim or BSA (pseudovirus:protein = 1:1) for 1 hour at room temperature, before intravaginal inoculation in the presence of CMC of 6 to 10 week-old female wildtype C57BL/B mice (n=6) (29). Genital tracts were washed with 2 x 50µL PBS at 24 and 72 hours p.i., and activity of the secreted Gaussia luciferase in the vaginal lavage fluid as a measure for infection was determined. Data of three independent experiments are presented relative to infectivity of the BSA control group at 72 hours which was set as 1. Statistical significance was determined using one-way ANOVA and Bonferroni's multiple comparison tests for the individual time points. *= $p<0.05$. Bars depict mean values, with error bars showing SEM.

4 Discussion

Infection with HPV is currently incurable, and co-infection with HIV, particularly in those regions of the world with high HIV prevalence like Southern Africa, contribute to the vicious cycle of viral acquisition, transmission and disease development. This emphasises the need for highly effective and easily accessible therapies with regards to HPV prevention and treatment (49).

Prophylactic vaccination is considered the most effective control of viral infections. Recently, highly efficacious prophylactic vaccines against high grade cervical intraepithelial diseases caused by the most prevalent oncogenic HPV types 16 and 18 have been developed (134). However, despite the great efforts exerted in HPV vaccination programs, these vaccines do not cover all the oncogenic HPV types present in malignant lesions and the extent of cross-protection against other oncogenic HPV types, of which there are more than twenty that have been identified, is largely unknown. In addition, the vaccines are ineffective for women already infected with high-risk HPV types (19). Therefore, cervical cancer still represents the fourth most common cancer in women worldwide (12). This clearly underscores the need for alternative interventions that broadly HPV infection.

This research focused on two proteins, rhVim and SP-A, which have been shown in previous studies to decrease infection, and it is theorised that they do so using very different mechanisms (36, 66). Since this was a feasibility study it was limited to the use of HPV16-PsVs, which represents the most common high-risk HPV type globally. Both *in vitro* experiments and an *in vivo* mouse model (29) were applied to characterise the modulatory effects of these two proteins on HPV infection. For ease of interpretation, SP-A will be discussed first followed by the discussion of rhVim.

4.1 The modulatory effect of surfactant protein A on HPV16-PsVs infection

Innate mucosal immune responses in the female reproductive tract, the first barrier associated with clearance of incoming HPV, is still an underexplored field. HPV infects epithelial cells at mucosal surfaces during primary infection. Due to the ability of HPV to evade several immune mechanisms, infiltration and activation of macrophages and DCs (the most likely antigen presenting cells) are usually ineffective, and as a result these viral infections lead to inept humoral and cellular immunity (26). Failure to develop effective immune responses results in the virus reaching the squamous epithelial cells where it remains concealed from the host immune system. The resulting persistent infection increases the likelihood of cancer development (34).

Therefore, an alternative approach for the prevention of HPV infection is the activation of the innate immune response leading to enhanced recognition and elimination of the virus before infection of its target cells. For this reason, SP-A, a molecule that has recently been shown to reduce HPV16-PsVs infection *in vitro* and *in vivo* (Ujma MSc thesis, 66) and has been well established as an innate immune molecule capable of clearing a broad range of viral and bacterial infections primarily in the lung (67, 71–75), was further explored in this study. These preliminary studies as well as the findings in this study have recently been published (82).

Previous studies in our laboratory have shown increased uptake of HPV16-PsVs by RAW264.7 macrophages upon pre-incubation of the pseudovirions with SP-A. Furthermore, a substantial (but not statistically significant) decrease in HPV16-PsVs infection was seen *in vivo* (Ujma MSc thesis, 66). These observations supported the hypothesis that SP-A may be modulating HPV16 infection by activation of the innate immune system and recognition of HPV16 by immune cells.

In order to refine the experimental conditions and to provide more accurate measurements of HPV16-PsVs infection in the murine cervicovaginal challenge model, viral particles encapsidating the secretable reporter Gaussia luciferase were used in time course experiments in order to detect luciferase activity from vaginal lavages daily without sacrificing the animals. The preliminary studies made use of the reporter firefly luciferase which gave much lower readings when compared to HPV16-PsVs encapsidating the Gaussia reporter gene. Firefly luciferase is not secretable and therefore, animals had to be killed and the genital tract dissected and lysed in

order to access the luciferase protein, where this may have resulted in experimental variation (66).

Vaginal lavages of HPV16-PsVs-infected C57BL/6 mice were taken under strict experimental conditions to minimise variation: vaginal vaults were rinsed with 2x 50µL sterile 1 X PBS by pipetting up and down 3 times and pooling the 2 lavages. This was followed by centrifugation to pellet the vaginal mucus. As a result of these strictly consistent experimental conditions, less experimental variations and a significant decrease in infection was observed at 72 hours p.i. (Figure 3.2A).

Since it was hypothesised that macrophages were likely to be involved in the SP-A-mediated reduction of HPV16-PsVs infection (Ujma MSc thesis, 66), macrophage recruitment was studied using IHC and confocal microscopy. It should be noted that for successful infection in the mouse model used, intravaginal administration of Nonoxynol-9 (N-9) was done a few hours before infection (29). N-9 is an over-the-counter spermicide and has been shown to disrupt animal and human vaginal epithelium resulting in undesired proinflammatory responses (135–139). This evidence makes it unsurprising that the overall recruitment of macrophages into the FRT due to N-9 treatment prior to viral challenge was independent of HPV (Figure 3.2B, upper panel). We therefore quantified macrophage recruitment into the basal epithelium by comparing infectious conditions of SP-A-coated virions with BSA controls only. A significant increase in the amount of macrophages at the site of infection (the basal epithelium) in the presence of SP-A was observed (Figure 3.2C).

To study selected innate immune cell populations for their ability to take up HPV16-PsVs in the presence or absence of SP-A in an *in vivo* context, single cell suspensions prepared from murine FRT tissue were analysed by flow cytometry over a time course of six hours. Experimental set up and optimisation of this protocol formed a part of this thesis, where the established protocol can now be used to study innate immune cell populations upon infection with other pathogens of interest. Using optimised conditions, it was found that all assessed populations, i.e. eosinophils, neutrophils, monocytes and macrophages, displayed strong SP-A-mediated viral uptake compared to control, with neutrophils being the most significant cellular responders to HPV16-PsVs infection in the presence of SP-A (Figure 3.5).

There are seemingly conflicting results between the co-localisation analysis performed in Figure 3.2C (which suggests an increase in the number of macrophages to the basal epithelial layer of the mouse FRT in the presence of SP-A) and the flow cytometric analyses of the single cell suspensions derived from mouse FRT shown in Figure 3.5B (suggesting no significant increase in the number of macrophages in the presence of SP-A). However, analyses of single cell suspensions do not qualitatively distinguish between macrophages located in the basal epithelium and the intermediate and upper layers of the epithelium. One could therefore speculate that it is indeed not the total number of macrophages in the FRT that changes (as observed by flow cytometry) but that migration of the macrophages occur in the presence of SP-A from the intermediate and superficial layers to the basal epithelial layers (as observed by confocal microscopy).

Based on the murine model used in this study, the data suggests that SP-A mediates opsonisation of incoming HPV16-PsVs, increased phagocytosis and killing by innate immune cells with an overall effect on dampening the infection (Figure 4.1). Besides enhanced phagocytosis, SP-A has been shown to aggregate pathogens thereby hindering their entry into host cells. Although this effect was not studied, the inhibitory effect of SP-A is not necessarily dependent on agglutination (80), and the data presented here strongly suggests an SP-A-mediated innate immune cell uptake of the pseudovirions. Although it has been demonstrated that there is a direct biochemical interaction between HPV16-PsVs and SP-A (66), which suggests opsonisation as the contributing factor for enhanced phagocytosis, it cannot be ruled out that the sheer presence of SP-A at the site of infection contributed to enhanced infiltration of innate immune cells and their rapid clearance of the invading viral particles. This will be concluded with further studies in future.

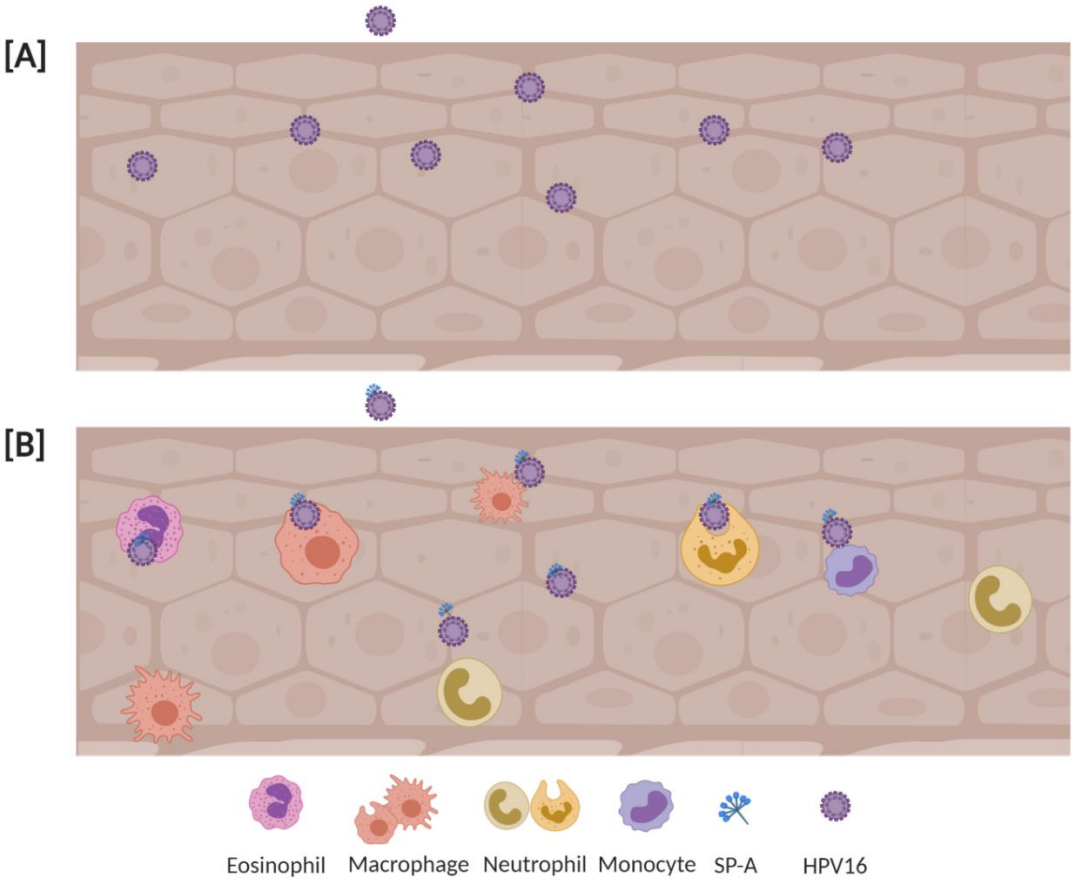

Figure 4.1: Model of the SP-A-mediated opsonisation of incoming HPV16-PsVs, resulting in increased phagocytosis and killing by innate immune cells. [A] HPV16-PsVs infection of the basal epithelium in the absence of SP-A. **[B]** HPV16-PsVs infection of the basal epithelium in the presence of SP-A. Opsonisation of HPV16-PsVs by SP-A results in an innate immune response characterised by innate immune cell infiltration of the basal epithelial layers and viral uptake.

4.2 The modulatory effect of recombinant human vimentin on HPV16-PsVs infection

Interaction with host cell surface molecules is one of the early (and crucial) steps leading to successful viral infection (140). In the case of HPV, it has been shown that HSPGs are the primary attachment factors in epithelial cells (123, 141). Specifically, the major capsid protein L1 binds to HSPGs on parts of the basement membrane of the FRT that have become exposed as a result of epithelial microabrasions and trauma (e.g. due to sexual intercourse or inflammation) (39).

Viral internalisation occurs approximately 2 to 4 hours after cell-surface binding (142). It has been shown that binding to the cell surface (or basement membrane in an *in vivo* context) results in a

conformational change of the viral capsid, which exposes the L2 minor capsid protein for subsequent furin cleavage (37). Furin cleavage is required for successful HPV infection and it has been hypothesised to result in a capsid conformation that is able to interact with a non-HSPG cell-surface receptor(s) (36, 40).

These crucial early steps in HPV infection make targeting viral receptors, or identifying novel molecules that prevent receptor engagement by incoming viral particles, promising strategies for the control of several viral infections (36, 140).

Vimentin, a type III IF protein, has been previously shown to modulate HPV16-PsVs infectious internalisation (36), independently of prior furin cleavage of the virions. The result was surprising as vimentin has been shown to facilitate infection of a number of viruses (108, 113–116, 121, 143).

It was hypothesised that binding of either cell surface or soluble recombinant vimentin protein with the viral particle interferes with the binding of the cell surface molecules utilised by HPV for binding and internalisation, either by concealing portions of the virus that interact with its receptor(s) or by causing steric hindrance (36). This study aimed to further characterise the precise mechanisms by which artificial supplementation with exogenous rhVim modulates the early steps of HPV16-PsVs infection.

As vimentin has been shown to form a filamentous network in the presence of NaCl (101), *in vitro* experiments were performed to determine whether rhVim in its filamentous form had a different effect on HPV16-PsVs infectious internalisation compared to non-filamentous form as used in previous experiments (36).

It is evident that in the absence or at low concentrations of NaCl vimentin remains in a globular state (Figure 3.6A), while in the presence of 100mM NaCl, rhVim forms a distinct filamentous network. Theses experimental conditions were used in further validation studies.

HPV16-PsVs internalisation by NIKS cells revealed that the decrease in infectious internalisation previously reported for rhVim coated viral particles in the absence of NaCl (36) was abolished when the rhVim was in its filamentous form (Figure 3.6B). One could speculate that rhVim in its filamentous form may be unable to conceal the portion of the viral particle necessary for

interaction of host cell-surface molecules. Another explanation could be that the formation of filaments may “hide” a majority of the HPV binding sites on vimentin which results in vimentin losing its ability to efficiently interact with HPV. Formation of filaments may even result in steric hindrance which could minimise the HPV-vimentin interaction points. Currently, by using cryogenic electron microscopy techniques, these precise regions of binding are being elucidated.

Since only globular vimentin was found to be capable of modulating HPV16-PsVs, all subsequent studies were performed in the absence of NaCl.

As HSPGs are used by HPVs for successful binding and internalisation in epithelial cells, it was investigated whether rhVim had any effect on HPV binding to HSPGs. By quantifying the co-localisation of Alexa Fluor 488-labelled HPV16-PsVs to stained surface HSPGs of NIKS cells, it was deduced that rhVim coated HPV16-PsVs resulted in less HSPG co-localisation than the HPV only and BSA controls (Figure 3.7B and 3.7C).

As HPV-HSPG co-localisation still occurred to a certain degree in the presence of rhVim, it could not be ruled out that it was solely HSPG binding which rhVim interferes with. HPV is believed to interact with a number of cell surface molecules (including the still unknown entry receptor (complex)) subsequent to the initial HSPG attachment; therefore, binding and internalisation by means of FACS assays were performed subsequent to removal of surface HSPGs by heparinase I treatment.

Binding of HPV16-PsVs to the cell surface of NIKS cells decreased as expected upon removal of HSPGs (Figure 3.8B). Although it has been suggested that HSPG binding is critical for successful HPV infection, these results do not show a complete reduction in infection upon heparinase I treatment. Similar results were seen in a study done by Culp *et al.,* where heparinase I treatment in HaCaT cells (a comparable human keratinocyte cell line to NIKS) also did not demonstrate a complete reduction in HPV11 infection (32). The same paper demonstrated that HaCaT cells secrete a yet unidentified extracellular matrix (ECM) absorption receptor which could absorb HPV particles and lead to its internalisation by adherent cells (32). This mode of internalisation in keratinocytes was independent of the HSPG internalisation pathway and could be an explanation for what was observed in NIKS cells in this study.

Regardless of the extent of heparinase I treatment on viral binding, cell-surface binding of HPV16-PsVs to NIKS cells decreased to an even greater extent when pre-coated with rhVim (Figure 3.8B). Similar trends were noted for viral internalisation (Figure 3.8C). The further decrease in both binding and internalisation in cells that were both heparinase I treated and then incubated with rhVim-coated HPV16-PsVs suggests that rhVim may be affecting viral particle binding to HSPGs as well as engagement with other unknown cell-surface binding molecules used by HPV in the early stages of infection.

To provide biological relevance to rhVim's modulation of HPV16-PsVs infection, *in vivo* studies as already described for the SP-A studies were performed.

Pre-incubation of HPV16-PsVs with rhVim led to a substantial decrease in infection when compared to the BSA control in mice (Figure 3.9B). This decrease in infection was observed 72 hours p.i., as the Gaussia luciferase readings for all the vaginal lavages at 24 hours p.i. were too low to quantify noticeable differences between the treatments. Due to time constraints, these results were derived from a single experiment and repeats will need to be performed in order to validate these observations.

Taken together, this study shed light on the mechanisms by which rhVim modulates HPV16-PsVs infectious internalisation. The data from this study suggests that non-filamentous rhVim, and not filamentous rhVim, modulates infectious internalisation of HPV16-PsVs *in vitro* at at least two steps, by preventing binding of the viral capsid to surface HSPGs, and by preventing attachment and interaction with the still unknown receptor/receptor complex (Figure 4.2). This is most likely independent of furin pre-cleavage of the viral capsid as demonstrated by Schäfer *et al* (36).

This study also suggests that rhVim is capable of modulating HPV16-PsVs infection in a complex biological setting.

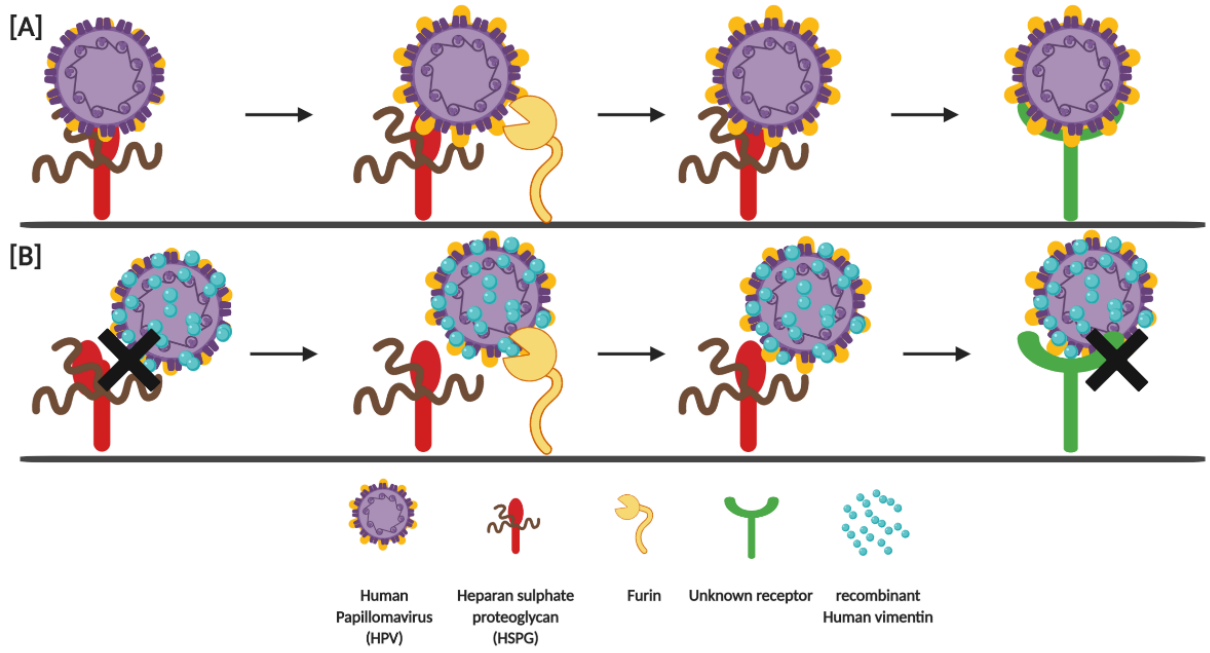

Figure 4.2: Model of rhVim's modulation of HPV16-PsVs infectious internalisation. **[A]** Cell-surface events that occur at the early stages of HPV entry into cultured cells. Mature HPV16-PsVs composed of both capsid proteins (L1 in purple and L2 in yellow) initially bind to HSPGs on the cell surface. This results in a conformational change that exposes the N-terminus of L2, allowing access to the furin recognition site followed by cleavage of this site. This cleavage further exposes L2, resulting in a capsid conformation that is able to interact with a non-HSPG cell-surface receptor(s). **[B]** Coating of HPV16-PsVs with rhVim prevents binding of the HPV16-PsVs to both HSPGs and the subsequent unknown receptor(s) used by HPV16 for successful internalisation and infection of cultured cells, where this is probably independent of furin cleavage. Figure adapted from (40).

5 Conclusion

In summary, this study assigned a novel role for SP-A and vimentin in the protection against HPV16-PsVs infection in the murine FRT. Although these two proteins demonstrate vastly different mechanisms, both lead to an overall decrease in HPV16-PsVs infection as shown in a murine infection model.

Both SP-A and vimentin can be artificially supplied exogenously, leading to recognition and binding of HPV particles and modulation of infection. Therefore, future research aims to develop these molecules into topical microbicides as an alternative and potentially broad-spectrum means to current prophylactic HPV vaccination.

The current research on the supplementation of SP-A as a means of reducing pathogenic infections is significantly more advanced than research on supplementation of rhVim, making SP-A, currently, a more ideal candidate for further studies in our laboratory into broad-spectrum therapies for sexually transmitted viral infections. *C. Trachomatis* and uropathogenic *E. coli,* are among the pathogens whose infection has been shown to decrease upon SP-A supplementation *in vivo* and *in vitro,* respectively (80, 144). Moreover, SP-A inhibits direct HIV infection of CD4 cells, yet the enhanced DC uptake with SP-A bound HIV *in vitro* emphasises the need for further research (78) particularly *in vivo*.

Nevertheless, the identification and characterisation of vimentin as a viral restriction factor capable of modulating the early events in HPV16-PsVs infection of epithelial cells, suggests it can be a candidate for drug development. Therefore, both SP-A and rhVim may potentially be developed into microbicides or lubricants to prevent HPV infection.

References

1. De Villiers EM, Fauquet C, Broker TR, Bernard HU, Zur Hausen H. 2004. Classification of papillomaviruses. Virology 324:17–27.

2. Bosch FX, Manos MM, Muñoz N, Sherman M, Jansen AM, Peto J, Schiffman MH, Moreno V, Kurman R, Shan K V, on Cervical Cancer (IBSCC) Study Group IBS. 1995. Prevalence of Human Papillomavirus in Cervical Cancer: a Worldwide Perspective. J Natl Cancer Inst 87:796–802.

3. Hausen H. 2002. Papillomaviruses and Cancer: From Basic Studies to Clinical Application. Nat Rev Cancer 2:342–350.

4. Munoz N, Bosch FX, Castellsague X, Diaz M, De Sanjose S, Hammouda D, Shah K V, Meijer CJLM. 2003. Against Which Papillomavirus Types Shall We Vaccinate and Screen? The International Perspective. Int J Cancer 111:278–285.

5. Munoz N, Castellsague X, Gonzales AB De. 2006. Chapter 1: HPV in the etiology of human cancer. Vaccine 3:1–10.

6. Sweetland S, Thomas D, Gonz B De, Unit E, Society DC, Health P, Hutchinson F, Epidemiolog- G, Rica C. 2006. Carcinoma of the cervix and tobacco smoking : Collaborative reanalysis of individual data on 13,541 women with carcinoma of the cervix and 23,017 women without carcinoma of the cervix from 23 epidemiological studies. Int J Cancer 118:1481–1495.

7. Palefsky JM, Holly EA. 2003. Chapter 6: Immunosuppression and Co-infection with HIV. Natl Cancer Inst m 31:41–46.

8. World HPV Information Center. 2017. Human Papillomavirus and Related Diseases Report - South Africa. HPV Inf Cent Rep 1–78.

9. Castle PE, Giuliano AR. 2003. Chapter 4: Genital Tract Infections, Cervical Inflammation, and Antioxidant Nutrients — Assessing Their Roles as Human Papillomavirus Cofactors. Natl Cancer Inst Monogr 7234:29–34.

10. Smith JS, Herrero R, Bosetti C, Mun N, Bosch FX, Castellsague X, Brule AJC Van Den,

Franceschi S, Ashley R. 2002. Herpes Simplex Virus-2 as a Human Papillomavirus Cofactor in the Etiology of Invasive Cervical Cancer. J Natl Cancer Inst 94:1604–1613.

11. Zhao Y, Cao X, Zheng Y, Tang J, Cai W, Wang H, Gao Y, Wang Y. 2012. Relationship Between Cervical Disease and Infection With Human Papillomavirus Types 16 and 18 , and Herpes Simplex Virus 1 and 2. J Med Virol 84:1920–1927.

12. Bray F, Ferlay J, Soerjomataram I. 2018. Global Cancer Statistics 2018: GLOBOCAN Estimates of Incidence and Mortality Worldwide for 36 Cancers in 185 Countries. CA Cancer J Clin 68:394–424.

13. De Vuyst H, Alemany L, Lacey C, Chibwesha CJ, Sahasrabuddhe V, Banura C, Denny L, Parham GP. 2013. The Burden of Human Papillomavirus Infections and Related Diseases in Sub-Saharan Africa. Vaccine 31:F32–F46.

14. Williamson A-L. 2015. The Interaction between Human Immunodeficiency Virus and Human Papillomaviruses in Heterosexuals in Africa. J Clin Med 4:579–592.

15. Berg M, Stenlund A. 1997. Functional Interactions between Papillomavirus E1 and E2 Proteins. J Virol 71:3853–3863.

16. Sverdrup F, Khan SA. 1994. Replication of Human Papillomavirus (HPV) DNAs Supported by the HPV Type 18 El and E2 Proteins. J Virol 68:505–509.

17. Doorbar J. 2013. The E4 protein; structure, function and patterns of expression. Virology 445:80–98.

18. Ashrafi GH, Haghshenas MR, Marchetti B, Brien PMO, Campo MS. 2005. E5 Protein of Human Papillomavirus Type 16 Selectively Downregulates Surface HLA Class I. Int J Cancer 113:276–283.

19. Ciesielska U, Nowińska K, Podhorska-okołów M. 2012. The Role of Human Papillomavirus in the Malignant Transformation of Cervix Epithelial Cells and the Importance of Vaccination Against This Virus. Adv Clinincal Exp Med 21:235–244.

20. Narisawa-saito M, Kiyono T. 2007. Basic mechanisms of high-risk human papillomavirus-induced carcinogenesis: Roles of E6 and E7 proteins. Cancer Sci 98:1505–1511.

21. Dyson N, Peter MH, Karl M, Ed H. 1989. The Human Papilloma Virus-16 E7 Oncoprotein is Able to Bind to the Retinoblastoma Gene Product. Science (80-) 243:934–937.

22. Chellappan S, Kraus VB, Kroger B, Munger K, Howley PM, Phelps WC, Nevins JR. 1992. Adeno virus E1A, simian virus 40 tumor antigen, and human papillomavirus E7 protein share the capacity to disrupt the interaction between transcription factor E2F and the retinoblastoma gene product. Proc Natl Acad Sci U S A 89:4549–4553.

23. Chow LT, Broker TR, Steinberg BM. 2010. The natural history of human papillomavirus infections of the mucosal epithelia. Authors J Compil 118:422–449.

24. Buck CB, Cheng N, Thompson CD, Lowy DR, Steven AC, Schiller JT, Trus BL. 2008. Arrangement of L2 within the Papillomavirus Capsid. J Virol 82:5190–5197.

25. Stanley MA. 2012. Epithelial Cell Responses to Infection with Human Papillomavirus. Clin Microbiol Rev 25:215–222.

26. Stanley M. 2010. HPV - immune response to infection and vaccination. Infect Agent Cancer 5:1–6.

27. Ozbun MA. 2019. Extracellular events impacting human papillomavirus infections: Epithelial wounding to cell signaling involved in virus entry. Papillomavirus Res 7:188–192.

28. Shope BRE, Hurst BEW. 1933. Infectious Papillomatosis of Rabbits. J Exp Med 58:607–624.

29. Roberts JN, Buck CB, Thompson CD, Kines R, Bernardo M, Choyke PL, Lowy DR, Schiller JT. 2007. Genital transmission of HPV in a mouse model is potentiated by nonoxynol-9 and inhibited by carrageenan. Nat Med 13:857–861.

30. Streeck RE, Giroglou T, Florin L, Scha F, Sapp M. 2001. Human Papillomavirus Infection Requires Cell Surface Heparan Sulfate. Am Soc Microbiol 75:1565–1570.

31. Johnson KM, Kines RC, Roberts JN, Lowy DR, Schiller JT, Day PM, Irol J V. 2009. Role of Heparan Sulfate in Attachment to and Infection of the Murine Female Genital Tract by Human Papillomavirus. Virology 83:2067–2074.

32. Culp TD, Budgeon LR, Christensen ND. 2006. Human papillomaviruses bind a basal extracellular matrix component secreted by keratinocytes which is distinct from a membrane-associated receptor. Virology 347:147–159.

33. Schäfer G, Blumenthal, Melissa J, Katz AA. 2015. Interaction of human tumor viruses with host cell surface receptors and cell entry. Viruses 7:2592–2617.

34. Cerqueira C, Ventayol S, Vogeley C. 2015. Kallikrein-8 Proteolytically Processes Human Papillomaviruses in the Extracellular Space To Facilitate Entry into Host Cells. J v 89:7038–7052.

35. Bienkowska-haba M, Patel HD, Sapp M. 2009. Target Cell Cyclophilins Facilitate Human Papillomavirus Type 16 Infection. Pathogens 5:1–11.

36. Schäfer G, Graham LM, Lang D, Blumenthal, Melissa JW, Marušič MB, Katz AA. 2017. Vimentin Modulates Infectious Internalization of Human Papillomavirus 16 Pseudovirions. J Virol 91:1–17.

37. Richards RM, Lowy DR, Schiller JT, Day PM. 2006. Cleavage of the papillomavirus minor capsid protein, L2, at a furin consensus site is necessary for infection. PNAS 103:1522–1527.

38. Selinka H-C, Florin L, Patel HD, Freitag K, Schmidtke M, Makarov VA, Sapp M. 2007. Inhibition of Transfer to Secondary Receptors by Heparan Sulfate-Binding Drug or Antibody Induces Noninfectious Uptake of Human Papillomavirus. J Virol 81:10970–10980.

39. Schiller JT, Day PM, Kines RC. 2019. Gynecologic Oncology Current understanding of the mechanism of HPV infection. Gynecol Oncol 118:S12–S17.

40. Day PM, Schiller JT. 2009. The role of furin in papillomavirus infection. Future Microbiol 4:1255–1262.

41. Moody CA, Laimins LA. 2010. Human papillomavirus oncoproteins: pathways to transformation. Nat Publ Gr 10:550–560.

42. Mcbride AA. 2017. ScienceDirect Playing with fire : consequences of human

papillomavirus DNA replication adjacent to genetically unstable regions of host chromatin. Curr Opin Virol 26:63–68.

43. Doorbar J. 2005. The papillomavirus life cycle. J Clin Virol 32S:7–15.

44. Arend WP, Palmer G, Gabay C. 2008. IL-1 , IL-18 , and IL-33 families of cytokines. Immunol Rev 223:20–38.

45. Park J, Kim E, Kwon H, Hwang E, Namkoong S, Um S. 2000. Inactivation of Interferon Regulatory Factor-1 Tumor Suppressor Protein by HPV E7 Oncoprotein. J Biol Chem 275:6764–6769.

46. Barnard P, Payne E, Mcmillan NAJ. 2000. The Human Papillomavirus E7 Protein Is Able to Inhibit the Antiviral and Anti-growth Functions of Interferon-alpha. Virology 277:411–419.

47. Ronco L V, Karpova AY, Vidal M, Howley PM. 1998. Human papillomavirus 16 E6 oncoprotein binds to interferon regulatory factor-3 and inhibits its transcriptional activity. Genes Dev 12:2061–2072.

48. Stanley M. 2005. Immune responses to human papillomavirus. Vaccine 24S1:1–7.

49. Konopnicki AD, Wit S De, Clumeck N. 2013. HPV and HIV coinfection: a complex interaction resulting in epidemiological , clinical and therapeutic implications. Future Virol 8:303–311.

50. Siddiqui MAA, Perry CM. 2006. Vaccine (Gardasil ®). Drugs 66:1263–1271.

51. Monie A, Hung CF, Roden R, Wu TC. 2008. Cervarix™: A vaccine for the prevention of HPV 16, 18-associated cervical cancer. Biol Targets Ther 2:107–113.

52. Zhai L, Tumban E. 2016. Gardasil-9: A global survey of projected efficacy. Antiviral Res 130:101–109.

53. Stanley M, Lowy DR, Frazer I. 2006. Chapter 12: Prophylactic HPV vaccines: Underlying mechanisms. Vaccine 24:106–113.

54. Denny L. 2015. Control of Cancer of the Cervix in Low- and Middle-Income Countries. Ann

Surg Oncol 22:728–733.

55. Tathiah N, Chb MB, Man DHI V, Epi MS, Phm M. 2015. Human papillomavirus (HPV) vaccination of adolescents in the South African private health sector: Lessons from the HPV demonstration project in KwaZulu-Natal. South African Med J 105:11–13.

56. Mofolo N, Sello M, Leselo M, Chabanku N, Ndlovu S, Naidoo Q, Joubert G, State F, Africa S, Africa S, Africa S, Mofolo N. 2014. Knowledge of cervical cancer , human papillomavirus and prevention among first-year female students in residences at the University of the Free State. African J Prim Heal Care Fmily Med 10:1–5.

57. Brouwer AF, Delinger RL, Eisenberg MC, Campredon LP, Walline HM, Carey TE, Meza R. 2019. HPV vaccination has not increased sexual activity or accelerated sexual debut in a college-aged cohort of men and women. BMC Public Health 19:1–8.

58. Chandra-mouli V, Mccarraher DR, Phillips SJ, Williamson NE, Hainsworth G. 2014. Contraception for adolescents in low and middle income countries : needs , barriers , and access. Reprod Heal 11:1–8.

59. Lowy DR, Schiller JT, Buck CB, Thompson CD, Roberts JN, Mu M. 2006. Carrageenan Is a Potent Inhibitor of Papillomavirus Infection. PLoS Pathog 2:671–680.

60. Marais D, Gawarecki D, Allan B, Ahmed K, Altini L, Cassim N, Hoffman M, Ramjee G, Williamson A. 2011. Original article The effectiveness of Carraguard , a vaginal microbicide , in protecting women against high-risk human papillomavirus infection 1226:1219–1226.

61. Fernández-Romero JA, Abraham CJ, Rodriguez A, Kizima L, Jean-Pierre N, Menon R, Begay O, Seidor S, Ford BE, Gil PI, Peters J, Katz D, Robbiani M, Zydowsky TM. 2012. Zinc Acetate/Carrageenan Gels Exhibit Potent Activity in vivo against High-Dose Herpes Simplex Virus 2 Vaginal and Rectal Challenge. Antimicrob Agents Chemother 56:358–368.

62. Skoler-karpoff S, Ramjee G, Ahmed K, Altini L, Plagianos MG, Friedland B, Govender S, Town C, Town C. 2019. Efficacy of Carraguard for prevention of HIV infection in women in South Africa: a randomised, double-blind , placebo-controlled trial. Lancet 372:1977–

1987.

63. Ujma S, Horsnell WGC, Katz A, Clark W. 2017. Non-Pulmonary Immune Functions of Surfactant Proteins A and D. J Innate Immun 9:3–11.

64. Pattle RE. 1955. Properties, Function, and Origin of the Alveolar Lining Layer. Nature 175:1125–1126.

65. Kishore U, Bernal AL, Kamran MF, Saxena S, Singh M, Sarma PU, Madan T, Chakraborty T. 2005. Surfactant proteins SP-A and SP-D in human health and disease. Arch Immunol Ther Exp (Warsz) 53:399–417.

66. Ujma SD. 2017. The role of surfactant protein A in immunity to HPV16 pseudovirus infection - MSc thesis. Univ Cape T.

67. Schlesinger LS. 1995. Pulmonary surfactant protein A mediates enhanced phagocytosis of Mycobacterium tuberculosis by a direct interaction with human macrophages. J Immunol 155:5343–5351.

68. Ghildyal R, Hartley C, Varrasso A, Meanger J, Dennis R, The S, Diseases I, Dec N, Meanger J, Voelker DR, Anders EM, Mills J. 1999. Surfactant Protein a Binds to the Fusion Glycoprotein of Respiratory Syncytial Virus and Neutralizes Virion Infectivity. J Infect Dis 180:2009–2013.

69. Kishore U, Greenhough TJ, Waters P, Shrive AK, Ghai R, Kamran MF, Reid KBM. 2006. Surfactant proteins SP-A and SP-D : Structure , function and receptors. Mol Immunol 43:1293–1315.

70. Wright JR. 2005. Immunoregulatory Function of Surfactant Porteins. Nat Rev Immunol 5:58–68.

71. Hartshorn KL, Crouch E, White MR, Colamussi ML, Kakkanatt A, Tauber B, Shepherd V, Sastry KN, Kevan L, Crouch E, White MR, Colamussi ML, Kakkanatt A, Shepherd V, Sastry KN. 1998. Pulmonary surfactant proteins A and D enhance neutrophil uptake of bacteria. Am Physiol Soc 274:958–969.

72. McDonough KA, Kress Y, Bloom BR. 1993. The interaction of Mycobacterium tuberculosis

with macrophages: A study of phagolysosome fusion. Infect Agents Dis 2:232–235.

73. Levine AM, Kurak KE, Bruno MD, Stark JM, Whitsett JA, Korfhagen TR, Respir AJ, Mol C. 1998. Surfactant Protein-A-Deficient Mice Are Susceptible to Pseudomonas aeruginosa Infection. Am J Respir Cell Mol Biol 19:700–708.

74. Hartshorn KL, White MR, Shepherd V, Reid KEN, Jensenius JC, Crouch EC, Kevan L, White MR, Reid K, Jensenius JC. 1997. Mechanisms of anti-influenza activity of surfactant proteins A and D: comparison with serum collectins. Am J Physiol 273:L1157–L1166.

75. Simoons-Smit AM, Kraan EM, Beishuizen A, Schijndel RJS Van, Vandenbroucke-Grauls CM. 2006. Herpes simplex virus type 1 and respiratory disease in critically-ill patients : real pathogen or innocent bystander? Eur Soc Clin Microbiol Infect Dis 12:1050–1059.

76. Garcia-verdugo I, Tanfin Z, Dallot E, Breuiller-fouche M. 2008. Surfactant Protein A Signaling Pathways in Human Uterine Smooth Muscle Cells 1. Biol Reprod 79:348–355.

77. Neill C, Umstead TM, Phelps DS, Lin Z, Floros J, Debra A. 2004. Surfactant protein A, an innate immune factor, is expressed in the vaginal mucosa and is present in vaginal lavage fluid. Immunology 111:91–99.

78. Gaiha GD, Dong T, Palaniyar N, Mitchell DA, Reid KBM, Clark HW. 2008. Surfactant Protein A Binds to HIV and Inhibits Direct Infection of CD4 + Cells, but Enhances Dendritic Cell-Mediated Viral Transfer. J Immunol 181:601–609.

79. Oberley RE, Goss KL, Ault KA, Crouch EC, Snyder JM. 2004. Surfactant protein D is present in the human female reproductive tract and inhibits Chlamydia trachomatis infection. Mol Hum Reprod 10:861–870.

80. Hashimoto J, Takahashi M, Saito A, Uehara Y, Hasegawa Y. 2019. Surfactant Protein A Inhibits Growth and Adherence of Uropathogenic Escherichia coli To Protect the Bladder from Infection. J Immunol 198:2898–2905.

81. Madsen AJ, Gaiha GD, Palaniyar N, Dong T, Mitchell DA, Clark HW. 2013. Surfactant Protein D Modulates HIV Infection of Both T-Cells and Dendritic Cells. PLoS One 8:59047–59055.

82. Ujma S, Carse S, Chetty A, Horsnell W, Clark H, Madsen J, Mackay R, Watson A, Griffiths M, Katz AA, Schäfer G. 2019. Surfactant Protein A Impairs Genital HPV16 Pseudovirus Infection by Innate Immune Cell Activation in A Murine Model. Pathogens 8:1–19.

83. Cooper G. 2000. The Cell: A molecular Approach, 2nd ed. Sunderland (MA): Sinauer Associates.

84. Lodish H, Berk A, Zipursky S. 2000. Molecular Cell Biology, 4th ed. W. H. Freeman, New York.

85. Jiu Y, Lehtimäki J, Tojkander S, Cheng F, Jäälinoja H, Liu X, Varjosalo M, Eriksson JE, Lappalainen P. 2015. Bidirectional Interplay between Vimentin Intermediate Filaments and Contractile Actin Stress Fibers. Cell Rep 11:1511–1518.

86. Conway JF, Parry DAD. 1988. Intermediate filament structure: 3. Analysis of sequence homologies. Int J Biol Macromol 10:79–98.

87. Marchuk D, McCrohon S, Fuchs E. 1984. Remarkable conservation of structure among intermediate filament genes. Cell 39:491–498.

88. Virtanen I, Lehto V, Lehtonen E, Vartio T, Stenman S, Kurki P, Wager O, Small J V, Dahl D, Badley RA. 1981. Expression of intermediate filaments in cultured cells. J Cell Sci 50:45–63.

89. Brown MJ, Hallam J a, Colucci-Guyon E, Shaw S. 2001. Rigidity of circulating lymphocytes is primarily conferred by vimentin intermediate filaments. J Immunol 166:6640–6646.

90. Azumi N, Battifora H. 1987. The distribution of vimentin and keratin in epithelial and nonepithelial neoplasms. A comprehensive immunohistochemical study on formalin- and alcohol-fixed tumors. Am J Clin Pathol 88:286–296.

91. Colucci-Guyon E, Portier M-M, Dunia I, Paulin D, Pournin S, Babinet C. 1994. Mice lacking vimentin develop and reproduce without an obvious phenotype. Cell 79:679–694.

92. Herrmann H, Bär H, Kreplak L, Strelkov S V, Aebi U. 2007. Intermediate filaments: from cell architecture to nanomechanics. Nat Rev Mol Cell Biol 8:562–573.

93. Spoden G, Freitag K, Husmann M, Boller K, Sapp M, Lambert C, Florin L. 2008. Clathrin- and caveolin-independent entry of human papillomavirus type 16 - Involvement of tetraspanin-enriched microdomains (TEMs). PLoS One 3:e3313.

94. Coulombe PA, Wong P. 2004. Cytoplasmic intermediate filaments revealed as dynamic and multipurpose scaffolds. Nat Cell Biol 6:699–706.

95. Toivola DM, Tao G, Habtezion A, Liao J, Omary MB. 2005. Cellular integrity plus: organelle-related and protein-targeting functions of intermediate filaments. Trends Cell Biol 15:608–617.

96. Ivaska J, Pallari HM, Nevo J, Eriksson JE. 2007. Novel functions of vimentin in cell adhesion, migration, and signaling. Exp Cell Res 313:2050–2062.

97. Ivaska J. 2011. Vimentin. Small GTPases 2:51–53.

98. Nieminen M, Henttinen T, Merinen M, Ichihara FM, Eriksson JE, Jalkanen S. 2006. Vimentin function in lymphocyte adhesion and transcellular migration. Nat Commun 8:156–162.

99. Byun Y, Chen F, Chang R, Trivedi M, Green KJ, Cryns VL. 2001. Caspase cleavage of vimentin disrupts intermediate filaments and promotes apoptosis. Cell Death Differ 8:443.450.

100. Premchandar A, Mücke N, Poznański J, Wedig T, Kaus-Drobek M, Herrmann H, Dadlez M. 2016. Structural dynamics of the vimentin coiled-coil contact regions involved in filament assembly as revealed by hydrogen-deuterium exchange. J Biol Chem 291:24931–24950.

101. Lopez CG, Saldanha O, Huber K, Köster S. 2016. Lateral association and elongation of vimentin intermediate filament proteins: A time-resolved light-scattering study. PNAS 113:11152–11157.

102. Herrmann H, Ha M, Brettel M, Mu SA, Goldie KN, Fedtke B, Lustig A, Franke WW, Mu ME. 1996. Structure and Assembly Properties of the Intermediate Filament Protein Vimentin: The Role of its Head, Rod and Tail Domains. Mol Biol 264:933–953.

103. Feher J. 2017. Cell structure.Quantitative Human Physiology2nd Editio. Academic Press.

104. Moisan E, Girard D. 2006. Cell surface expression of intermediate lament proteins vimentin and lamin B1 in human neutrophil spontaneous apoptosis. J Leukoc Biol 79:489–498.

105. Bhattacharya R, Gonzalez AM, DeBiase PJ, Trejo HE, Goldman RD, Flitney FW, Jones JCR. 2009. Recruitment of vimentin to the cell surface by β3 integrin and plectin mediates adhesion strength. J Cell Sci 122:1390–1400.

106. Mor-Vaknin N, Punturieri A, Sitwala K, Markovitz D. 2003. Vimentin is secreted by activated macrophages. Nat Cell Biol 5:77–81.

107. Shigyo M, Tohda C. 2016. Extracellular vimentin is a novel axonal growth facilitator for functional recovery in spinal cord-injured mice. Sci Rep 6:28293.

108. Steinmetz NF, Cho C-F, Ablack A, Lewis JD, Manchester M. 2012. Cowpea mosaic virus nanoparticles target surface vimentin on cancer cells. Nanomedicine 6:351–364.

109. Thiagarajan PS, Yakubenko VP, Elsori DH, Yadav SP, Febbraio M, Willard B, Tan CD, Rene E, Cathcart MK. 2013. Vimentin is an endogenous ligand for the pattern recognition receptor Dectin-1. Cardiovasc Res 99:494–504.

110. Satelli A, Brownlee Z, Mitra A, Meng QH, Li S. 2015. Circulating tumor cell enumeration with a combination of epithelial cell adhesion molecule- and cell-surface vimentin-based methods for monitoring breast cancer therapeutic response - Satelli.PDF. Clin Chem 61:259–266.

111. Sukumaran B, Mastronunzio JE, Narasimhan S, Fankhauser S, Uchil PD, Levy R, Graham M, Colpitts TM, Lesser CF, Fikrig E. 2011. Anaplasma phagocytophilum AptA modulates Erk1/2 signalling. Cell Microbiol 13:47–61.

112. Kumar Y, Valdivia RH. 2008. Article Actin and Intermediate Filaments Stabilize the Chlamydia trachomatis Vacuole by Forming Dynamic Structural Scaffolds. Cell Host Microbe 4:159–169.

113. Koudelka KJ, Destito G, Plummer EM, Trauger SA, Siuzdak G, Manchester M. 2009. Endothelial Targeting of Cowpea Mosaic Virus (CPMV) via Surface Vimentin. PLoS Pathog

5:1–10.

114. Das S, Ravi V, Desai A. 2011. Japanese encephalitis virus interacts with vimentin to facilitate its entry into porcine kidney cell line. Virus Res 160:404–408.

115. Liang J, Yu C, Liao C, Lin Y. 2011. Vimentin binding is critical for infection by the virulent strain of Japanese encephalitis virus. Cell Microbiol 13:1358–1370.

116. Miller MS, Hertel L. 2009. Onset of Human Cytomegalovirus Replication in Fibroblasts Requires the Presence of an Intact Vimentin Cytoskeleton. J Virol 83:7015–7028.

117. Du N, Cong H, Tian H, Zhang H, Zhang W, Song L, Tien P. 2014. Cell Surface Vimentin Is an Attachment Receptor for Enterovirus 71. J Virol 88:5816–5833.

118. Ksiazek TG, Erdman D, Goldsmith CS, Zaki SR, Peret T, Emery S, Tong S, Urbani C, Comer JA, Lim W, Rollin PE, Dowell SF, Ling A-E, Humphrey CD, Shieh W-J, Guarner J, Paddock CD, Rota P, Fields B, DeRisi J, Yang J-Y, Cox N, Hughes JM, LeDuc JW, Bellini WJ, Anderson LJ. 2003. A Novel Coronavirus Associated with Severe Acute Respiratory Syndrome Thomas. N Engl J Med 348:1953–1965.

119. Ding Y, He L, Zhang Q, Huang Z, Che X, Hou J, Wang H, Shen H, Qiu L, Li Z, Geng J, Cai J, Han H, Li X, Kang W, Weng D, Liang P, Jiang S. 2004. Organ distribution of severe acute respiratory syndrome (SARS) associated coronavirus (SARS-CoV) in SARS patients: Implications for pathogenesis virus transmission pathways. J Pathol 203:622–630.

120. Li W, Moore MJ, Vasilieva N, Sui J, Wong S kee, Berne MA, Somasundaran M, Sullivan JL, Luzuriga K, Greenough TC, Choe H, Farzan M. 2003. Angiotensin-converting enzyme 2 is a functional receptor for the SARS coronavirus. Nature 426:450–452.

121. Yu YT, Chien S, Chen I, Lai C, Tsay Y, Chang SC. 2016. Surface vimentin is critical for the cell entry of SARS-CoV. J Biomed Sci 23:1–10.

122. Buck CB, Pastrana D V., Lowy DR, Schiller JT. 2005. Generation of HPV pseudovirions using transfection and their use in neutralization assays. Methods Mol Med 119:445–462.

123. Joyce JG, Tung JS, Przysiecki CT, Cook JC, Lehman ED, Sands JA, Jansen KU, Keller PM.

1999. The L1 major capsid protein of human papillomavirus type 11 recombinant virus-like particles interacts with heparin and cell-surface glycosaminoglycans on human keratinocytes. J Biol Chem 274:5810–5822.

124. Verhaegent M, Christopoulos TK. 2002. Recombinant Gaussia luciferase: Overexpression, purification, and analytical application of a bioluminescent reporter for DNA hybridization. Anal Chem 74:4378–4385.

125. Schäfer G, Kabanda S, Rooyen B Van, Bergant M, Banks L, Parker MI. 2013. The role of inflammation in HPV infection of the Oesophagus. BMC Cancer 13.

126. Michelle A, Bergant M, Campos SK, Michael P, Banks L, Maru B. 2012. Human Papillomavirus L2 Facilitates Viral Escape from Late Endosomes via Sorting Nexin 17 ˇ c. Traffic 13:455–467.

127. Schäfer G, Graham LM, Lang D, Blumenthal MJ. 2017. Vimentin modulates infectious internalisation of HPV16 pseudovirions. J Virol 91.

128. Varsani A, Williamson A, Jaffer MA, Rybicki EP. 2006. A deletion and point mutation study of the human papillomavirus type 16 major capsid gene. Virus Res 122:154–163.

129. Manders EMM, Verbeek FJ, Aten JA. 1993. Measurement of co-localization of objects in dual-colour confocal images. J Microsc 169:375–382.

130. Niruthisard S, Roddy RE, Chutivongse S. 1991. The effects of frequent nonoxynol-9 use on the vaginal and cervical mucosa. Sex Transm Dis 18:176—179.

131. Anisimovfi E, Bartfik P, Vl D, Hirsch I, B B, V V. 1990. Presence and type specificity of papillomavirus antibodies demonstrable by immunoelectron microscopy tests in samples from patients with warts. J Gen Virol 71:419–422.

132. Schopferer M, Bär H, Hochstein B, Sharma S, Mücke N, Herrmann H, Willenbacher N. 2009. Desmin and Vimentin Intermediate Filament Networks : Their Viscoelastic Properties Investigated by Mechanical Rheometry. J Mol Biol 388:133–143.

133. Giroglou T, Florin L, Schafer F, Streeck RE, Sapp M. 2000. Human Papillomavirus Infection Requires Cell Surface Heparan Sulfate. Virology 75:1565–1579.

134. Apter D, Kitchener H, Castellsague X, Teixeira JC, Skinner SR, Hedrick J, Jaisamrarn U, Limson G, Garland S, Szarewski A, Romanowski B, Aoki FY, Schwarz TF, Poppe WAJ, Bosch FX, Jenkins D, Hardt K, Zahaf T, Descamps D, Struyf F, Lehtinen M, Dubin G. 2009. Efficacy of human papillomavirus (HPV)-16/18 AS04-adjuvanted vaccine against cervical infection and precancer caused by oncogenic HPV types (PATRICIA): final analysis of a double-blind, randomised study in young women. Lancet 374:301–314.

135. Fichorova RN, Tucker LD, Anderson DJ. 2001. The Molecular Basis of Nonoxynol-9 – Induced Vaginal Inflammation and Its Possible Relevance to Human Immunodeficiency Virus Type 1 Transmission. J Infect Dis 184:418–428.

136. Patton DL, Kidder G, Sweeney C, Rabe LK, Hillier SL. 1999. Effects of multiple applications of benzalkonium chloride and nonoxynol 9 on the vaginal epithelium in the pigtailed macaque (Macaca nemestrina). Am J Obstet Gynecol 180:1080–1087.

137. Jain JK, Li A, Minoo P, Nucatola DL, Felix JC. 2005. The effect of nonoxynol-9 on human endometrium. Contraception 71:137–142.

138. Betis K. 1980. Studies of Nonoxynol-9 I. The Effect on the Vaginas of Rabbits and Rats. Fertil Steril 33:455–450.

139. Smith-mccune K, Chen JC, Greenblatt RM, Shanmugasundaram U, Shacklett BL, Hilton JF, Johnson B, Irwin JC, Giudice LC. 2015. Unexpected Inflammatory Effects of Intravaginal Gels (Universal Placebo Gel and Nonoxynol-9) on the Upper Female Reproductive Tract : A Randomized Crossover Study. PLoS One 20:1–21.

140. Letian T, Tianyu Z. 2010. Cellular receptor binding and entry of human papillomavirus. Virology 7:1–7.

141. Roden RBS, Kirnbauer R, Jenson AB, Lowy DR, Schiller JT. 1994. Interaction of Papillomaviruses with the Cell Surface. J Virol 68:7260–7266.

142. Culp TD, Christensen ND. 2004. Kinetics of in vitro adsorption and entry of papillomavirus virions 319:152–161.

143. Kim J, Fahad A, Shanmukhappa K, Kapil S. 2006. Defining the Cellular Target (s) of Porcine

Reproductive and Respiratory Syndrome Virus Blocking Monoclonal Antibody 7G10 Defining the Cellular Target (s) of Porcine Reproductive and Respiratory Syndrome Virus Blocking Monoclonal Antibody 7G10. J Virol 80:689–696.

144. Oberley RE, Ault KA, Neff TL, Khubchandani KR, Crouch EC, Snyder JM, Rebecca E, Ault KA, Neff TL, Kavita R, Crouch EC, Surfac- JMS. 2004. Surfactant proteins A and D enhance the phagocytosis of Chlamydia into THP-1 cells. Am J Physiol - Lung Cell Mol Physiol 287:296–306.

145. Buck C., Pastrana DV, Lowy DR, Schiller J., Thompson CD, Pang YY, Cardone G, Moyer AL, Cheng N, Dvoretzky I, Steven AC, Trus BL. 2015. Production of Papillomaviral Vectors (Pseudoviruses). Natl Cancer Inst.

Appendix

Composition of solutions used

Complete medium (DMEM): Dulbecco's Modified Eagle Medium (DMEM), 10% foetal calf serum (FCS) (Biochrom), Penicillin (100U/mL) and Streptomycin (100mg/mL).

F-medium: 3 vol Ham's F 12 medium, 1 vol DMEM, 5% FCS, Penicillin (100U/mL), Streptomycin (100mg/mL), 0.4µg/mL hydrocortisone, 5µg/mL insulin, 8.4ng/mL cholera toxin, 10ng/mL epidermal growth factor (EGF), 24µg/mL adenine.

Trypan Blue: 0.4% trypan blue in 1 X PBS.

5X HSB buffer: 125mM HEPES; 2.5M NaCl; 0.1% Brij58; 5mM $MgCl_2$; 500µM EDTA; 2.5% ethanol; filter sterilised.

Light CsCl: 54g CsCl in 200 mL 1xHSB buffer, filter sterilised.

Heavy CsCl: 77.6g CsCl in 200 mL 1xHSB buffer, filter sterilised.

KCl isotonic buffer: 20mM Tris, 100mM NaCl, 1.5mM $CaCl_2$, pH 7.0

FACS wash: 0.5% BSA in 1 X PBS.

FACS fix: 1% (v/v) formaldehyde in FACS wash.

Blocking solution: 1% BSA in 1X PBS.

Supplementary Figures

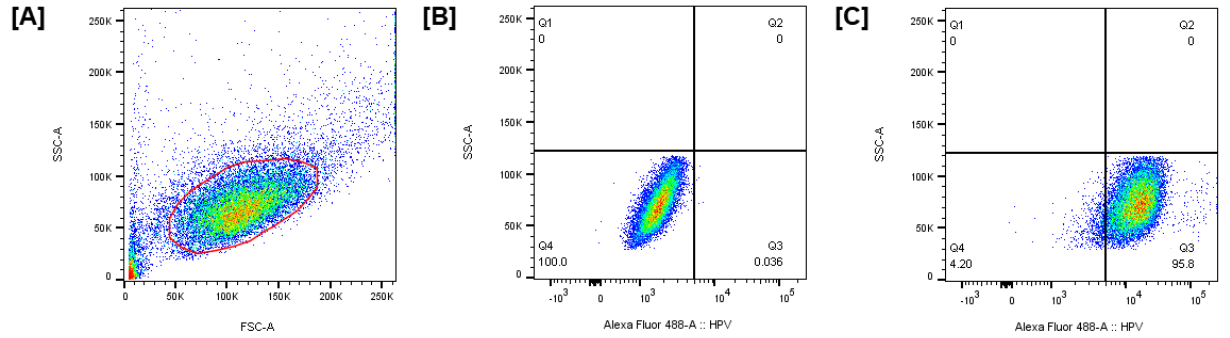

Supplementary Figure 1: Flow cytometry analysis of NIKS cell populations, following infection with AF488-HPV16-PsVs. [A] Shows a representation of the viable cell population using a dot plot of FSC versus SSC representative dot plots of fluorescence in the FL1 channel plotted against side scatter for an internalisation assay. **[B]** Shows the gating strategy using the dot plot showing forward scatter (FSC) versus side scatter (SSC) of the negative control using the BD FlowJo™ software. **[C]** Shows a shift of the cell population to the lower right quadrant upon internalisation of AF488-HPV16-PsVs.

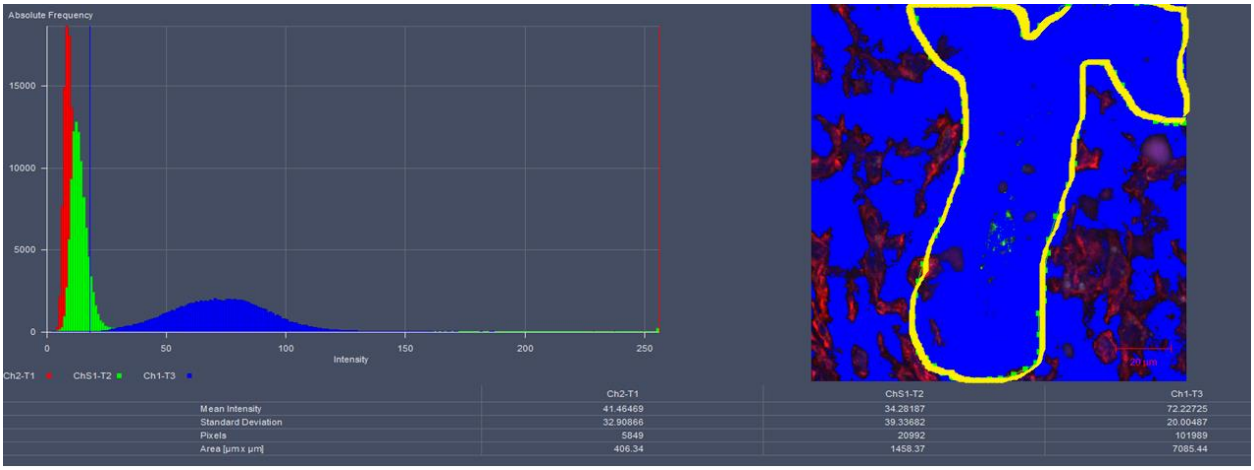

Supplementary Figure 2: Outlining of the basal epithelium of female C57BL/6 mice genital tracts for quantification of macrophage recruitment. The area of F4/80 staining in the basal layer of the epithelium of 10 randomly chosen images was quantified by setting the lower and upper thresholds at 18 and 256, respectively, to remove any background signal.